الجمهورية الجزائرية الديمقراطية الشعبية
DEMOCRATIC AND POPULAR REPUBLIC OF ALGERIA
وزارة التعليم العالي والبحث العلمي
MINISTRY OF HIGHER EDUCATION AND SCIENTIFIC RESEARCH

Mohamed Khider University, Biskra
Faculty of Sciences and technology
Department of Electrical Engineering
Ref : ……

جامعة محمد خيضر بسكرة
كلية العلوم و التكنولوجيا
قسم الهندسةالكهربائية
المرجع:.....

Contribution to Robust Control Synthesis Application to Robotics or Aerodynamics Systems

Presented to the Faculty of Sciences and Technology in Fulfillment of the Requirements for the Degree of Doctorate (Es-Science) in Electronics

Field: Electrical Engineering
Option: Electronics

Presented by:
Mohamed Redouane KAFI

Supervised by:
Prof. Abderrazak DEBILOU

Publicly defended on: July 06, 2017

Jury members:

Dr. Mebarka BELAHCEN	Chairwoman	Mohamed Khider University, Biskra
Prof. Abderrazak DEBILOU	Supervisor	Mohamed Khider University, Biskra
Dr. Latifa ABDOU	Examinator	Mohamed Khider University, Biskra
Dr. Med Assaad HAMIDA	Examinator	University Kasdi Merbah Ouargla
Prof. Noureddine ATAMNA	Examinator	University Hadj Lakhdar Batna
Prof. Djamel MELAAB	Examinator	University Hadj Lakhdar Batna

2017

Abstract

This thesis contributes to the development of robust control design strategies for uncertain nonlinear mimo systems, in which a model based control approach robust control (H_2,H_∞) framework is introduced and an intelligent control model free control is suggested.

In reality an allusion to the Modelizations of the systems CE 150 and TRMS is proposed for the research seems important because they are prerequisite to test the designed robust control law. The investigation starts by a neighboring optimal control law which is coupled with estimation to solve the trajectory tracking and/or regulator problem of a twin-rotor multi-input multi-output system (TRMS) is introduced. The above mentioned technique is applied through the linearization of the TRMS model around its operating point.

Since CE-150 helicopters are known for their varying operating conditions along with external disturbances, a local model network H_∞ control is proposed as a second alternative, for CE-150 helicopter stabilization. The proposed strategy capitalizes on recent developments on H_∞ control and its promising results in robust stabilization of plants under unstructured uncertainties. Using the fact that the system can be linearized at different operating points, a mixed sensitivity H_∞ controller is designed for the linearized system, and combined within a network to make transitions between them. The proposed control structure ensures robustness, decoupling of the system dynamics while achieving good performance.

Alternatively, another approach interval type-2 fuzzy controller is proposed for TRMS control problem because of and owing to, respectively, the nuance existing between model based control approach and model free control, and their simplicity and efficiency. The main strength of the proposed control algorithm is its robustness with respect to parametric uncertainties and noise measurement. The suggested approaches are validated through a set of computer simulations which illustrate the effectiveness of the proposed control scheme; the obtained results are presented to illustrate the controller's performance in various operating conditions, and have been successfully applied.

A custom real-time control platform design for a quadrotor is introduced and the control framework is designed to be universal but yet, flexible for implementation of various control and navigation algorithms. The developed platform is modular and is presented in three categories: hardware, software and communication. System identification is also presented for parameters measurement and estimation. Moreover, a ground station with a graphical user interface is designed for remote control and monitoring. A wireless bidirectional communication unit is also designed to bridge the quadrotor and the ground station. The developed cost effective control platform is validated by simulation and experimental test.

keywords: Estimation, output feedback, optimal control, H_∞ control, helicopter, CE150, TRMS, UAV, local model network, robust stabilization, Type 2 fuzzy logic, real-time control platform.

Contribution la synthse de loi de Commandes Robustes Application aux Systmes Robotiss ou Arodynamiques

Rsum

La prsente thse se veut comme contribution au dveloppement d'une stratgie de synthse relative aux commandes robustes, pour des systmes MIMO non linaires incertains. Dans cette perspective des approches de commande base de modle par la technique (H_2,H_∞) ont t introduites dune part et dautre part, une commande intelligente est suggre pour le cas sans modle. La modlisation des systmes CE-150 et TRMS introduits et proposs dans le prsent travail de recherche semble pertinente et ce, au regard de leur importance pour des tests de lois de commandes robustes synthtises. Dans un premier temps, une loi de commande optimale voisine, associe un estimateur, fut introduite en guise de rsolution du problme de suivi de trajectoire et/ou de rgulation du systme MIMO twin rotor (TRMS). Cette technique est applique travers la linarisation du modle TRMS autour de ses points dquilibres.

Dans un second temps, vu que lhlicoptre CE-150 est connu pour ses multiples modes de fonctionnement, outre de ses perturbations externes, une commande H_∞ par rseaux de modles locaux est propose comme une deuxime alternative afin de stabiliser lhlicoptre en question. Cette alternative capitalise les dveloppements rcents de la commande H_∞, et ses rsultats probants en termes de stabilisation robuste des systmes avec des incertitudes non structures. Le systme est linaris autour de nombreux points de fonctionnement ; une commande H_∞ sensibilit mixte fut synthtise avant quelle ne soit combine dans un rseau afin dassurer une transition plus souple. La structure de commande propose assure la robustesse, le dcouplage des dynamiques du systme tout en garantissant de bonnes performances.

Alternativement cela, une autre approche base sur la commande flou par intervalle type-2 est propose pour le problme de commande du TRMS, en raison de la diffrence existant entre les commandes base de modle et celles sans modle, ainsi que pour leur simplicit et efficacit. La force majeure de lalgorithme de commande propos rside dans son robustesse lgard des incertitudes paramtriques et les bruits de mesures.

Les approches proposes sont valides travers une srie de simulations qui montrent clairement lefficacit de la structure des commandes suggres, alors que les rsultats obtenus savrent concluants en illustrant parfaitement les performances des commandes dans diverses conditions de fonctionnement. La conception dune plateforme de commande en temps rel pour

le quadrotor fut introduite et conue pour tre flexible et universelle pour toute implmentation de diffrents algorithmes de commande et de navigation. Dveloppe, la plateforme en question est la fois de conception modulaire et compose de trois parties ; en loccurrence matriel, logiciel et communication.

Lindentification du systme (quadrotor) a permis la mesure et lestimation de diffrents paramtres, outre, une station sol avec interface graphique est dveloppe pour la tlcommande et le monitoring. Par ailleurs, une unit de communication bidirectionnelle wifi est conue pour relier le quadrotor la station sol. Ainsi la plateforme dveloppe est valide par des tests de simulations et dexprimentation.

Mots Cls: Estimation, retour de sortie, control optimal, commande H_∞, hlicoptre, CE150, TRMS, UAV, rseau de modles locaux, stabilisation robuste, logique flou Type 2, plateforme de commande en temps-rel.

ملخص

تقدم هذه الأطروحة مساهمة في تطوير إستراتجية إنشاء تحكمات قوية للأنظمة اللاخطية متعددة المداخل والمخارج و الغير مؤكدة. في هذا المنظور تم إدراج مقاربات التحكم المعتمدة على نموذج عن طريق التقنية (H_2, H_∞) من ناحية، و من ناحية أخرى طريقة تحكم ذكية أقترحت في حالة غياب النموذج.

في هذا البحث تم التطرق إلى نمذجة الأنظمة CE-150 و TRMS، و ذلك بالنظر لأهميتها في اختبار قوانين التحكمات القوية المنشئة.

في البداية، تم اعتماد قانون تحكم جواري أمثل مرفق بنظام تقدير لحل مشكلة تتبع المسار و/أو التنظيم متعدد المداخل و المخارج، ثنائي المراوح (TRMS)، و يتم تطبيق هذه التقنية من خلال النموذج الخطي للجهاز حول نقاط توازنه.

ثم بعد ذلك، نظرا لأن مجال عمل المروحية CE-150 واسع و متعدد بالإضافة إلى الاضطرابات الخارجية، نقترح تحكم H_∞عن طريق شبكة النماذج المحلية كبديل ثاني، لتحقيق استقرار المروحية. الإستراتيجية المقترحة تضمن تطويرات حديثة ذات نتائج واعدة في تحقيق استقرار قوي مع وجود إرتيابات ليست لها بنية محددة.

بعد استخراج النموذج الخطي للنظام حول العديد من نقاط التشغيل، تم تصميم تحكمات H_∞حساسية مختلطة، قبل أن يتم دمجها في الشبكة من أجل ضمان انتقال سلس. بنية التحكم المقترحة تضمن المتانة، وفصل ديناميكيات النظام مع ضمان الأداء الجيد.

كبديل ثاني لما سبق، نقترح طريقة أخرى تعتمد على التحكم الغامض صنف 2 لحل مشكلة السيطرة على TRMS، و ذلك بسبب الفرق الموجود بين طرق التحكم المرتكزة على نموذج و الغير مرتكزة عليه، بالإضافة إلى بساطته وكفاءته. القوة الرئيسية لخوارزمية التحكم المقترحة تكمن في صلابتها فيما يتعلق بارتيابات المعاملات وضجيج القياسات.

يتم التحقق من صحة مقاربات التحكم المقترحة من خلال سلسلة من عمليات المحاكاة تظهر بوضوح فعالية طرق التحكم المقترحة، لأن النتائج المحصلة توضح تماما الأداء الجيد حتى في ظروف التشغيل المختلفة.

وقدم تصميم منصة للتحكم في الوقت الحقيقي لطائرة عمودية رباعية المراوح بدون طيار، مصممة لتكون مرنة ومتعددة الاستعمالات لتنفيذ مختلفة خوارزميات التحكم والملاحة، المنصة المعنية ذات تصميم وحدوي وتتكون من ثلاثة أجزاء: وهي المعدات والبرمجيات والاتصالات.

يسمح نظام تحديد الهوية (لطائرة عمودية رباعية المراوح) بقياس وتقدير مختلف المعاملات، وعلاوة على ذلك تم تصميم محطة أرضية ذات واجهة مستخدم رسومية للتحكم عن بعد والرصد.

تم تصميم وحدة الاتصالات اللاسلكية في إتجاهين للربط بين الطائرة العمودية رباعية المراوح والمحطة الأرضية. وقد تم التحقق من جودة منصة التحكم وفعاليتها من خلال المحاكاة والاختبارات التجريبية.

الكلمات المفتاحية: تقدير، رجوع المخارج، تحكم الأمثل، تحكم H_∞، هليكوبتر، CE150، TMS، طائرة بدون طيار، شبكة نماذج محلية، استقرار قوي، منطق غامض صنف 2، منصة تحكم في وقت الحقيقي.

Acknowledgement

First of all, I have to thank God, and then I have to thank my supervisor Professor Abderrezak DEBILOU, and Professor Hichem CHAOUI, respectively, in Mohamed Khider Univerity-Biskra (ALGERIA) and Tennessee Technological University- Cookeville, Tennessee (USA) In reality, the thesis writing process has been a long journey for me that would not have been possible without the support of so many people, like Suruz Miah (Bradley University- USA), Ahmed CHERITI (UQ TR- CANADA) and Rabi BELKACEMI (TEN TECH University-USA), who introduced me to and acquainted me with the field of system control and provided me a precious guidance during the realization of my work.

I need, also, to thank Professor Ahmed Bouterfaia (Rector of Mohamed Khider Univerity-Biskra, and the ex Rector of Kasdi Merbah University - Ouargla) who helped me a great deal despite the administrative as well as the academic commitments I still do have; I have as well to thank Professor Mohammed Tahar HLILAT (Rector of the Kasdi Merbah University- Ouargla) Professor Mouard KORICHI, Professor Abdelhakim SENOUSSI, Dr. Mohammed Seghir HALIMI, Dr. Djelloul BOURAHLA, Dr.Hanane AMIRAT (Kasdi Merbah University-Ouargla) who supported me physically and morally either by their psychological assistance or intellectual contribution; I might have never been able to finish with my thesis without their reinforcement.

I have to deny the social, psychological, moral and even the physical endeavour of my parents and my wonderful Wife who have encouraged, coaxed and sometimes even goaded me into sticking with my project even though the chances seem slim that it become realizable. For that, and for being the best son and the best husband and most of the time a father that I could have ever want, thank you ALL.

Dedication

To my parents,
To my wife,
To my kids,
To my sisters, brothers
and to the one I love.

Table of Contents

List of Tables **xi**

List of Figures **xii**

1 Introduction **1**

1.1 Motivation 1

1.2 Contributions 2

1.3 The thesis Structure 4

Nomenclature **1**

2 Systems Modelizations **6**

2.1 Introduction 6

2.2 CE-150 Helicopter Nonlinear Model Description 6

2.2.1 CE-150 State-Space Model and Linearization 11

2.2.2 CE-150 Model simulation 14

2.3 Two-DOF Helicopter TRMS (33-949) Description 18

2.3.1 TRMS (33-949) State-Space Model and Linearization 19

2.3.2 TRMS Model Simulation 26

2.4 Conclusion 26

3 Neighboring Optimal Control of Partially-Observed Twin Rotor Multi-Input Multi-Output System **30**

3.1 Introduction 30

3.2 Neighboring Optimal Control 32

3.3 Optimal State Estimation 35

3.4 Simulation Results 38

3.5 Conclusion 41

4 Local Model Network **42**

4.1 Introduction . . . 42

4.2 Generalized H_∞ Control Problem . . . 44

4.3 Local Model Networks based H_∞ Control . . . 45

4.4 Simulation Results . . . 48

4.5 Conclusion . . . 50

5 Interval Type-2 Fuzzy Logic Control of a Twin-Rotor Multi-input Multi-output System **58**

5.1 Introduction . . . 58

5.2 Interval Type-2 FLSs . . . 60

5.2.1 Type-2 Fuzzification . . . 61

5.2.2 Type-2 Rule Base . . . 61

5.2.3 Type-2 Fuzzy Inference Engine . . . 61

5.2.4 Type Reduction . . . 62

5.2.5 Defuzzification . . . 62

5.3 Interval Type-2 Fuzzy Logic Control Strategy . . . 62

5.4 Results and Discussion . . . 64

5.5 Conclusion . . . 70

6 Design and Realization of a Real-Time Control Platform for Quadrotor Unmanned Aerial Vehicles **71**

6.1 Introduction . . . 71

6.2 Dynamics . . . 72

6.3 Real-Time Control Platform Design . . . 74

6.3.1 Hardware . . . 75

6.3.2 Communication . . . 77

6.3.3 Software . . . 77

6.4 System Identification . . . 78

6.5 Control Strategy . . . 78

6.6 Simulation and Experimental Results . . . 80

6.6.1 Setup . . . 80

6.6.2 Simulation Results . . . 82

6.6.3 Experimental results . . . 82

6.7 Conclusion . . . 83

7 Conclusion and future works **85**

7.1 Conclusion 85

7.2 future works 86

List of Tables

2.1 Physical parameters of the TRMS [44]. 22

5.1 Fuzzy rules for type-1 and type-2 FLCs. 64

6.1 Quadrotor's physical parameters. 80

List of Figures

2.1 Helicopter CE-150. 7
2.2 Two degrees of freedom, Helicopter CE-150. 7
2.3 Torque's acting on the helicopter body in the vertical planes. 8
2.4 Torques acting on the helicopter body in the horizontal planes. 9
2.5 Complete system dynamics, Helicopter CE-150. 12
2.6 CE-150 Open loop step response for reference $\psi^* = 1$ and $\varphi^* = 0$ 15
2.7 CE-150 Open loop step response for reference $\psi^* = 0$ and $\varphi^* = 1$ 16
2.8 CE-150 Open loop step response for reference $\psi^* = 1$ and $\varphi^* = 1$ 17
2.9 Feedback TRMS helicopter. 18
2.10 Non-linear simulink model of the TRMS. 20
2.11 TRMS Open loop step response for reference $\psi^* = 1$ and $\varphi^* = 0$ 27
2.12 TRMS Open loop step response for reference $\psi^* = 0$ and $\varphi^* = 1$ 28
2.13 TRMS Open loop step response for reference $\psi^* = 1$ and $\varphi^* = 1$ 29

3.1 Step response for reference $\psi^* = 0.5$ and $\varphi^* = 0.5$, neighboring optimal control 39
3.2 Time-varying step response for reference ψ^* and φ^*, neighboring optimal control 40

4.1 The two-port block diagram for H_∞ control. 44
4.2 Local model network control. 46
4.3 Switching. 47
4.4 A mixed sensitivity configuration. 47
4.5 control structure for H_∞ local model network. 49
4.6 Validity function and switching mechanism. 49
4.7 LMN, Unit step response for reference $\psi^* = 0,25$ and $\varphi^* = 0$ 51
4.8 LMN, Unit step response for reference $\psi^* = 0$ and $\varphi^* = 0,25$. 52

4.9 LMN, Unit step response for reference $\psi^* = 0,5$ and $\varphi^* = 0$. 53
4.10 LMN, Unit step response for reference $\psi^* = 0$ and $\varphi^* = 0,5$. 54
4.11 LMN, Unit step response for reference $\psi^* = 0,5$ and $\varphi^* = 0,5$. 55
4.12 LMN, Time change step response for ψ^* and φ^*. 56

5.1 Fuzzy logic control scheme. 63
5.2 Fuzzy membership functions: (a) type-1; and (b) type-2. 65
5.3 interval Type2 FLC, Step response for reference $\psi^* = 0.5$ rad and $\varphi^* = 0$ rad. 67
5.4 interval Type2 FLC, Step response for reference $\psi^* = 0$ rad and $\varphi^* = 0.5$ rad. 68
5.5 interval Type2 FLC, Step response for reference $\psi^* = 0.5$ rad and $\varphi^* = 0.5$ rad. 69

6.1 GAUI 330 X-S quad flyer. 74
6.2 Platform architecture. 75
6.3 Illustration of the ground station interface. 76
6.4 Trust factor experiment testbed. 78
6.5 Quadrotor platform's simulation. 81
6.6 Assembled structure. 82
6.7 Quadrotor platform's experiment. 83

Chapter 1

Introduction

1.1 Motivation

The objective of automatic control in general is to influence the behavior of a given physical plant so that the response becomes conform to some desired specification. The plants, in reality, are classified into different categories such as nonlinear or linear systems, constrained system or unconstrained systems and small or large scale systems. The treatment and analysis to design linear systems has been well developed, and it could be found in [75]. Yet, almost all the plants are, actually, nonlinear, multivariables, and subject to physical constraints. Therefore, the design linear systems requires different techniques and treatments to properly design and handle the nonlinear constrained systems.

Recently, researchers have divided control law design approaches for nonlinear systems into three categories. the first category is based on linearization of nonlinear systems [55]; it is possible, however, to use a linear approximation around a prescribed operating point for analysis and controller design. Despite the simplicity of control laws, there are many situations where non linearities cannot be neglected. Phenomena such as saturation, hysteresis, deadzone, dry friction, to mention just few examples, are a of common nonlinearities that often arise in practice because this control system stability and performance are not guaranteed for full operating range . The second category deals with nonlinear controllers design based on nonlinear systems dynamics. In such cases, a nonlinear model is needed to obtain a more accurate representation of the dynamics of the system. Yet, the more complex is nonlinear systems dynamics, the more arise the design approach difficulties [59]. These approaches take for granted a precise mathematical system model and tend to work theoretically in an appropriate way. However, their very performance degrades in the presence of varying operating conditions, structured and unstructured dynamical un-

certainties, and external disturbances. In real complex physical system, deriving a precise mathematical model might be a difficult task to undertake. Other factors might be unexpected, such as parameters variation and noise. Thus, the system's dynamics cannot be efficiently based on presumably accurate mathematical models. The third category consists of nonlinear controllers design based on intelligence methods which are free model based such as artificial neural networks (ANNs) and fuzzy logic systems (FLSs) [4, 41]. These techniques have been considered various applications as efficient tools capable of providing robust approximation for mathematically ill-defined systems that may be subjected to structured and unstructured uncertainties [62, 92]. The universal approximation theorem is the major force behind the increasing popularity of such methods as it underlines that they are theoretically capable of uniformly bringing any continuous real function and any degree of accuracy together. miscellaneous artificial neural network and fuzzy logic models have been suggested to resolve many complex problems which have led to a satisfactory performance [61, 90], providing an alternative to conventional control techniques. The constrained plant under full range of operational conditions usually requires meeting several sets of objectives. It is impossible to achieve all control objectives by a single controller. It thus calls for application of multiple local model networks (LMN) controllers each of them being best fit into specific operational conditions. It is then inevitable to switch between controllers during the plant operation.

The two degrees of freedom helicopter system is given as an example. The two typical control strategies H_2, and H_∞ minimization strategy are employed with local model network (LMN) that depends on the operational condition. The most suitable control strategy is selected to apply to the plant under the full range of operational conditions.

Finally type-2 fuzzy logic control with soft computing is also applied to the system in question to show the observed difference.

1.2 Contributions

Nonlinear dynamic systems are governed by complex dynamics and hence are inevitably subject to the ubiquitous presence of high, particularly unstructured, modeling nonlinearities. The presence of such nonlinearities significantly changes the dynamics of nonlinear systems [14]. So, modeling a system's dynamics based on presumably accurate mathematical models cannot be applied efficiently in this case. This raises the importance to consider alternative approaches for the control of this type of systems to keep up with their increasingly demanding design requirements.

The main contributions idea is to design robust control structures for complex non linear dynamic systems, principally, based on robust optimal (H_2/H_∞) approach. Then local model networks (LMN) for soft switching mechanism between H_∞ controllers are eventually achieved to get a Softly Switched (LMN-H_∞), that could be applied to full range states operating of nonlinear systems. Moreover, type-2 fuzzy logic control is developed for the control of 2-DOF helicopter system in the presence of dynamical modeling and parametric uncertainties of various magnitudes. The ultimate contribution is to design and realize a real-time control platform for autonomous quadrotor unmanned aerial vehicles (UAVs). The control framework is designed to be universal but, yet, flexible for the implementation of various control and navigation algorithms. The proposed design approach which favors versatility is modular, while the implemented quadrotor control platform is cost effective and could be used as a benchmark to demonstrate the effectiveness of a variety of controllers. To sum up, the salient contributions of the present research are:

1. The Neighboring Optimal Control of Partially-Observed Twin Rotor Multi-Input Multi-Output System has been designed to solve the trajectory tracking and the regulator problems.

2. A local model network based H_∞ control technique is proposed to solve the stabilization problem of CE-150 helicopters.

3. A powerful approach, based on the type-2 fuzzy logic controller, is proposed for attitude stabilization of two degrees of freedom helicopter (TRMS).

4. A real-time control platform for quadrotor UAVs is realized to be universal and flexible, and allows implementation of various control algorithms.

The papers that have been published and those which are in process and expected to be published are listed as follow:

- Kafi, M. R., Chaoui, H., Miah, S., Debilou, A. (2017). Local model networks based mixed-sensitivity H-infinity control of CE-150 helicopters. Control Theory and Technology, 2017, vol. 15, no 1, p. $34-44$. springer. (doi:$10.1007/s11768-017-5073-x$).

- M. R. Kafi, H. Chaoui, B. Hamane and A. Debilou, "Design and realization of a real-time control platform for quadrotor unmanned aerial vehicles," $20153rd$ International Conference on Control, Engineering Information Technology (CEIT), Tlemcen, Algeria, 2015, pp. $1-6$. (doi: $10.1109/CEIT.2015.7232995$).

- S. Miah, M. R. Kafi, H. Chaoui and In Soo Ahn, "Neighboring optimal control of partially-observed twin rotor multi-input multi-output system," 2016 IEEE 25th International Symposium on Industrial Electronics (ISIE), Santa Clara, CA, USA, 2016, pp. 393-398. (doi: 10.1109/ISIE.2016.7744922).

- Kafi, M. R., Chaoui, H., Miah, S., Debilou, A. "Interval Type-2 Fuzzy Logic Control of a Twin-Rotor Multi-input Multi-output System" submitted to International Journal of Control, Automation and Systems, Springer (under reviewing).

- H. Chaoui, S. Miah, M. R. Kafi and B. Hamane, "Neural network balance control of hopping robots in flight phase under unknown dynamics," 2015 3rd International Conference on Control, Engineering Information Technology (CEIT), Tlemcen, 2015, pp. 1-5. (doi: 10.1109/CEIT.2015.7232996).

1.3 The thesis Structure

This thesis is divided into five chapters with a general introduction and a general conclusion.

Chapter two is entitled Systems Modelizations. It is mainly devoted to the presentation of systems operating under wide range of operational conditions for control purpose. This chapter deals with the physical modeling of the two 2-DOF multivariable nonlinear systems (CE-150 helicopter of Humusoft and TRMS 33-949 helicopter from Feedback Instruments) is detailed (studied), and the mathematical model which is deduced.

Chapter three, which is entitled Neighboring Optimal Control of Partially-Observed Twin Rotor Multi-Input Multi-Output System, emphasizes the proposed neighboring optimal control law coupled with a state estimation technique to solve the trajectory tracking and the regulator problems of a TRMS model. The latter is linearized around an operating point. Since the internal dynamical states (except the azimuth and elevation angles) are not measurable, an optimal filter to estimate them is designed. The proposed control law takes into account both process and measurement uncertainties of a TRMS model. Simulation results are presented to demonstrate the performance of the proposed control law.

Chapter four is entitled Local Model Network. It investigates the feasibility of local model network based H_∞ control technique to solve the stabilization problem of CE-150 helicopters. Considering the fact that the system could be linearized around a set of operating points, an H_∞ controller is designed for the linearized system. The mixed sensitivity

problem is considered by means of its transformation into a standard H_∞ problem and then solved for a stabilizing gain that satisfies the desired criteria. The obtained controllers are integrated within a network to guaranty full range operational conditions. Finally, Simulation results are presented.

Chapter five deals with Interval Type-2 Fuzzy Logic Control of a Twin-Rotor Multi-input Multi-output System. Actually, the proposed interval type 2 fuzzy approach is based on triangular membership functions and operator experience. Two controllers are designed to control the position of the yaw and the pitch angles of systems, and then validated through a set of simulation results. The latter illustrate the effectiveness of the proposed control scheme for larger magnitudes of uncertainties with severe nonlinearities.

Chapter six is entitled Design and Realization of a Real-Time Control Platform for Quadrotor Unmanned Aerial Vehicles. The realized control framework consists of three major parts: hardware, software and communication. It is mainly conceived to be universal and flexible, as it is adequate for the implementation of various control and navigation algorithms.

The general conclusion summarizes the overall proposed approaches and the obtained results, as it unveils the suggestions for further researches and future trends.

Chapter 2

Systems Modelizations

2.1 Introduction

Modeling nonlinear systems is an interesting challenging problem [33, 76, 82, 1, 79, 54]. In addition, most control techniques are model based. Hence, the first step in the control design process is to develop appropriate mathematical models of the system derived either from physical laws or experimental data. It is obvious that some information about controlled plant is required to allow the design of controllers with satisfactory performance. A plant model could be also used to investigate properties and behavior of the modeled plant without a risk of damage in violating technological constraints of the real plant. In this chapter, the models used in this research are introduced. The detailed mechanical and electrical components are presented, and a valid state space model is derived. In this research, the considered nonlinear multivariable complex systems are both Humsoft CE-150 and feedback instrument TRMS 33-949 helicopters. These systems are chosen because they include almost all the problems relative to the nonlinear systems, which are multivariable, instability in open loop, strong cross-coupling, to mention just a few.

2.2 CE-150 Helicopter Nonlinear Model Description

With reference to [3], a laboratory helicopter whose body is connected to a fixed base is considered. Hence, two degrees of freedom of the helicopter are enabled where the elevation angle ψ (rotation around horizontal axis) and the azimuth angle φ (rotation vertical axis) describe the motion of the helicopter body. The parameters describing the helicopter motion is depicted in Fig. 2.3. The body is actuated by two DC motors which drive the

Figure 2.1: Helicopter CE-150.

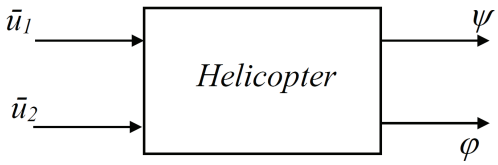

Figure 2.2: Two degrees of freedom, Helicopter CE-150.

main and tail propellers. The rotor axes acting on these propellers are orthogonal to each other.

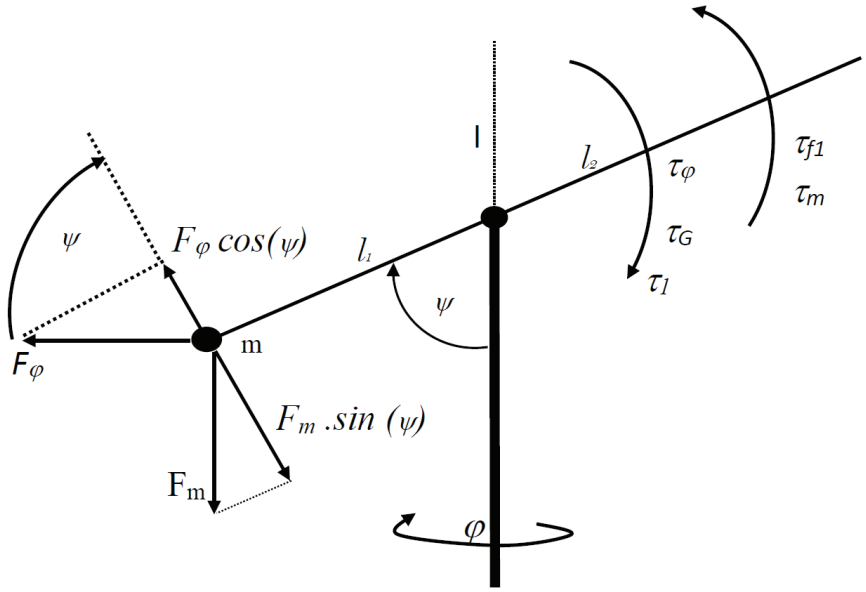

Figure 2.3: Torque's acting on the helicopter body in the vertical planes.

Suppose that $\bar{u}_1(t)$ and $\bar{u}_2(t)$ represent the voltages driving the main and tail motors, respectively, at time $t \geq 0$. As such, the helicopter model can be treated as a two-input two-output nonlinear multi-variable system (Fig.2.2). Considering the forces acting on the vertical helicopter body, the dynamics of the elevation angle is given by:

$$I\ddot{\psi} = \tau_1 + \tau_{\dot{\varphi}} - \tau_{f_1} - \tau_m + \tau_G, \tag{2.1}$$

Satisfying the following relations:

$$\tau_m = F_m l_1 \sin\psi = mgl_1 \sin\psi = \tau_g sin\psi \tag{2.2}$$

$$\tau_{\dot{\varphi}} = ml_1\dot{\varphi}^2 \sin\psi cos\psi = \frac{1}{2}ml_1\dot{\varphi}^2 \sin 2\psi \tag{2.3}$$

$$\tau_1 = k_{\omega 1}\omega_1^2 \tag{2.4}$$

$$\tau_{f1} = C_\psi \text{sign}\dot{\psi} + B_\psi\dot{\psi} \tag{2.5}$$

$$\tau_G = K_G\dot{\varphi}\omega_1 \cos\psi, \text{ for } \dot{\varphi} \ll \omega_1, \tag{2.6}$$

Where

I moment of inertia of the helicopter body around horizontal axis
$\tau_{\dot{\varphi}}$ centrifugal torque
τ_m gravitational torque
τ_G gyroscopic torque
τ_{f1} friction torque (coulomb and viscous)
τ_1 elevation driving torque (main propeller influence)
τ_{ω_1} main propeller angular velocity
m mass
g gravity
l_1 distance from z-axis to main rotor
k_{ω_1} main rotor constant
k_G gyroscopic coefficient
B_ψ viscous friction coefficient (around y-axis)
C_ψ Coulomb friction coefficient (around y-axis)

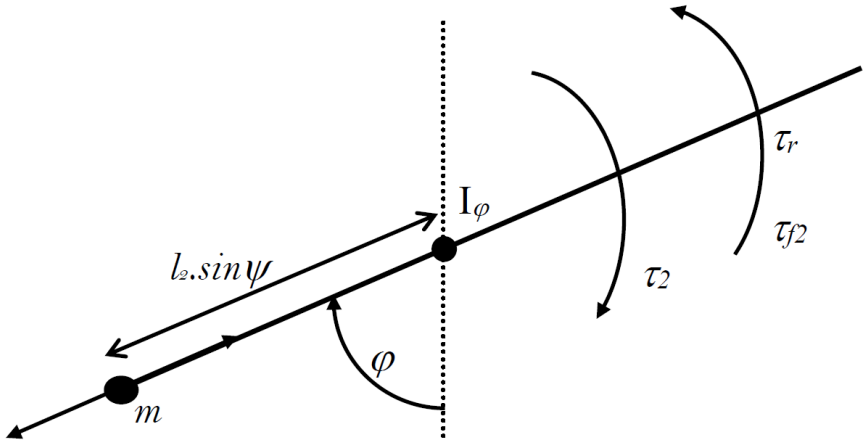

Figure 2.4: Torques acting on the helicopter body in the horizontal planes.

Similar to the elevation dynamics, we consider the forces in the horizontal plain (see Fig. 2.4) taking into account the forces acting on the helicopter body in the direction of the azimuth angle φ. The dynamics of φ is given by:

$$I_\psi \ddot{\varphi} = \tau_2 - \tau_{f_2} - \tau_r, \tag{2.7}$$

Satisfying the following relations:

$$I_\psi = I \sin\psi \tag{2.8}$$

$$\tau_2 = k_{\omega_2} l_2 \sin\psi \omega_2^2 \tag{2.9}$$

$$\tau_{f_2} = C_\varphi \text{sign}\dot{\varphi} + B_\varphi \dot{\varphi}, \tag{2.10}$$

Where

I_ψ	moment of inertia around vertical axis,
τ_2	stabilizing motor driving torque,
τ_{f_2}	friction torque (coulomb and viscous),
τ_r	main motor reaction torque,
l_2	distance from z-axis to stabilizing tail rotor
k_{ω_2}	constant for the tail rotor,
ω_2	angular velocity of the tail rotors,
B_φ	viscous friction coefficient around z-axis, and
C_φ	Coulomb friction coefficient around z-axis.

Similar to the body dynamics in elevation, no connection between the speed of the side propeller and friction torque around vertical rotational axis has been introduced into the derivation of an analytical model of the helicopter dynamics [43]. The torque τ_r is significant and arises from the torque generated by the main motor acting on rotating body. Note that the propulsion system of the CE 150 helicopter model are mainly driven by two independent DC motors. Under certain assumptions on the DC motor dynamics as stated in [3], the DC motor and propeller dynamics are given by the following equations:

$$i_j = \frac{1}{R_j}(\bar{u}_j - k_{b_j}\omega_j) \tag{2.11a}$$

$$\tau_j = k_{ij} i_j \tag{2.11b}$$

$$\tau_{c_j} = C_j \text{sign}(\omega_j) \tag{2.11c}$$

$$\tau_{p_j} = B_{p_j}\omega_j + D_{p_j}\omega_j^2 \tag{2.11d}$$

$$I_j \dot{\omega}_j = \tau_j - \tau_{c_j} - B_j\omega_j - \tau_{p_j}, \tag{2.11e}$$

Where $j \in \{1, 2\}$ represents the motor index ($j = 1$ for main motor and $j = 2$ for tail motor),

$\bar{u}_j$	control input voltage,
i_j	armature current,
ω_j	rotor angular velocity,
τ_j	motor torque,
τ_{c_j}	coulomb friction load torque,
τ_{p_j}	air resistance load torque,
R_j	armature resistance,
k_{ij}	torque constant,
k_{bj}	back-emf constant,
I_j	rotor and propeller moment of inertia,
B_j	viscous friction coefficient,
C_j	coulomb friction coefficient,
B_{p_j}	air resistance coefficient (laminar flow),
$D_p \in \mathbb{R}$	air resistance coefficient (turbulent flow).

The input variables are the electrical voltages $\bar{u}_1$ and $\bar{u}_2$, and the output variables (measured by sensors) are ψ and φ angles. The objective of control is to synthesize control $\bar{\mathbf{u}} = [\bar{u}_1 \;\; \bar{u}_2]^T$ to bring the angles ψ and φ to the desired angles ψ^* and φ^*. Figure 2.5 shows the block diagram of a complete CE-150 model dynamic, achieved with certain neglecting parameters of helicopter model (without loss of generality) and using a linearization of some parts of the system. The description of parameters, such as T_1, T_2 (time constants of main and tail motor, respectively), a_i, b_i ($i = 1, 2, 3$, square functions' parameters), I, B_ψ, τ_G, K_G, I_ψ, and B_φ, are detailed in [3] and are omitted here for conciseness purpose.

2.2.1 CE-150 State-Space Model and Linearization

In this section, the nonlinear model of CE-150, which is described by (2.1)–(2.11), will be first analyzed by determining the system's equilibrium points, and then linearizing around them.

By denoting the state vector $\mathbf{x} \in \mathbb{R}^8, \mathbf{x} \equiv [x_1, x_2, ..., x_8]^T \equiv [\psi, \dot{\psi}, \varphi, \dot{\varphi}, \omega_1, \dot{\omega}_1, \omega_2, \dot{\omega}_2]^T$,

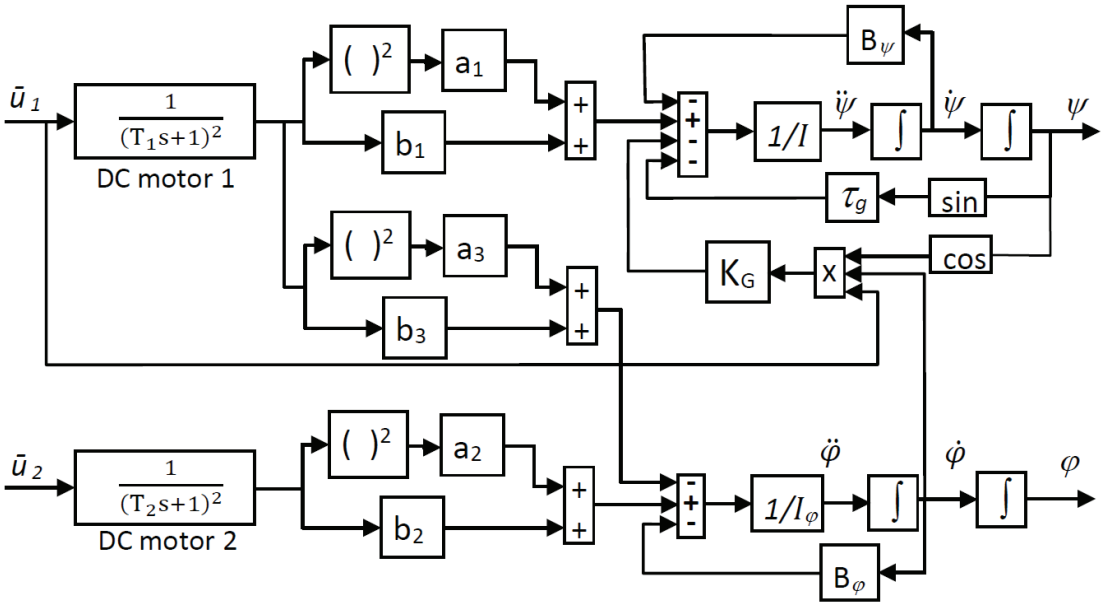

Figure 2.5: Complete system dynamics, Helicopter CE-150.

the models described by (2.1)–(2.11) can be written as a state-space model given by:

$$\dot{x}_1 = x_2 \tag{2.12a}$$

$$\dot{x}_2 = \frac{1}{I} b_1 x_5 + \frac{1}{I} a_1 x_5^2 - \frac{1}{I} \tau_g \sin x_1 - \frac{1}{I} B_\psi x_2 - \frac{1}{I} K_G x_4 \cos x_1 . \bar{u}_1 \tag{2.12b}$$

$$\dot{x}_3 = x_4 \tag{2.12c}$$

$$\dot{x}_4 = -\frac{1}{I_\varphi} b_3 x_5 - \frac{1}{I_\varphi} a_3 x_5^2 + \frac{1}{I_\varphi} b_2 x_7 + \frac{1}{I_\varphi} a_2 x_7^2 - \frac{1}{I_\varphi} B_\varphi x_4 \tag{2.12d}$$

$$\dot{x}_5 = x_6 \tag{2.12e}$$

$$\dot{x}_6 = -\frac{1}{T_1^2} x_5 - \frac{2}{T_1} x_6 + \frac{1}{T_1^2} \bar{u}_1 \tag{2.12f}$$

$$\dot{x}_7 = x_8 \tag{2.12g}$$

$$\dot{x}_8 = -\frac{1}{T_2^2} x_7 - \frac{2}{T_2} x_8 + \frac{1}{T_2^2} \bar{u}_2 . \tag{2.12h}$$

The compact form of (2.12a)–(2.12h) can be expressed as:

$$\dot{\mathbf{x}} = \mathbf{f}(\mathbf{x}, \bar{\mathbf{u}}), \tag{2.13}$$

where $\bar{\mathbf{u}} \in \mathbb{R}^2$ and $\bar{\mathbf{u}} \equiv [\bar{u}_1, \bar{u}_2]^T$ is the control input vector and $\mathbf{f} : \mathbb{R}^8 \times \mathbb{R}^2 \to \mathbb{R}^8$. Note that all the state variables, x_1 to x_8 and inputs $\bar{u}_1$ and $\bar{u}_2$ are functions of time (t), which

is dropped here for clarity.

By setting $\mathbf{f}(\mathbf{x}, \bar{\mathbf{u}}) = 0$ in (2.13), the equilibrium points are obtained by solving the following equations:

$$b_1 x_5 + a_1 x_5^2 - \tau_g \sin x_1 = 0 \tag{2.14a}$$
$$-b_3 x_5 - a_3 x_5^2 + b_2 x_7 + a_2 x_7^2 = 0 \tag{2.14b}$$
$$\bar{u}_1 - x_5 = 0 \tag{2.14c}$$
$$\bar{u}_2 - x_7 = 0, \tag{2.14d}$$

with $x_2 = x_4 = x_6 = x_8 = 0$ and $x_3 = \alpha \in \mathbb{R}$ is simply a constant. Clearly, $\bar{u}_1 = x_5$ and $\bar{u}_2 = x_7$. The solution for x_5 and x_7 can be obtained from (2.14a) and (2.14b) assuming the fact that $x_1 \equiv \psi$ (elevation angle) takes the value from $[0, \pi]$. By doing so, we get:

$$x_5 = \frac{-b_1 \pm \sqrt{b_1^2 + 4a_1 \tau_g \sin x_1}}{2a_1}$$
$$x_7 = \frac{-b_2 \pm \sqrt{b_2^2 + 4a_2(b_3 x_5 + a_3 x_5^2)}}{2a_2}.$$

For $x_1 = 0,\ 5\pi/16$, and $9\pi/16$, the three different equilibrium points are:

$$(\mathbf{x}_*^{[1]}, \bar{\mathbf{u}}_*^{[1]}) = ([0, 0, \alpha, 0, 0, 0, 0, 0]^T, [0, 0]^T),$$
$$(\mathbf{x}_*^{[2]}, \bar{\mathbf{u}}_*^{[2]}) = ([\frac{5\pi}{16}, 0, \alpha, 0, 0.49, 0, 0.39, 0]^T, [0.49, 0.39]^T),$$
$$\text{and}$$
$$(\mathbf{x}_*^{[3]}, \bar{\mathbf{u}}_*^{[3]}) = ([\frac{9\pi}{16}, 0, \alpha, 0, 0.55, 0, 0.44, 0]^T, [0.55, 0.44]^T),$$

for $a_1 = 0.1165$, $a_2 = 0.268$, $a_3 = 0.1959$, $b_1 = 0.062$, $b_2 = 0.0408$, $b_3 = 0.0202$, $T_1 = 0.1$, $T_2 = 0.25$, $I = 184$, $I_\varphi = 494.3$, $B_\psi = 0.08$, $B_\varphi = 0.04$, $K_G = 0.3185$, and $\tau_g = 0.071$.

Given an equilibrium point $(\mathbf{x}_*, \bar{\mathbf{u}}_*)$ and assuming the fact that the CE-150 model operates around the equilibrium point, we linearize the nonlinear model (2.13) using the

first-order Taylor's series (neglecting the higher-order terms) as:

$$\Delta\dot{\mathbf{x}} = \mathbf{A}\Delta\mathbf{x} + \mathbf{B}\Delta\bar{\mathbf{u}}, \tag{2.16}$$

where

$$\mathbf{A} = \frac{\partial f}{\partial \mathbf{x}}\Big|_{(\mathbf{x}_*, \bar{\mathbf{u}}_*)} = \begin{bmatrix} \frac{\partial f_1}{\partial x_1} & \cdots & \frac{\partial f_1}{\partial x_8} \\ \vdots & & \vdots \\ \frac{\partial f_8}{\partial x_1} & \cdots & \frac{\partial f_8}{\partial x_8} \end{bmatrix}_{(\mathbf{x}_*, \bar{\mathbf{u}}_*)} \quad \text{and}$$

$$\mathbf{B} = \frac{\partial f}{\partial \bar{u}}\Big|_{(\mathbf{x}_*, \bar{\mathbf{u}}_*)} = \begin{bmatrix} \frac{\partial f_1}{\partial \bar{u}_1} & \frac{\partial f_1}{\partial \bar{u}_2} \\ \vdots & \vdots \\ \frac{\partial f_8}{\partial \bar{u}_1} & \frac{\partial f_8}{\partial \bar{u}_2} \end{bmatrix}_{(\mathbf{x}_*, \bar{\mathbf{u}}_*)}$$

2.2.2 CE-150 Model simulation

It is helpful to look at the way the open-loop system behaves before designing a controller for a plant.

To show dynamic of CE-150 system in open loop case. Responses for Step inputs $(\psi, \varphi) = (1, 0)$, $(\psi, \varphi) = (0, 1)$ and $(\psi, \varphi) = (1, 1)$ are considered, the simulation results in Fig. 2.6, Fig. 2.7 and Fig. 2.8 respectively show the instability of azimuth subsystem, with remarkable offset of elevations subsystem.

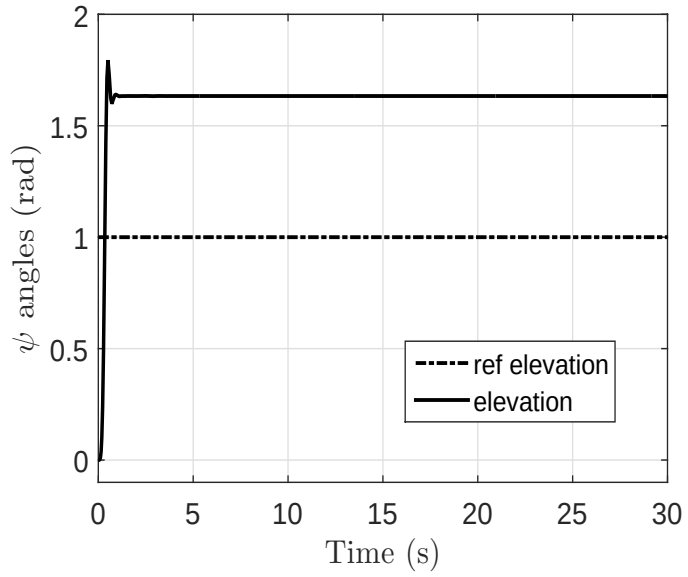

(a)

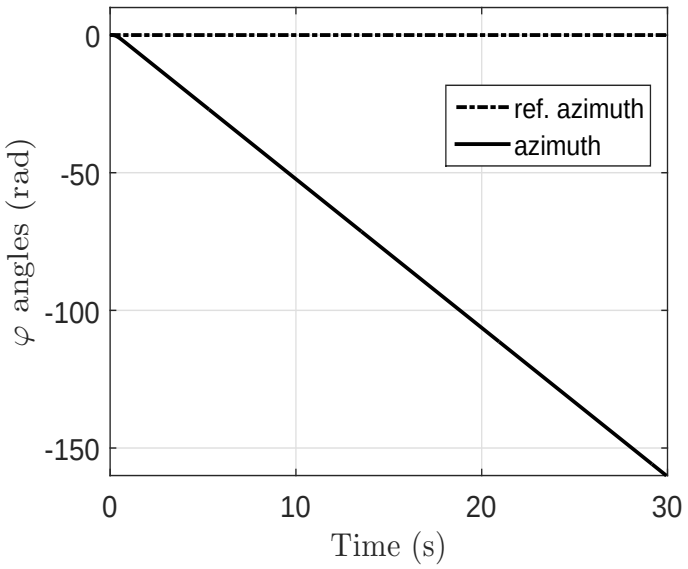

(b)

Figure 2.6: CE-150 Open loop step response for reference $\psi^* = 1$ and $\varphi^* = 0$: (a) Elevation response; and (b) azimuth response.

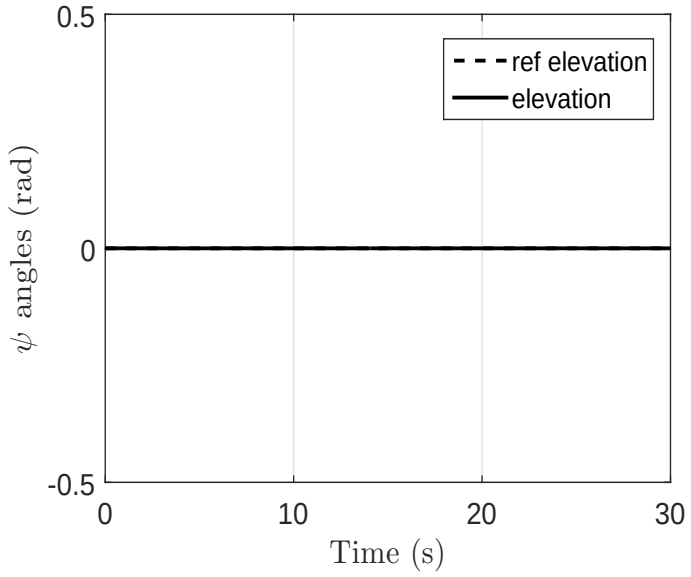

(a)

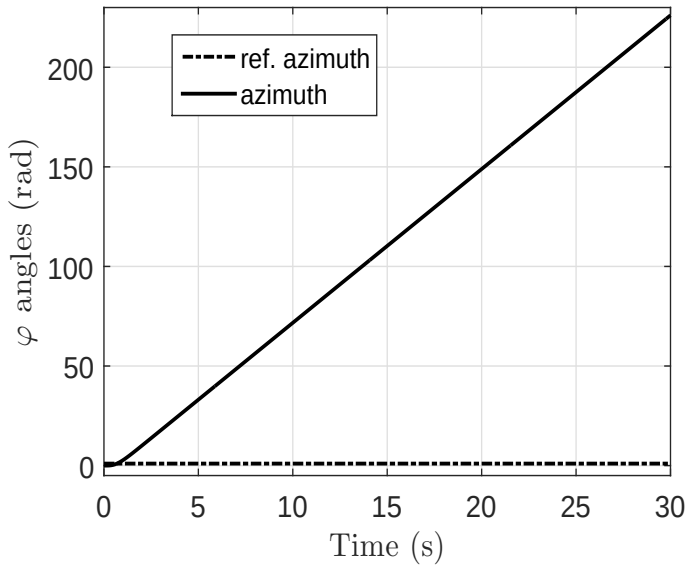

(b)

Figure 2.7: CE-150 Open loop step response for reference $\psi^* = 0$ and $\varphi^* = 1$: (a) Elevation response; and (b) azimuth response.

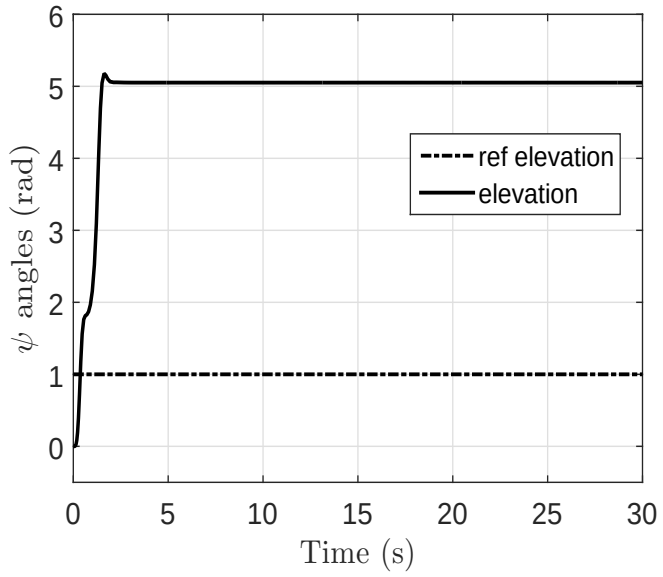

(a)

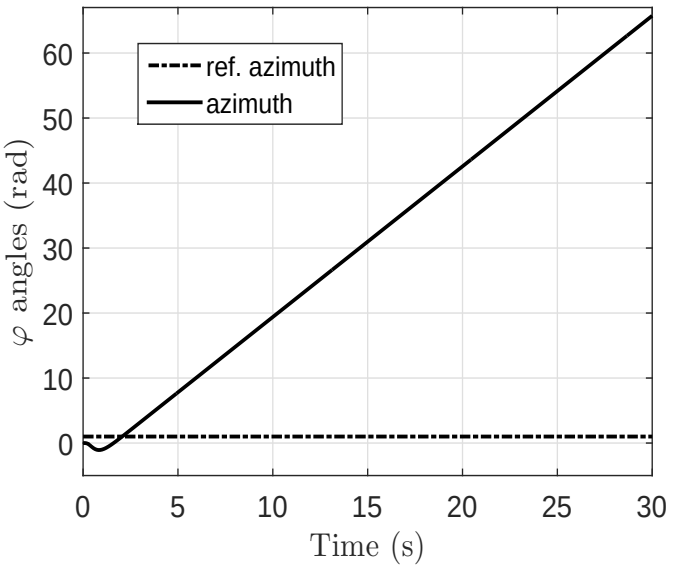

(b)

Figure 2.8: CE-150 Open loop step response for reference $\psi^* = 1$ and $\varphi^* = 1$: (a) Elevation response; and (b) azimuth response.

2.3 Two-DOF Helicopter TRMS (33-949) Description

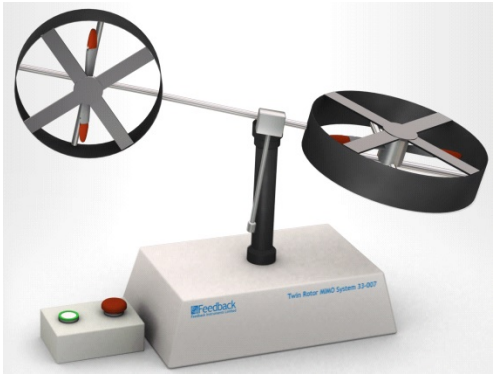

Figure 2.9: Feedback TRMS helicopter.

The electro-mechanical structure of a twin robot multi-input multi-output system is shown in Figure 2.9. An orthogonal connection of two rotors (main and tail rotors) is established by a beam pivoted on a fixed base where each rotor is mounted at the end of the beam. Hence, the beam can rotate in both vertical and horizontal planes. As opposed to a conventional helicopter model where its aerodynamic force is controlled by changing the angle of attack of the blades, the aerodynamic force of a TRMS is controlled by speed of two DC motors mounted as main and tail rotors. The aerodynamic force at the main rotor allows the beam to rotate vertically (elevation angle) while that at the tail rotor makes the beam to rotate horizontally (azimuth angle). Therefore, the manipulated variables (control) are the voltages applied to the DC motors. Following [44], [77], the momentum equations for the main and tail rotors of a TRMS model are given by:

$$I_1\ddot{\Psi} = M_1 - M_{FG} - M_{B\Psi} - M_G \tag{2.17a}$$

$$I_2\ddot{\varphi} = M_2 - M_{B\varphi} - M_R, \tag{2.17b}$$

where M_1 and M_2 are the total momentum of the main and tail rotors, respectively, $M_{B\Psi}$ is the momentum of the friction forces, M_{FG} is the gravity momentum, and M_R is the cross-reaction momentum. Furthermore,

$$M_1 = a_1\tau_1^2 + b_1\tau_1 \tag{2.18a}$$
$$M_{FG} = M_g sin\Psi \tag{2.18b}$$
$$M_{B\Psi} = B_{1\Psi}\dot{\Psi} + B_{2\Psi}sign(\dot{\Psi}) \tag{2.18c}$$
$$M_G = K_{gy}M_1\dot{\Psi}cos\Psi \tag{2.18d}$$

$$M_2 = a_2\tau_2^2 + b_2\tau_2 \tag{2.19a}$$
$$M_{B\varphi} = B_{1\varphi}\dot{\varphi} + B_{2\varphi}sign(\dot{\varphi}) \tag{2.19b}$$
$$M_R = \frac{k_c(T_0 s + 1)}{T_p s + 1}\tau_1, \tag{2.19c}$$

where τ_1 and τ_2 are the momentum produced by main and tail motors, respectively. The input voltages of the main and tail motors are respectively denoted by u_1 and u_2 which are related to the main and tail motors momentum as:

$$\tau_1 = \frac{k_1 u_1}{T_{11}s + T_{10}} \tag{2.20a}$$
$$\tau_2 = \frac{k_2 u_2}{T_{21}s + T_{20}}, \tag{2.20b}$$

with s being the Laplace variable. The nonlinear state-space representation of the TRMS model (2.17)-(2.20), is shown in Figure 2.10 (which is also provided by the manufacturer). As noted in [44], the parameters of this system (see Table 2.1) have been chosen more or less experimentally. It is verified that when the physical system is at rest both the pitch and yaw angle sensors reading are zero. Therefore, in this project, the origin of physical system is taken as an operating point.

2.3.1 TRMS (33-949) State-Space Model and Linearization

In this section, the mathematical approximation of original nonlinear model of the 2-DOF helicopter (TRMS) [44] is developed by using Newtons's second law, from which the state apace representation is obtained. Be denoting the state vector $\mathbf{x} \in \mathbb{R}^6$ and $\mathbf{x} \equiv [x_1, x_2, ..., x_6]^T \equiv [\psi, \varphi, \dot{\psi}, \dot{\varphi}, i_h, i_v]^T$, the models described by [44, 87, 48] can be

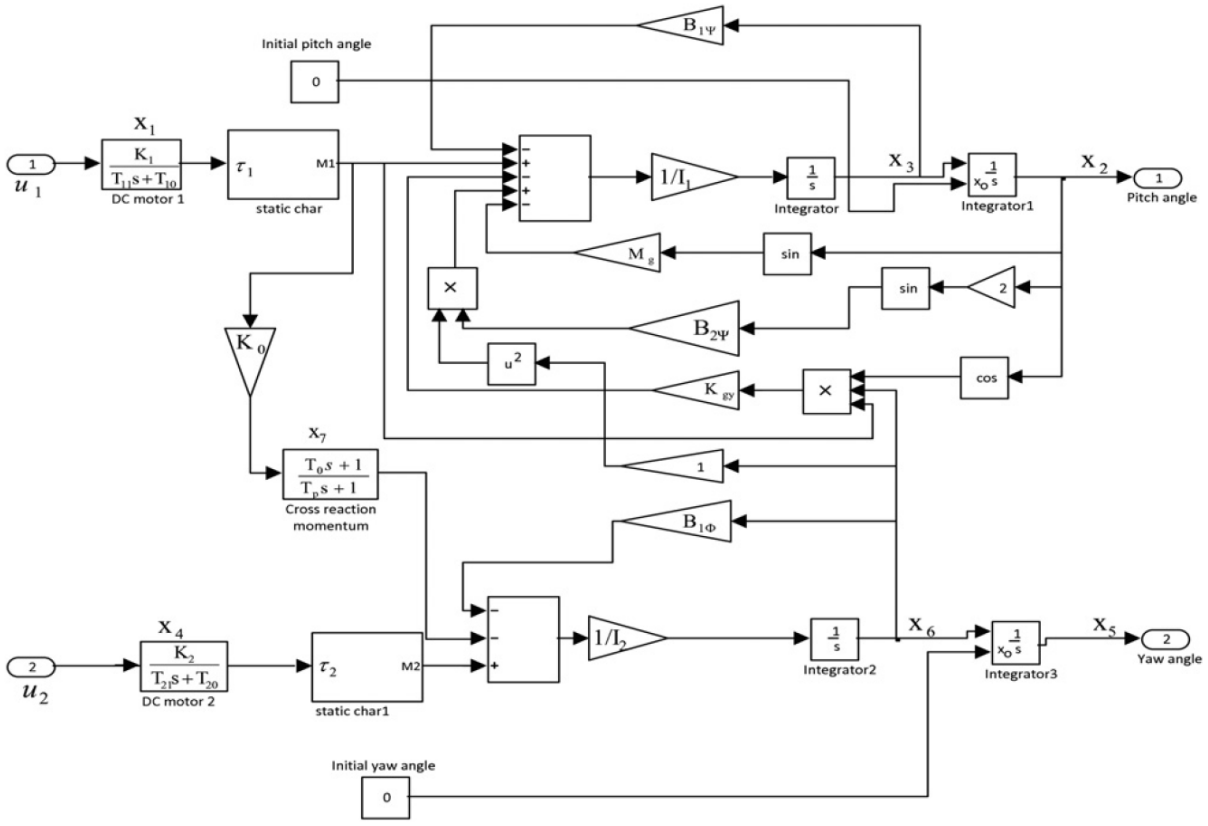

Figure 2.10: Non-linear simulink model of the TRMS.

written as a state-space model given by:

$$\dot{x}_1 = x_3 \tag{2.21a}$$

$$\dot{x}_2 = x_4 \tag{2.21b}$$

$$\dot{x}_3 = \frac{1}{j_h}[l_t S_f F_h(\omega_t) cos x_2 - k_h x_3 - x_3 x_4 (D-E) sin 2x_2 - j_{mr}\omega_m(x_6) x_4 sin x_2] \tag{2.21c}$$
$$+ \frac{j_{mr}}{T_{mr}}(u_v - x_6)\frac{d\omega_m(x_6)}{dx_6} cos x_2$$

$$\dot{x}_4 = 9.1[l_m S_f F_v(\omega_m) - g(0.0099 cos x_2 + 0.0168 sin x_2) - k_v x_4] \tag{2.21d}$$
$$+ 9.1[-0.0252 x_3^2 sin 2x_2 r + \frac{j_{tr}}{T_{tr}}(u_h - x_5)\frac{d\omega_t(x_5)}{dx_5}$$

$$\dot{x}_5 = \frac{1}{T_{tr}}(u_h - x_5) \tag{2.21e}$$

$$\dot{x}_6 = \frac{1}{T_{mr}}(u_v - x_6) \tag{2.21f}$$

The compact form of (2.21a)–(2.21f) can be expressed as:

$$\dot{X} = f(X, \bar{\mathbf{u}}), \tag{2.22}$$

where $\bar{\mathbf{u}} \in \mathbb{R}^2$ and $\bar{\mathbf{u}} \equiv [u_v, u_h]^T$ is the control input vector, and $\mathbf{f} : \mathbb{R}^6 \times \mathbb{R}^2 \to \mathbb{R}^6$. Note that all the state variables, x_1 to x_6 and inputs $\bar{u}_v$ and $\bar{u}_h$ are functions of time (t), which is dropped here for clarity.

With u_v/u_h being the input voltage of the DC motor for the main/tail propeller, the armature current i_v/i_h can be obtained by solving the following differential equations [44]

$$\frac{di_v}{d_t} = \frac{1}{T_{mr}}(u_v - i_v) \tag{2.23a}$$

$$\frac{di_h}{d_t} = \frac{1}{T_{tr}}(u_h - i_h), \tag{2.23b}$$

Where, l_m/l_t is the main/tail length of the beam, j_{mr}/j_{tr} is the moment of inertia for the main/tail propeller subsystem, T_{mr}/T_{tr} is the time constant of the main/tail motor-propeller system and $\omega_m\omega_t$ is the rotational speed of the main/tail rotor DC motor. Moreover, k_v/k_h is the friction constant of the main/tail propeller subsystem and Sf is the balanced scale and u_v/u_h is the control input for the main/tail DC motor. The propulsive force to move the joined beam in the vertical/horizontal direction is denoted by F_v/F_h. The propulsive force is approximately described by a non-linear function of the angular velocity ω_m/ω_t. Gravitational acceleration is symbolized as g and D, E, G are constants.

Table 2.1: Physical parameters of the TRMS [44].

Symbol	Definition	Value
l_m	length of the main part of the beam	0.236 m
l_t	length of the tail part of the beam	0.25 m
K_v	friction coefficient of the vertical axis	0.0095
K_h	friction coefficient of the horizontal axis	0.0054
j_{mr}	moment of inertia of the DC motor main	1.6543x10^{-5}kg m^2
j_{tr}	moment of inertia of the DC motor tail propeller	2.65x10^{-5}kg m^2
T_{mr}	time constant of the main rotor	1.432 s
T_{tr}	time constant of the tail rotor	0.3842 s
D	mechanical related constant	1.6065x10^{-3}kg m^2
E	mechanical related constant	4.90092x10^{-2}kg m^2
G	mechanical related constant	6.3306x10^{-3}kg m^2
S_f	balance scale	8.43318x10^{-4}
g	gravitational constant	9.81 m/s^2

Furthermore

$$j_h = Dsin^2x_2 + Ecos^2x_2 + G \tag{2.24a}$$

$$\omega_m(x_6) = 99.99x_6^6 + 599.73x_6^5 - 129.26x_6^4 - 1283.64x_6^3 + 63.45x_6^2 + 1283.41x_6 \tag{2.24b}$$

$$\omega_m(x_5) = 2020x_5^5 - 194.69x_5^4 - 4283.15x_5^3 + 262.27x_5^2 + 3768.83x_5 \tag{2.24c}$$

$$F_v(\omega_m) = -3.48x10^{-12}\omega_m^5 + 1.09x10^{-9}\omega_m^4 + 4.123x10^{-6}\omega_m^3 - 1.632x10^{-4}\omega_m^2 + 9.544x10^{-2}\omega_m \tag{2.24d}$$

$$F_h(\omega_t) = -3x10^{-14}\omega_m t5 - 1.595x10^{-11}\omega_t^4 + 2.511x10^{-7}\omega_t^3 - 1.808x10^{-4}\omega_t^2 + 8.01x10^{-2}\omega_t \tag{2.24e}$$

Table 2.1 lists the physical parameters of the TRMS and their values.

The non-linear state equation of the TRMS in (2.21)-(2.24) can be represented as:

$$\dot{X} = f(X, u_h, u_v), \quad Where\ X = [x_1, x_2, ..., x_6]^T$$

$$f(X, u_h, u_v) = [f_1(X, u_h, u_v), f_2(X, u_h, u_v), ..., f_6(X, u_h, u_v)]^T \tag{2.25}$$

In order to reduce the complexity of the position controller, the complex TRMS model is divided into an HS and a VS following the approach in [87, 89]. While designing the controller for the subsystem, a linear part is added to and the same is then subtracted from

the non-linear part for facilitating pseudo-separation whereas the overall system remains the same. The state equations are then written as:

$$\begin{aligned} \dot{x}_h &= \bar{A}_h x_h + \bar{B}_h u_h + \Delta F_h \\ \dot{x}_v &= \bar{A}_v x_v + \bar{B}_v u_v + \Delta F_v \end{aligned} \tag{2.26}$$

For the above horizontal and vertical subsystems, the states and parameters are defined as:

$$\begin{aligned} x_h &= [x_1, x_3, x_5]^T \\ \Delta F_h &= [0, \Delta f_h(x_h, x_v, u_v), 0]^T \\ x_v &= [x_2, x_4, x_6]^T \\ \Delta F_v &= [0, \Delta f_v(x_v, x_h, u_h), 0]^T \end{aligned}$$

Here

$$\bar{A}_h = \begin{bmatrix} a_{h11} & a_{h12} & a_{h13} \\ a_{h21} & a_{h22} & a_{h23} \\ a_{h31} & a_{h32} & a_{h33} \end{bmatrix} = \begin{bmatrix} \frac{\partial f_1}{\partial x_1} & \frac{\partial f_1}{\partial x_3} & \frac{\partial f_1}{\partial x_5} \\ \frac{\partial f_3}{\partial x_1} & \frac{\partial f_3}{\partial x_3} & \frac{\partial f_3}{\partial x_5} \\ \frac{\partial f_5}{\partial x_1} & \frac{\partial f_5}{\partial x_3} & \frac{\partial f_5}{\partial x_5} \end{bmatrix}_{X=0} = \begin{bmatrix} 0 & 1 & 0 \\ 0 & -\frac{k_h}{E+G} & \frac{301.88 l_t S_f}{E+G} \\ 0 & 0 & -T_{tr}^{-1} \end{bmatrix} \tag{2.27}$$

$$\bar{B}_h^T = \begin{bmatrix} b_{h11} & b_{h21} & b_{h31} \end{bmatrix} = \begin{bmatrix} \frac{\partial f_1}{\partial u_h} & \frac{\partial f_3}{\partial u_h} & \frac{\partial f_5}{\partial u_h} \end{bmatrix} = \begin{bmatrix} 0 & 0 & T_{tr}^{-1} \end{bmatrix} \tag{2.28}$$

$$\bar{B}_v^T = \begin{bmatrix} b_{v11} & b_{v21} & b_{v31} \end{bmatrix} = \begin{bmatrix} \frac{\partial f_2}{\partial u_v} & \frac{\partial f_4}{\partial u_v} & \frac{\partial f_6}{\partial u_v} \end{bmatrix} = \begin{bmatrix} 0 & 0 & T_{mr}^{-1} \end{bmatrix} \tag{2.29}$$

$$\begin{aligned} \bar{A}_h &= \begin{bmatrix} a_{v11} & a_{v12} & a_{v13} \\ a_{v21} & a_{v22} & a_{v23} \\ a_{v31} & a_{v32} & a_{v33} \end{bmatrix} = \begin{bmatrix} \frac{\partial f_2}{\partial x_2} & \frac{\partial f_2}{\partial x_4} & \frac{\partial f_2}{\partial x_6} \\ \frac{\partial f_4}{\partial x_2} & \frac{\partial f_4}{\partial x_4} & \frac{\partial f_4}{\partial x_6} \\ \frac{\partial f_6}{\partial x_2} & \frac{\partial f_6}{\partial x_4} & \frac{\partial f_6}{\partial x_6} \end{bmatrix}_{X=0} \\ &= \begin{bmatrix} 0 & 1 & 0 \\ -0.153g & -9.1k_v & 1114.65 l_m S_f \\ 0 & 0 & -T_{mr}^{-1} \end{bmatrix} \end{aligned} \tag{2.30}$$

$$\begin{aligned} \Delta f_h(x_h, x_v, u_v) = \frac{1}{j_h}[l_t S_f F_h(\omega_t) cos x_2 - k_h x_3 - x_3 x_4 (D-E) sin 2x_2 - j_{mr}\omega_m(x_6) x_4 sin x_2 \\ + \frac{j_{mr}}{T_{mr}}(u_v - x_6)\frac{d\omega_m(x_6)}{dx_6} cos x_2] - a_{h21}x_1 - a_{h22}x_3 - a_{h23}x_5 \end{aligned} \tag{2.31}$$

$$\Delta f_v(x_v, x_v, u_h) = 9.1[l_m S_f F_v(w_m) - g(0.0099cosx_2 + 0.0168sinx_2) - k_v x_4 \\ - 0.0252x_3^2 sin2x_2 + \frac{j_{tr}}{T_{tr}}(u_h - x_5)\frac{dw_t(x_5)}{dx_5}] - a_{v21}x_2 - a_{v22}x_4 - a_{v23}x_6 \tag{2.32}$$

In (2.26), ΔF_h and ΔF_v are considered as the uncertainty in the TRMS. The system in (2.26) can be partitioned into the regular form

$$\begin{aligned} \dot{z}_{1h} &= a_{11h}z_{1h} + a_{12h}z_{2h} + f_{1h} \\ \dot{z}_{2h} &= a_{21h}z_{1h} + a_{22h}z_{2h} + b_{h31}u_h + f_{2h} \end{aligned} \tag{2.33}$$

where

$$\begin{aligned} z_{1h} &= [x_1 \ x_3]^T \\ z_{2h} &= x_5 \\ a_{11h} &= \begin{bmatrix} a_{h11} & a_{h12} \\ a_{h21} & a_{h22} \end{bmatrix} \\ a_{12h} &= \begin{bmatrix} a_{h13} \\ a_{h23} \end{bmatrix} \\ a_{21h} &= [a_{h31} \ a_{h32}] \end{aligned}$$

Here,

$$\begin{aligned} f_{1h} &= \begin{bmatrix} 0 \\ \Delta f_h(x_h, x_v, u_v) \end{bmatrix} \\ f_{2h} &= 0 \end{aligned}$$

Therefore the state space model of the TRMS-HS can be expressed as:

$$\begin{bmatrix} \dot{z}_{1h} \\ \dot{z}_{2h} \end{bmatrix} = A_h \begin{bmatrix} z_{1h} \\ z_{2h} \end{bmatrix} + \begin{bmatrix} 0 \\ B_{2h} \end{bmatrix} u_h + \begin{bmatrix} \Delta\bar{F}_h \\ 0 \end{bmatrix} \tag{2.34}$$

where

$$\begin{aligned} A_h &= \begin{bmatrix} a_{11h} & a_{12h} \\ a_{21h} & a_{22h} \end{bmatrix} \\ B_{2h} &= b_{h31} \\ \Delta\bar{F}_h = f_{1h} &= \begin{bmatrix} 0 \\ \Delta f_h(x_h, x_v, u_v) \end{bmatrix} \end{aligned}$$

Similarly the TRMS-VS can be expressed as:

$$\begin{aligned} \dot{z}_{1v} &= a_{11v}z_{1v} + a_{12v}z_{2v} + f_{1v} \\ \dot{z}_{2v} &= a_{21v}z_{1v} + a_{22v}z_{2v} + b_{v31}u_v + f_{2v} \end{aligned} \tag{2.35}$$

Where

$$
\begin{aligned}
z_{1v} &= [x_2 \ x_4]^T \\
z_{2v} &= x_6 \\
a_{11v} &= \begin{bmatrix} a_{v11} & a_{v12} \\ a_{v21} & a_{v22} \end{bmatrix} \\
a_{12v} &= \begin{bmatrix} a_{v13} \\ a_{v23} \end{bmatrix} \\
a_{21v} &= [a_{v31} \ a_{v32}] \\
a_{22v} &= a_{v33}
\end{aligned}
$$

Here,

$$
\begin{aligned}
f_{1v} &= \begin{bmatrix} 0 \\ \Delta f_v(x_h, x_v, u_h) \end{bmatrix} \\
f_{2v} &= 0
\end{aligned}
$$

Therefore the state space model of the TRMS-VS can be expressed as:

$$
\begin{bmatrix} \dot{z}_{1v} \\ \dot{z}_{2v} \end{bmatrix} = A_v \begin{bmatrix} z_{1v} \\ z_{2v} \end{bmatrix} + \begin{bmatrix} 0 \\ B_{2v} \end{bmatrix} u_v + \begin{bmatrix} \Delta \bar{F}_v \\ 0 \end{bmatrix} \tag{2.36}
$$

where

$$
A_h = \begin{bmatrix} a_{11v} & a_{12v} \\ a_{21v} & a_{22v} \end{bmatrix}, B_{2v} = b_{v31}, \Delta \bar{F}_v = f_{1v} = \begin{bmatrix} 0 \\ \Delta f_v(x_v, x_h, u_h) \end{bmatrix} \tag{2.37}
$$

Let the desired reference vector be:

$r_{iv}(r_{ih})$ for $z_{iv}(z_{ih})$, $i = 1, 2$. Then

$$
\begin{aligned}
r_{1v} &= [r_{xv} \ 0]^T \\
r_{2v} &= 0
\end{aligned}
$$

and

$$
\begin{aligned}
r_{1h} &= [r_{xh} \ 0]^T \\
r_{2h} &= 0
\end{aligned}
$$

Hence the error vectors $e_{iv}(e_{ih})$ are obtained as:

$$
\begin{aligned}
e_{1v} &= z_{1v} - r_{1v}, \ e_{2v} = z_{2v} - r_{2v} \\
e_{1h} &= z_{1h} - r_{1h}, \ e_{2h} = z_{2h} - r_{2h}
\end{aligned} \tag{2.38}
$$

Without loss of generality, the desired vectors are assumed to be zero [8], hence the error state space model becomes:

$$\dot{E}_v = A_v E_v + B_v u_v + \Delta F_v \tag{2.39}$$

$$\dot{E}_h = A_h E_h + B_h u_h + \Delta F_h \tag{2.40}$$

where $E_v(E_h) \in R^3$ is the error state vector and $u_v(u_h) \in R^1$ is the control input. Here $A_v(A_h)$ and $B_v(B_h)$ are known matrices with proper dimensions.

2.3.2 TRMS Model Simulation

It is helpful to look at the way the open-loop system behaves before designing a controller for a plant.

To show dynamic of TRMS system in open loop case. response for Step inputs $(\psi, \varphi) = (1, 0)$, $(\psi, \varphi) = (0, 1)$ and $(\psi, \varphi) = (1, 1)$ are considered, the simulation results in Fig. 2.11, Fig. 2.12 and Fig. 2.13 respectively show the instability of azimuth subsystem, with remarkable divergence of elevations subsystem.

2.4 Conclusion

In this chapter, modeling nonlinear systems for control purpose has been detailed. Two types of nonlinear aerodynamic twin rotor multi-input multi-output systems (CE-150 and TRMS 33-949 helicopters) have been introduced. The twin rotor MIMO system (TRMS) is an example of a highly coupled nonlinear system perturbed by mismatched uncertainty. Simulation model has been provided and its analysis confirms that the systems are multivariable two degree-of-freedom (DOF), and strong cross-coupling between the main and the tail rotor with nonlinear dynamic equation in both vertical and horizontal planes. In addition to uncertain dynamic, further effects of friction torque force would provoke an additional uncertainty. The twin rotor is a good example for complex nonlinear multivariable control systems which could not be easily handled by classical control for full range of operating area. In the next chapter, a neighboring optimal control of partially-observed systems would be dealt with.

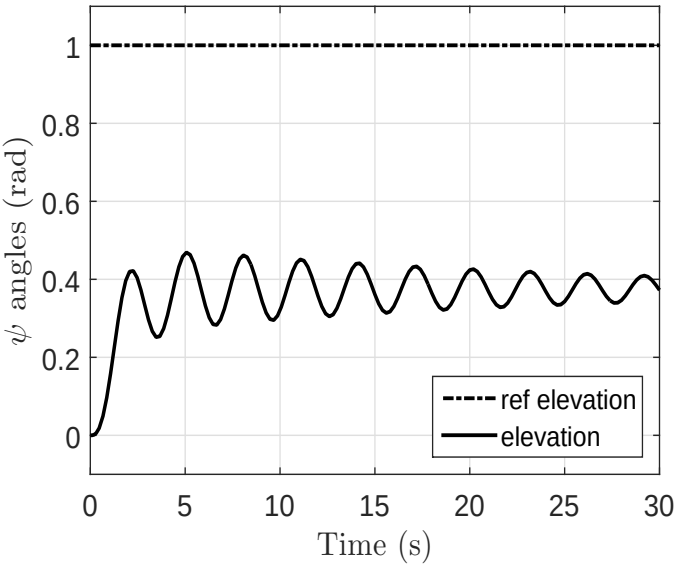

(a)

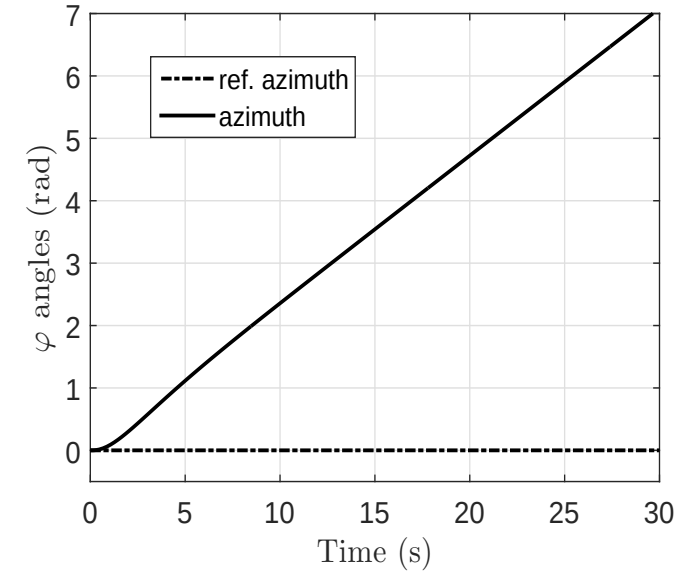

(b)

Figure 2.11: TRMS Open loop step response for reference $\psi^* = 1$ and $\varphi^* = 0$: (a) Elevation response; and (b) azimuth response.

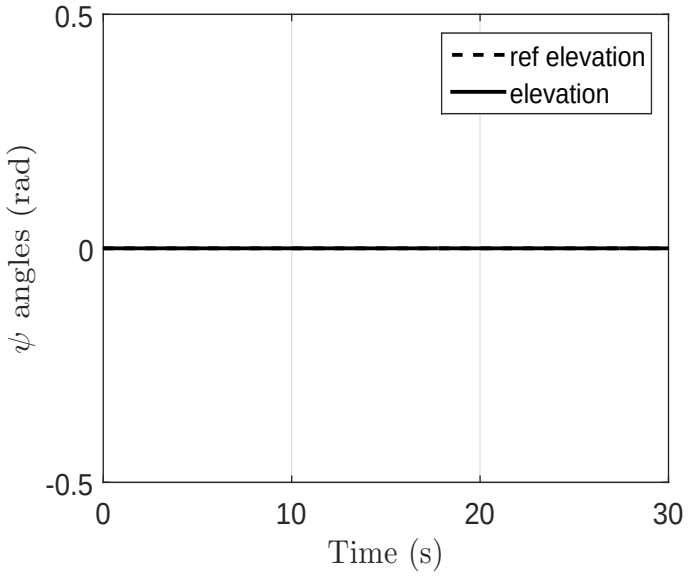

(a)

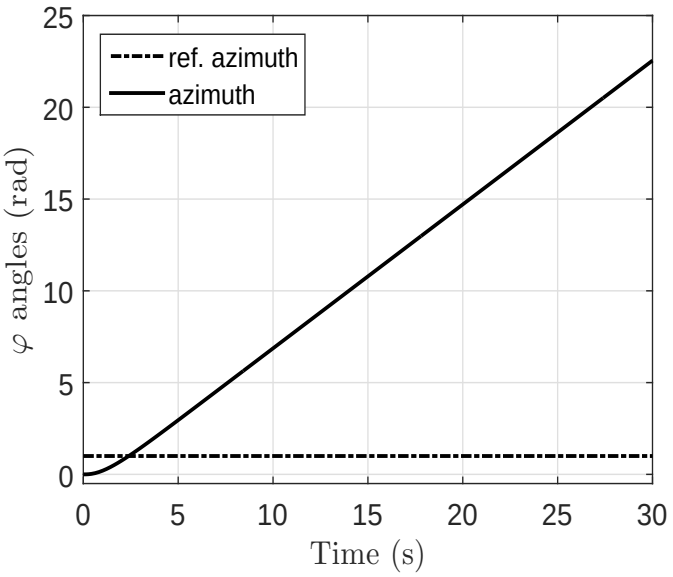

(b)

Figure 2.12: TRMS Open loop step response for reference $\psi^* = 0$ and $\varphi^* = 1$: (a) Elevation response; and (b) azimuth response.

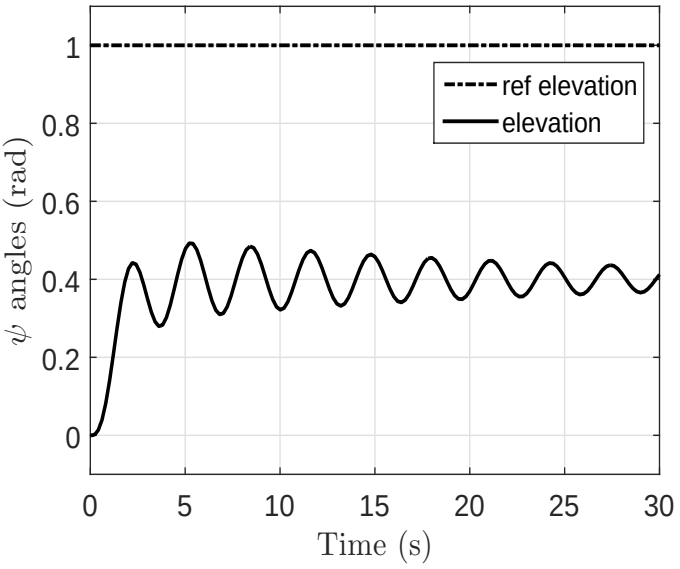

(a)

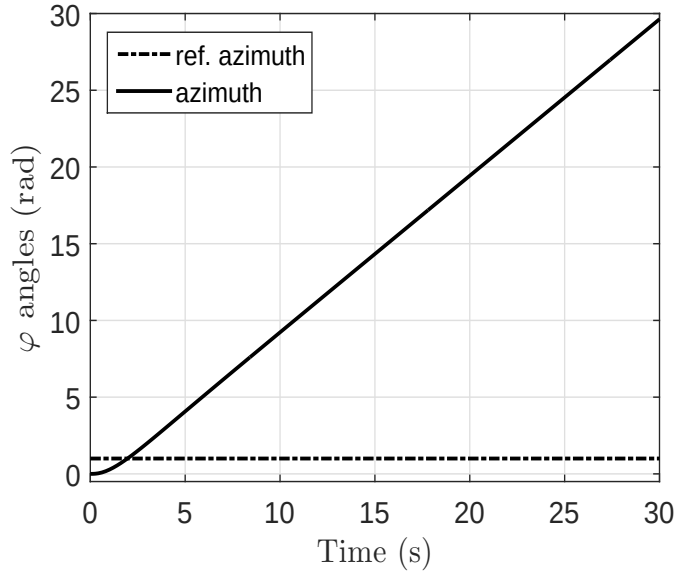

(b)

Figure 2.13: TRMS Open loop step response for reference $\psi^* = 1$ and $\varphi^* = 1$: (a) Elevation response; and (b) azimuth response.

Chapter 3

Neighboring Optimal Control of Partially-Observed Twin Rotor Multi-Input Multi-Output System

3.1 Introduction

Unmanned aerial vehicles (UAVs) have received an increasing interest due to the absence of on-board human pilots and have been recently used successfully to unveil the efficiency of miscellaneous control strategies [58], [63], [30]. In the last decade, twin rotors have become increasingly popular thanks to their ability to hover and maneuver in tight and dangerous places [7]. However, varying operating conditions along with structured and unstructured uncertainties, such as severe nonlinearities and external disturbances, are among the numerous challenges that need to be addressed before their wide-spread use in everyday real-life applications. Unlike quad-rotors that exhibit a good degree of decoupling among rotors, which makes them easy to control, twin rotors are openloop unstable systems due to their inherent characteristics such as nonlinearity, time-varying, uncertainty, and strong coupling between rotors [39], [37], [23]. As such, solving the regulator and/or tracking problem of a TRMS is a challenging task. This chapter addresses the regulator problem of a TRMS model around a nominal operating point despite its aforementioned inherent characteristics. The destabilizing effect of high nonlinearities has been thoroughly studied in many control systems. Failing to compensate for modeling uncertainties in controlling such systems can have negative consequences, such as severe tracking errors, limit cycles, chattering, and excessive noise [16], [30], [45]. In a modeling effort of the twin rotor system, fuzzy logic is combined with an optimization algorithm in [73]. Many control laws, on the one hand, have been proposed for TRMS including classical, robust and adaptive

control laws [26], [80], [18]. Yet their performance is limited since they generally consider only structured uncertainties. Linear control design methods [77] are used for their simplicity. However, linearization does not guarantee the stability in all operating conditions. A decoupling deadbeat control technique is proposed for a twin rotor system [93]. Although it shows better convergence than classical PID control, it suffers from sensitivity to parameters that are often changing dynamically and with uncertain dynamics. To overcome this weakness, genetic algorithms are used to tune a PID controller in [48] for a TRMS. On the other hand, an adaptive second-order sliding mode controller is also proposed in [70] for a TRMS. However, robustness to parameter variations and uncertain disturbances is obtained only when sliding mode truly occurs. In addition, most of these controllers do not take into account both structured and unstructured uncertainties. The presence of high, particularly unstructured, uncertainties such as nonlinearities significantly changes the system's dynamics [13]. This raises the urgency to consider alternative approaches for the control of this type of systems to keep up with their increasingly demanding design requirements.

Studies have shown that the design of robust controllers for mathematically ill-defined systems that may be subjected to structured and unstructured uncertainties was made possible with computational intelligence tools, such as artificial neural networks and fuzzy logic controllers [29]. The approximation capabilities have been the main driving force behind the increasing popularity of such methods as they are theoretically capable of uniformly approximating any continuous real function to any degree of accuracy. This has led to the recent advances in the area of intelligent control [10], [13]. Satisfactory performance was achieved with various neural network models for complex systems control [18], [21]. Despite the success witnessed by neural network-based control systems, they remain incapable of incorporating any human-like expertise already acquired about the dynamics of the system in hand, which is considered one of the main weaknesses of such soft computing methodologies. On the other hand, fuzzy logic control provides human reasoning capabilities to deal with uncertainties [52], [87] while their learning ability is almost inexistent as opposed to artificial neural networks. In the last decade, many researchers have put their efforts into combining between the advantages of these two methods. Recently, hybrid control laws gave fuzzy logic controllers more powerful abilities, such as adaptive learning, parallelism and generalization. Better control performance was achieved by using neural networks to adjust and optimize parameters of fuzzy controllers through offline or online learning. However, stability and robustness analysis of such heuristic methods cannot be easily derived.

This work aims to design a neighboring optimal control law for a TRMS around its

nominal operating point. Since the nonlinear mathematical model of a TRMS was already linearized around the operating point, the neighboring optimal control law is then designed to regulate the azimuth and elevation angles of a TRMS to their desired ones. As the internal dynamic states (except azimuth and elevation angles) of a TRMS are not measurable, the controller is coupled with a optimal estimator. The TRMS's process and measurement uncertainties associated with the azimuth and elevation angles are taken into considerations while designing the neighboring optimal control law. This is the first attempt in designing a neighboring optimal control law coupled with estimation to address the regulator problem of a noisy TRMS model.

3.2 Neighboring Optimal Control

The main theoretical results of this work is presented in this section where neighboring optimal control law for regulating the TRMS's azimuth and elevation angles to the desired ones are applied. Assuming $(\mathrm{q}^0, \mathrm{u}^0)$ as the TRMS's nominal operating point such that

$$\dot{\mathrm{q}}^0 = \mathrm{f}(\mathrm{q}^0, \mathrm{u}^0) = 0 \tag{3.1}$$

and the TRMS operates in the finite time interval $\mathcal{I} \equiv [0, t_f]$, with $t_f > 0$; we define the cost function as

$$\mathrm{J} = \Phi[t_f, \mathrm{q}(t_f)] + \int_0^{t_f} \ell[t, \mathrm{q}(t), \mathrm{u}(t)]dt, \tag{3.2}$$

where

$$\Phi[t_f, \mathrm{q}(t_f)] = \frac{1}{2}[\mathrm{q}(t_f) - \mathrm{q}^0(t_f)]^T P(t_f)[\mathrm{q}(t_f) - \mathrm{q}^0(t_f)] \tag{3.3a}$$

$$\ell[t, \mathrm{q}(t), \mathrm{u}(t)] = \frac{1}{2}[\mathrm{q}(t) - \mathrm{q}^0(t)]^T Q(t)[\mathrm{q}(t) - \mathrm{q}^0(t)] + \frac{1}{2}[\mathrm{u}(t) - \mathrm{u}^0(t)]^T \hat{R}(t)[\mathrm{u}(t) - \mathrm{u}^0(t)] \tag{3.3b}$$

with $P \in \mathbb{R}^{7\times7}$ and $Q \in \mathbb{R}^{7\times7}$ being the symmetric positive definite matrices of appropriate dimensions that signify relative importance along the error components of the TRMS's states and $\hat{R} \in \mathbb{R}^{7\times7}$ is a symmetric positive definite matrix that imposes the penalty on control efforts.

Defining the perturbations from the nominal optimal solutions as

$$\begin{aligned} \Delta\mathrm{q}(t) &= \mathrm{q}(t) - \mathrm{q}^0(t) \\ \Delta\mathrm{u}(t) &= \mathrm{u}(t) - \mathrm{u}^0(t) \end{aligned} \quad t \in \mathcal{I} \tag{3.4}$$

the TRMS's model (2.22) can be rewritten as:

$$\dot{\mathrm{q}} = \mathrm{f}(\mathrm{q}, \bar{\mathbf{u}}),$$

and expanded as the Taylor series

$$\begin{aligned} \dot{\mathrm{q}}^0(t) + \Delta\dot{\mathrm{q}}(t) = \mathrm{f}[\mathrm{q}^0(t), \mathrm{u}^0(t)] + \frac{\partial \mathrm{f}}{\partial \mathrm{q}}[\mathrm{q}^0(t), \mathrm{u}^0(t)]\Delta\mathrm{q}(t) \\ + \frac{\partial \mathrm{f}}{\partial \mathrm{u}}[\mathrm{q}^0(t), \mathrm{u}^0(t)]\Delta\mathrm{u}(t) + \mathcal{O}[\Delta\mathrm{q}, \Delta\mathrm{u}] \end{aligned} \tag{3.5}$$

where $\mathcal{O}[\Delta\mathrm{q}, \Delta\mathrm{u}]$ is the higher order terms of $\Delta\mathrm{q}$ and $\Delta\mathrm{u}$. Using the model (3.1) and assuming the perturbation variables to be relatively small, the above expression can be truncated to first degree, yielding the TRMS's linear kinematic constraint

$$\Delta\dot{\mathrm{q}}(t) = F(t)\Delta\mathrm{q}(t) + G(t)\Delta\mathrm{u}(t), \quad \Delta\mathrm{q}(0) = \Delta\mathrm{q}_0 \tag{3.6}$$

where

$$F(t) = \frac{\partial \mathrm{f}}{\partial \mathrm{q}}(\mathrm{q}^0, \mathrm{u}^0) \qquad \textit{and} \qquad G(t) = \frac{\partial \mathrm{f}}{\partial \mathrm{u}}(\mathrm{q}^0, \mathrm{u}^0)$$

The cost function (3.2) can be expanded as:

$$J[\mathrm{q}^0 + \Delta\mathrm{q}] \cong J[\mathrm{q}^0] + \Delta J[\Delta\mathrm{q}] + \Delta^2 J[\Delta\mathrm{q}] \tag{3.7}$$

However, the optimality guarantees that the first variation of $J[.]$ (i.e, $\Delta J[\Delta\mathrm{q}]$) is zero [68], which yields:

$$J[\mathrm{q}^0 + \Delta\mathrm{q}] \cong J[\mathrm{q}^0] + \Delta^2 J[\Delta\mathrm{q}] \tag{3.8}$$

where the second variation of $J[.]$ can be expressed as:

$$\Delta^2 J[\Delta\mathrm{q}] = \frac{1}{2}\Delta\mathrm{q}^T(t_f)\Phi_{qq}(t_f)\Delta\mathrm{q}(t_f) + \frac{1}{2}\int_0^{t_f} \begin{bmatrix} [\Delta\mathrm{q}^T \Delta\mathrm{u}^T] & \begin{bmatrix} \ell_{qq} & \ell_{qu} \\ \ell_{uq} & \ell_{uu} \end{bmatrix} & \begin{bmatrix} \Delta\mathrm{q} \\ \Delta\mathrm{u} \end{bmatrix} \end{bmatrix} dt \tag{3.9}$$

subject to (3.6). Let us rewrite the expression (3.9) as:

$$\Delta^2 J[\Delta \mathrm{q}] = \frac{1}{2}\Delta \mathrm{q}^T(t_f)\mathrm{P}(t_f)\Delta \mathrm{q}(t_f) + \frac{1}{2}\int_0^{t_f} \left[[\Delta \mathrm{q}^T \Delta \mathrm{u}^T] \quad \begin{bmatrix} \mathrm{Q} & \mathrm{M} \\ \mathrm{M}^T & \mathrm{R} \end{bmatrix} \quad \begin{bmatrix} \Delta \mathrm{q} \\ \Delta \mathrm{u} \end{bmatrix} \right] dt \tag{3.10}$$

where

$$\begin{aligned} \mathrm{P}(t_f) &\equiv \Phi_{qq}(t_f) \equiv \frac{\partial^2 \Phi}{\partial \mathrm{q}^2}(t_f, \mathrm{q}^0(t_f)) \\ \mathrm{Q} &\equiv \ell_{qq} \equiv \frac{\partial^2 \ell}{\partial \mathrm{q}^2}(t, \mathrm{q}^0, \mathrm{u}^0) \\ \mathrm{M} &\equiv \ell_{qu} \equiv \frac{\partial^2 \ell}{\partial \mathrm{q} \partial \mathrm{u}}(t, \mathrm{q}^0, \mathrm{u}^0), \quad \textit{and,} \\ \mathrm{R} &\equiv \ell_{uu} \equiv \frac{\partial^2 \ell}{\partial \mathrm{u}^2}(t, \mathrm{q}^0, \mathrm{u}^0) \end{aligned}$$

Since $\mathrm{M}(t) = 0$, it follows from (3.10) that:

$$J = \frac{1}{2}\Delta \mathrm{q}^T(t_f)\mathrm{P}(t_f)\Delta \mathrm{q}(t_f) + \frac{1}{2}\int_0^{t_f} \left[[\Delta \mathrm{q}^T \Delta \mathrm{u}^T] \quad \begin{bmatrix} \mathrm{Q} & 0 \\ 0 & \mathrm{R} \end{bmatrix} \quad \begin{bmatrix} \Delta \mathrm{q} \\ \Delta \mathrm{u} \end{bmatrix} \right] dt \tag{3.11}$$

where $\Delta^2 J[\Delta \mathrm{q}]$ is replaced by J for simplicity in notation and the equation (3.11) now defines the quadratic cost functional.

Theorem 1 (linear-quadratic control law): Consider the TRMS's linear kinematic model (3.6) and its quadratic cost functional given by (3.11). The optimal linear-quadratic state feedback control law is given by:

$$\Delta \mathrm{u}^o(t) = -\mathrm{R}^{-1}(t)\mathrm{G}^T(t)\mathrm{P}(t)\Delta \mathrm{q}(t) = -\mathrm{C}(t)\Delta \mathrm{q}(t), \tag{3.12}$$

where C(t) et is the (2 x 7) neghboring-optimal control gain matrix and P(t) is the solution of the differential matrix Riccati equation:

$$\dot{\mathrm{P}} = -\mathrm{F}^T(t)\mathrm{P}(t) - \mathrm{Q}(t) - \mathrm{P}(t)\mathrm{F}(t) + \mathrm{P}(t)\mathrm{G}(t)\mathrm{R}^{-1}(t)\mathrm{G}^T(t)\mathrm{P}(t), \quad \mathrm{P}(t_f) = \mathrm{P}_f \tag{3.13}$$

The proof Theorem 1 is similar to the one given in [68]. It is interesting to note that

the solution for P(t) and, therefore, for C(t) is independent of Δq(t). Variations in Δq(0) or Δq(t_f) have no effect on C(t), although the linear-optimal control history is obviously affected by state perturbations [86]. It is clear from Theorem 1 that once the solution of the differential matrix Riccati equation (3.13) is available, the feedback control law given by (3.12) can be formally constructed. From the perturbation (3.4), the total control is formed as the sum of the nominal and the perturbation optimal controls as stated in the introduction of chapter one:

$$\mathrm{u}(t) = \mathrm{u}^o(t)\Delta\mathrm{u}^o(t) = \mathrm{u}^o(t) - \mathrm{C}(t)[\hat{\mathrm{q}}(t) - \mathrm{q}^o(t)] \tag{3.14}$$

where $\hat{\mathrm{q}}(t)$ is the TRMS's estimated states which will be determined in section 3.3. Substituting perturbed optimal control (3.12) in (3.6) yields the perturbed stated feedback system

$$\begin{aligned} \Delta\dot{\mathrm{q}} &= [\mathrm{F}(t) - \mathrm{G}(t)\mathrm{R}^{-1}(t)\mathrm{G}^T(t)\mathrm{P}(t)]\Delta\mathrm{q}(t), \\ &\equiv \mathrm{A}(t)\Delta\mathrm{q}(t), \quad \Delta\mathrm{q}(0) = \Delta\mathrm{q}_0 \neq 0, \end{aligned} \tag{3.15}$$

with $\mathrm{A}(t) \equiv [\mathrm{F}(t) - \mathrm{G}(t)\mathrm{R}^{-1}(t)\mathrm{G}^T(t)\mathrm{P}(t)]$ and the corresponding state trajectory can then be described by

$$\Delta\mathrm{q}(t) = \Phi(t,0)\Delta\mathrm{q}(0), \tag{3.16}$$

where $\Phi(t,0) = e^{tA(t)}$ is the state transition matrix. The feedback model (3.15) with the quadratic cost functional (3.10) is similar to the optimal linear quadratic regulator problem, which is stable in the Laypunov sense [2]. In other words, the optimality condition guarantees the controllers' stability.

3.3 Optimal State Estimation

The TRMS employed in this work is subject to external disturbance (process noise) and is driven by the control law given in (3.14). Note that the TRMS's control input u(t) in (3.14) requires the state feedback which is subject to noise. Hence, dynamic measurements (azimuth (yaw) angle Ψ and elevation (pitch) angle φ) must be taken into account for

the TRMS to estimate its current state $\hat{\mathrm{q}}(t)$. These measurements are also subject to noise of the TRMS's operating environment. Thus, estimating the TRMS's state in noisy environments is a challenging task. In the following, an optimal filter is presented to filter out the noise embedded in TRMS's angle measurements for estimating its states. Since the TRMS itself is subject to process noise, the model (2.22) can be rewritten as:

$$\dot{\mathrm{q}}(t) = \mathrm{f}[\mathrm{q}(t), \mathrm{u}(t), \xi(t)], \tag{3.17}$$

where $\xi(t)$ is the noise associated with control input u(t). The Taylor series expansion of (3.17), neglecting the higher order terms, yields:

$$\Delta\dot{\mathrm{q}}(t) = \mathrm{F}(t)\Delta\mathrm{q}(t) + \mathrm{G}(t)\Delta\mathrm{u} + \mathrm{L}(t)\Delta\xi(t)], \quad \Delta\mathrm{q}(0) = \Delta\mathrm{q}_0 \tag{3.18}$$

where,

$$\mathrm{L}(t) = \frac{\partial \mathrm{f}}{\partial \xi}[\mathrm{q}^o(t), \mathrm{u}^o(t), \xi^o(t)], and \Delta\xi(t) = \xi(t) - \xi^o(t) \tag{3.19}$$

Note that $\xi^o(t) = 0$ because the deterministic solution of (3.1) has no process noise. The expected values of the initial state and co-variance are:

$$\begin{aligned} \mathbb{E}[\mathrm{q}(0)] &= \hat{\mathrm{q}}_0, \\ \mathbb{E}\left\{[\mathrm{q}(0) - \hat{\mathrm{q}}_0][\mathrm{q}(0) - \hat{\mathrm{q}}_0]^T\right\} &= \mathrm{S}_0. \end{aligned} \tag{3.20}$$

For simplicity, assume that the TRMS's input and measurement noise are a white, zero-mean Gaussian random process. If W_C and N_C are spectral density matrices of the TRMS process and measurement noise, respectively, the following expression holds:

$$\begin{aligned} \mathbb{E}\left[\xi^T(t) \quad \xi^T(t)\right] &= \left[\bar{\xi}^T \quad \bar{\xi}^T\right] \\ \mathbb{E}\left\{\begin{bmatrix}\xi(\tau)\\ \xi(\tau)\end{bmatrix} \quad \left[\xi^T(t) \quad \xi^T(t)\right]\right\} &= \begin{bmatrix} W_c(t) & 0 \\ 0 & N_c(t)\end{bmatrix}.\delta(t-\tau) \end{aligned} \tag{3.21}$$

where $\delta(.)$ is the dirac delta function defined by:

$$\delta(t-\tau) = \begin{cases} \infty, & \tau = t \\ 0, & \tau \neq t \end{cases}$$

$$\lim_{t \to k} \int_{t-k}^{t+k} \delta(t-\tau)d\tau = 1 \quad \text{(unit impulse function)}.$$

The TRMS's *a priori* state estimate is described by:

$$\hat{\mathrm{q}}(t) = \hat{\mathrm{q}}_0 + \int_0^t \mathrm{f}[\hat{\mathrm{q}}(t), \mathrm{u}(t)]dt. \tag{3.22}$$

The TRMS's measurement model is simply

$$\mathrm{z}(t) = \mathrm{Hq}(t) + \xi(t), \tag{3.23}$$

where the measurement matrix $\mathrm{H} \in \mathbb{R}^{2x7}$. The optimal filter gain can then be computed as:

$$\mathbb{K}_c = \mathrm{S}(t)\mathrm{H}^T(t)\mathrm{N}_C^{-1}(t), \tag{3.24}$$

where the state covariance matrix $\mathrm{S}(t)$ is the solution of the differential matrix Riccati equation

$$\begin{aligned} \dot{\mathrm{S}}(t) = \mathrm{F}(t)\mathrm{S}(t) + \mathrm{S}(t)\mathrm{F}^T(t) + \mathrm{L}(t)\mathrm{W}_C(t)\mathrm{L}^T(t) \\ -\mathrm{S}(t)\mathrm{H}^T(t)\mathrm{N}_C^{-1}(t)\mathrm{H}(t)\mathrm{S}(t), \quad \mathrm{S}(0) = \mathrm{S}_0. \end{aligned} \tag{3.25}$$

Using the current angle measurement, $\mathrm{z}(t)$ given in (3.23), the TRMS's *a posteriori* state estimate is determined by solving the following state model:

$$\dot{\hat{\mathrm{q}}}(t) = \mathrm{f}[\hat{\mathrm{q}}(t), \mathrm{u}(t)] + \mathbb{K}_c \left\{ \mathrm{z}(t) - \mathrm{h}[\hat{\mathrm{q}}(t)] \right\}, \quad \hat{\mathrm{q}}(0) = \hat{\mathrm{q}}_0. \tag{3.26}$$

The next section illustrates the performance of the neighboring optimal controller coupled with estimation using optimal Kalman filter.

3.4 Simulation Results

The purpose of this section is to sustain the neighboring optimal controller illustrated in section 3.2 through a set of computer simulations. For that, the parameters of the TRMS model are chosen as in chapter 2. The equilibrium point of the TRMS model is the origin, i.e.,

$$(q^o; u^o) = (0; 0)$$

The parameters of the cost function (3.11) are set as:

$$Q = diag(100, 5, 1, 1, 1, 1), \quad and \quad R = diag(1, 1)$$

The process and measurement noise covariance matrices are:

$$W_C = diag(1, 1, 1, 1, 1, 1) \quad and \quad N_C = diag(1, 1)$$

The optimal state estimator gain $\mathbb{K}_C$ is calculated as in (3.24) where the error covariance matrix $S(t)$ is solved using the algebraic Riccati model (3.25). First, we consider a case where the outputs of the TRMS model, (ψ, φ), are required to regulate on the fixed reference (or desired) azimuth, $\psi^* = 0,5$ rad, and elevation, $\varphi^* = 0,5$ rad, angles, respectively. Fig. 3.1 shows the performance of the feedback control law (3.14) in stabilizing the TRMS's outputs to desired ones. As can be seen from Fig. 3.1(a), initially $(\psi, \varphi) = (0, 0)$ rad, the TRMS's output reached the desired angles in about 7 s and maintained 0,5 rad regardless of the measurement noise of the outputs that are fed back to the control inputs, as expected. The main and tail motor voltages (inputs) are determined the by control law (3.14) and are shown in Fig. 3.1(b). Initial main and tail motor voltages are 4.1V and 0.2V and they are maintained at about 1.2V and 0.45V, respectively. Note that the full-state of the TRMS need to be estimated, $\hat{q}$ in order to compute the control inputs according to the control law (3.14). The full state of the TRMS is estimated and computed according to the model (3.26). Second, we consider a case where the TRMS is supposed to track desired time-varying azimuth and elevation angles.

The results for this case are summarized in Fig. 3.2, where the desired azimuth and elevation angles are defined with time-varying step signals (See Fig. 3.2(a)). Similar to the previous setup, the TRMS took about 7s to settle down to desired angles as it is natural. It is interesting to notice that the TRMS can still track the desired angles after sharp changes in the desired angles. Fig. 3.2(b) reveals the main and tail motor voltages

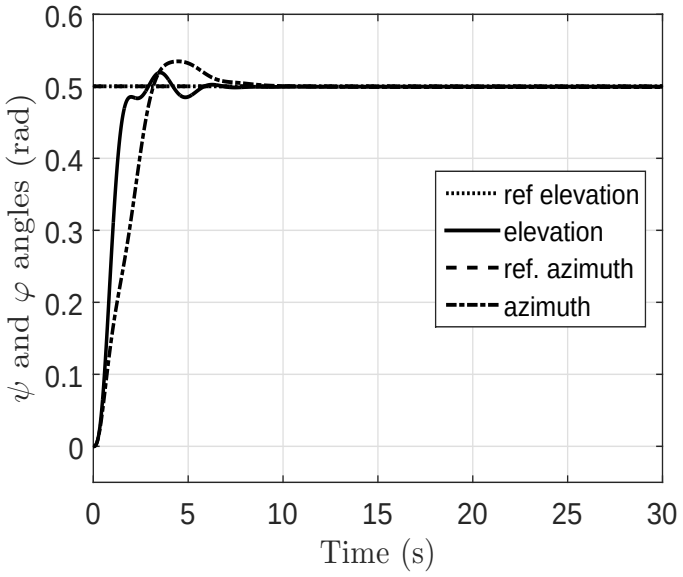

(a)

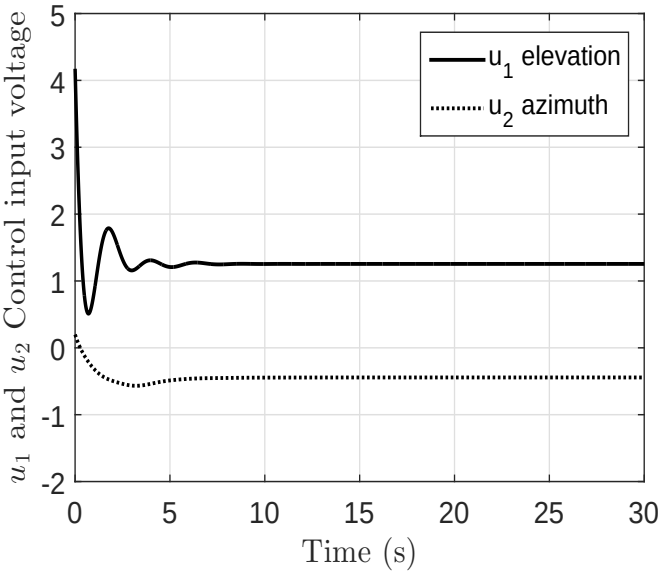

(b)

Figure 3.1: Step response for reference $\psi^* = 0.5$ and $\varphi^* = 0.5$: (a) stabilizing performance; and (b) control inputs (main and tail motor's input voltages).

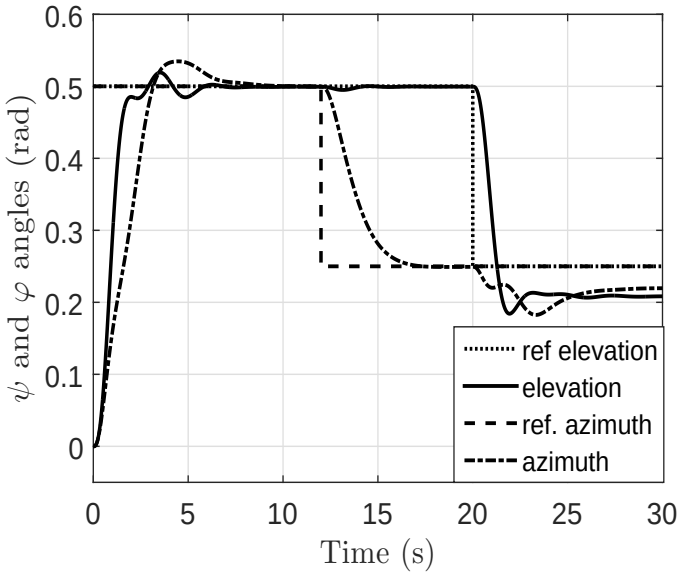

(a)

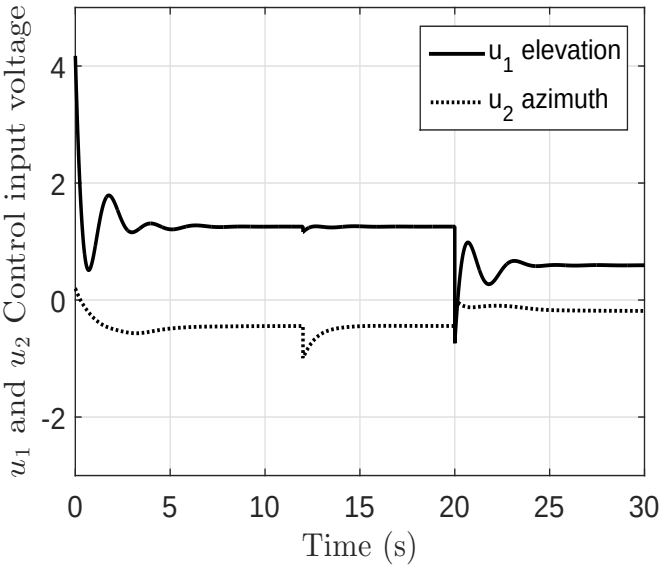

(b)

Figure 3.2: Time-varying step response for reference ψ^* and φ^*: (a) tracking performance; and (b) control inputs.

where fluctuations of the input voltages are due to the sharp changes in the desired output angles of the TRMS. As can be noticed, both stabilization and tracking performance of the neighboring optimal control law coupled with estimation for a TRMS model is satisfactory. However, there is a non-zero settling error for tracking desired azimuth and elevation angles as time goes to infinity. This is due to the fact that the linear model of the TRMS was based on a fixed operating point. Nevertheless, this settling error could be zero if a linear quadratic control law is designed based on the quadratic cost functional taking into account the time-varying desired trajectory of the outputs.

3.5 Conclusion

In this chapter, a neighboring optimal control law coupled with a state estimation technique for solving the trajectory tracking and the regulator problems of a TRMS model were proposed. The TRMS model is linearized around an operating point. Since the internal dynamical states (except the azimuth and elevation angles) are not measurable, an optimal filter to estimate them was designed. Hence, the proposed control law takes into account both process and measurement uncertainties of a TRMS model. A set of computer simulation results demonstrates the performance of the proposed control law. As can be seen from the simulation results, the desired trajectories of both azimuth and elevation angles are achieved with satisfactory asymptotic errors, as expected.

Chapter 4

Local Model Network

4.1 Introduction

Helicopters have received a thorough attention and have been extensively used lately to demonstrate the effectiveness of different kinds of controllers. They are considered as a well challenging established standard for many control problems, and have been used in various applications such as transportation and above-ground monitoring [63, 30]. Varying operating conditions along with structured and unstructured uncertainties, such as external disturbances, are among the numerous challenges that need to be addressed to successfully control such highly complex nonlinear unstable systems. Unlike quadrotors that exhibit a good degree of decoupling which makes them easier to control, helicopters are open-loop unstable systems, their dynamics is highly nonlinear, time-varying, uncertain, and strongly coupled.

Various flight control techniques have been proposed in the literature for the helicopter flight control problem [64, 91, 66, 46, 28, 47, 69], including robust adaptive control [46, 45], state-dependent Riccati equation control [5], sliding mode control [85], trajectory tracking control [53, 84], backstepping control [91, 47, 65], fuzzy control [52, 51] and neural network control [32, 29]. In [45], robust nonlinear motion control of a helicopter is developed. In spite of the simplicity of control law design based on linearization around an operating point of the states, the control system's performance and stability are achieved for only the approximated system and are not guaranteed for the overall system. On the other hand, fuzzy logic based controllers are incapable of incorporating any learning already acquired about the dynamics of the system in hand and neural network based controllers remain incapable of incorporating any human-like expertise. Moreover, these tools achieve outstanding performance at the expense of a heavy computation. Furthermore, they are

based on heuristic which makes tuning not trivial [10, 11].

Another aspect is that local model network theory has received a thorough attention and an increasing interest from the control community [72]. This is due to its simplicity since it is based on a combination of a set of linear controllers, where each of them corresponds to an appropriate operating point. Thus, the resulting control system is able to achieve good performance for a large operating range in the presence of plant's nonlinearities and uncertainties. Moreover, H_∞ control is considered as one of the promising robust control techniques. Its limitation is essentially a frequency domain optimization method for designing robust control systems. H_∞ refers to the space of stable and proper transfer functions. It has evolved since the initial seminal work of Zames [96]. The Book by Francis records the progress in the initial development of the subject [31], much of which was concerned with solving the Nehari optimization problem. The state-space methods of solving the H_∞ design problems is well-established as a very practical and a simple means of computing H_∞ controllers (see [25]). The polynomial approach for solving these problems have also been developed over the last few years [57, 34] and seen recent advances through the use of J spectral factorization algorithms [56, 35]. Besides, the control of a helicopter is a challenging problem since the system is multivariable, nonlinear, unstable in open loop, in addition to uncertain parameters, and at least of the sixth order, depending on the modeling precision. All inputs and outputs are coupled. To effectively handle strongly coupled nonlinearities, model uncertainties and time-varying unknown perturbations, local model networks are combined, in this research, with H_∞ control for helicopter stabilization.

The contribution in this Chapter is to propose a local model network based H_∞ controller for CE-150 helicopter stabilization problem. Local model networks provides a conceptually powerful combination of fuzzy logic and conventional linear control techniques providing an alternative approach for the control of nonlinear systems. Using nonlinear systems linearization at different significant operating points, H_∞ controller is designed for the linearized system, which is then combined in a local model network control structure. Therefore, decoupling of the system dynamics is achieved which is a key in obtaining good performance in the presence of uncertainties. The rest of the chapter is organized as follows: Section 4.2 presents a brief over view about H_∞ control synthesis. The local model networks based H_∞ control synthesis is detailed in Section 4.3. In Section 4.4, simulation results are reported and discussed. Conclusion with few remarks and suggestions is also presented.

4.2 Generalized H_∞ Control Problem

Consider a feedback control system whose block diagram representation is shown in Fig. 4.1, where $\mathbf{w}(s)$, $\mathbf{u}(s)$, $\mathbf{z}(s)$, and $\mathbf{v}(s)$ are vector-valued signals: $\mathbf{w}(s)$ is the exogenous signal including disturbances, sensor noise, and reference signals; the output $\mathbf{z}(s)$ is an error (performance) signal; $\mathbf{v}(s)$ is the measured output; and $\mathbf{u}(s)$ is the control (manipulated) signal, with s being the Laplace variable. The transfer function matrices $\mathbf{P}(s)$ and $\mathbf{K}(s)$ are real-rational and proper, and represent, respectively, the generalized plant transfer function and the controller transfer function, respectively. The generalized plant transfer function $\mathbf{P}(s)$ can be partitioned as:

$$\mathbf{P}(s) = \begin{bmatrix} \mathbf{P_{11}(s)} & \mathbf{P_{12}(s)} \\ \mathbf{P_{21}(s)} & \mathbf{P_{22}(s)} \end{bmatrix}.$$

Droping the argument (s) when no ambiguity arises. The system shown in Fig. 4.1 can be written as

$$\begin{bmatrix} \mathbf{z} \\ \mathbf{v} \end{bmatrix} = \mathbf{P}(s) \begin{bmatrix} \mathbf{w} \\ \mathbf{u} \end{bmatrix} = \begin{bmatrix} \mathbf{P_{11}} & \mathbf{P_{12}} \\ \mathbf{P_{21}} & \mathbf{P_{22}} \end{bmatrix} \begin{bmatrix} \mathbf{w} \\ \mathbf{u} \end{bmatrix} \tag{4.1a}$$

$$\mathbf{u} = \mathbf{K}\mathbf{v} \tag{4.1b}$$

The system (4.1) is also referred to as a linear fractional transformation (LFT) on $\mathbf{K}(s)$, and $\mathbf{P}(s)$ is the coefficient matrix for the LFT.

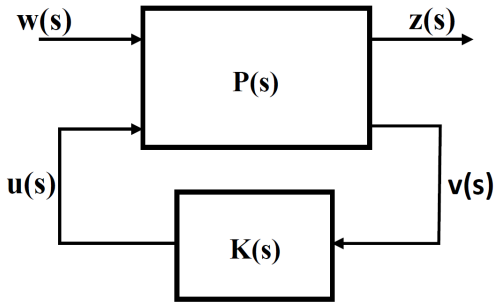

Figure 4.1: The two-port block diagram for H_∞ control.

For positive integers $\bar{m}, p > 0$, the transfer function representation of the system (4.1)

is given by:

$$\mathbf{z} = \mathbf{P}_{11}\mathbf{w} + \mathbf{P}_{12}\mathbf{u} \tag{4.2a}$$

$$\mathbf{v} = \mathbf{P}_{21}\mathbf{w} + \mathbf{P}_{22}\mathbf{u} \tag{4.2b}$$

$$\mathbf{u} = \mathbf{K}\mathbf{v}, \tag{4.2c}$$

where, $\mathbf{z} \in \mathbb{R}^{\bar{m}+p}$, $\mathbf{v} \in \mathbb{R}^{p}$, $\mathbf{u} \in \mathbb{R}^{\bar{m}}$, and $\mathbf{w} \in \mathbb{R}^{\bar{m}+p}$. Denoting $\mathbf{T}_{zw}(s)$ as the closed loop transfer function between the regulated outputs and the exogenous inputs, we write

$$\mathbf{z} = \mathbf{T}_{zw}(s)\mathbf{w} \tag{4.3}$$

where, $\mathbf{T}_{zw} = \mathbf{P}_{11} + \mathbf{P}_{12}\mathbf{K}(\mathbf{I} - \mathbf{P}_{22}\mathbf{K})^{-1}\mathbf{P}_{12}$, with $\mathbf{I}$ being the identity matrix of appropriate dimension. The above expression for the closed loop transfer function $\mathbf{T}_{zw}$ is the LFT. The H_∞ control aims to find a stable closed-loop controller $\mathbf{K}(s)$ that minimizes the infinity norm of $\mathbf{T}_{zw}(s)$ while stabilizing the generalized plant $\mathbf{P}(s)$. One solution to the H_∞ control problem is the γ-iteration, where the controller $\mathbf{K}(s)$ is determined such that $\|\mathbf{T}_{zw}\|_\infty < \gamma$. For such a solution, an initial γ is chosen from $[\gamma^-, \gamma^+]$ with γ^- and γ^+ are the initial minimum and maximum values of γ, respectively. In the next iteration, γ is chosen using bisection method, for example. This process continues until a minimal γ is found that minimizes $\|\mathbf{T}_{zw}(s)\|_\infty$ and the plant transfer function $\mathbf{P}(s)$ is stabilized.

4.3 Local Model Networks based H_∞ Control

In essence, based on the interpolation models and weighted by their associated validity functions, Local model networks (LMNs) operate. The output of an LMN with ℓ local models can be expressed as:

$$\bar{\mathbf{u}} = \sum_{i=1}^{\ell} u_i(\bullet)\Phi_i(\bullet), \tag{4.4}$$

where $(\bullet)$ is an indicator of the operating point which is usually the reference or the output signal, $\Phi_i(\bullet)$ is the corresponding validity function of the i^{th} controller, u_i is control output of i^{th} controller, and $\bar{\mathbf{u}}$ is the LMN's output. The validity functions determine the validity region of their corresponding LMs. They can be interpreted as the operating point dependent on the weighting factors which determine the contribution of their associated LMs to the final output. In order to have a smooth transition among the local models, the validity functions should be smooth and take their values between 0 and 1. Furthermore,

the validity functions must form a partition of unity to have reasonable interpretation of the local models,

$$\sum_{i=1}^{\ell} \Phi_i(\bullet) = 1. \tag{4.5}$$

Usually, when the validity functions do not automatically sum up to 1, the partition of unity is achieved through normalization. This principle is illustrated in Fig. 4.2.

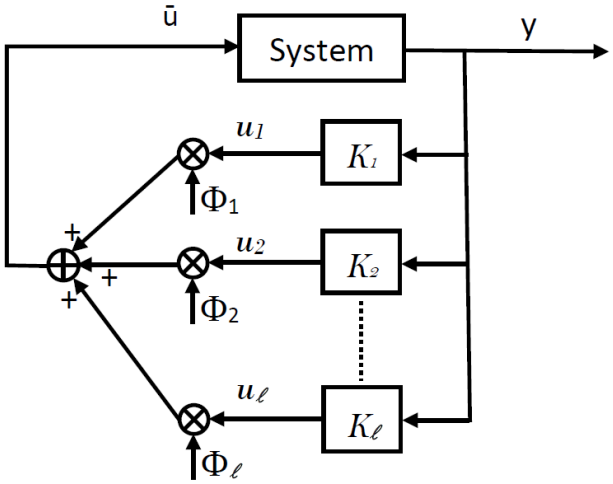

Figure 4.2: Local model network control.

The control law is given by:

$$\bar{\mathbf{u}} = \Phi_1 u_1 + \Phi_2 u_2 + \ldots + \Phi_\ell u_\ell \tag{4.6}$$

Where, Φ_i is a function that depends on the operating point and must satisfy the condition (4.5). The functions Φ_i allow us to privilege each compensator in its functional domain. A simple choice of the functions Φ_i is based on the use of trapezoidal functions as indicated in Fig 4.3.

In region (1), the compensator $\mathbf{K}_1$ is in operation, whereas in region (2) the system is controlled by linear combination of $\mathbf{K}_1$ and $\mathbf{K}_2$. However, the compensator $\mathbf{K}_2$ is used in region (3). For acceptable behavior of the system, the operating point is described by a variable which is slowly varying with time.

For simple cases, we can use the reference or the output as an indicator of the operating point. We note that the control principle presented in this paragraph comes closer to the principle of the adaptive control with advantage that parameter identification and

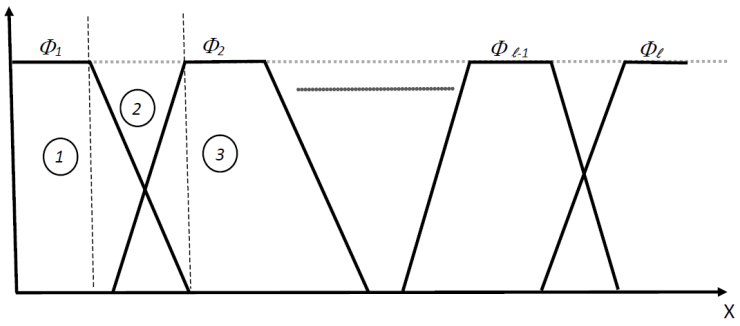

Figure 4.3: Switching.

estimation part is avoided, which yield less computational load and better time response. In this work, ℓ is taken to be equal to 3.

On the other hand, mixed-sensitivity H_∞ control design consists of synthesising a controller $\mathbf{K}(s)$ to minimize low frequency disturbances at the plant output and the high frequency control effort while providing robustness to additive uncertainty at high frequencies. Fig. 4.4 shows a feedback control system with augmented plant, where $\mathbf{G}(s)$ is a plant, and $\mathbf{W_s}(s)$ and $\mathbf{W_T}(s)$ are weighting matrices. In this chapter, mixed-sensitivity H_∞ control is applied to CE-150 helicopter model. Therefore, the sensitivity function $\mathbf{S}(s)$, and the complementary sensitivity function $\mathbf{T}(s)$ are defined as follow:

$$\mathbf{S(s)} = (\mathbf{I} + \mathbf{G(s)K(s)})^{-1} \tag{4.7}$$

$$\mathbf{T(s)} = \mathbf{G(s)K(s)}\,(\mathbf{I} + \mathbf{G(s)K(s)})^{-1} \tag{4.8}$$

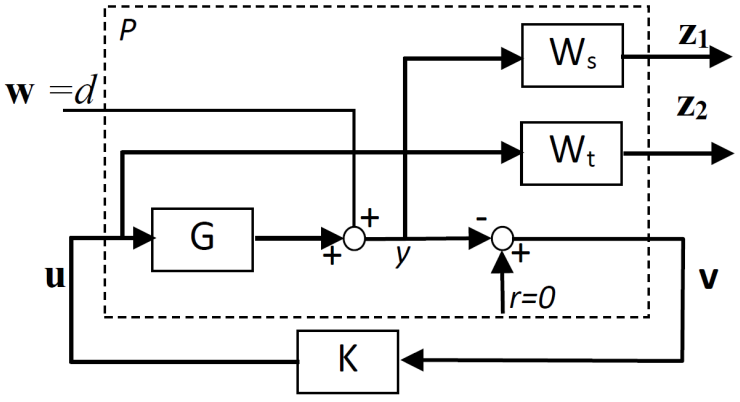

Figure 4.4: A mixed sensitivity configuration.

It is noteworthy from (4.7) that the minimisation of $\mathbf{T}(s)$ at high frequencies leads to robustness to uncertainties. Therefore, designing a control law to meet the specifications consists of a proper selection of the weighting matrices $\mathbf{W_s}(s)$ and $\mathbf{W_T}(s)$, which capture the desired closed-loop dynamics. Then, the design of a stabilizing controller $\mathbf{K}(s)$ is carried-out by minimizing the following cost function,

$$\left\| \begin{matrix} \mathbf{W_s(s)\ S(s)} \\ \mathbf{W_T(s)\ T(s)} \end{matrix} \right\|_\infty \tag{4.9}$$

The selection process of the weighting matrices is repeated until satisfactory performance and robustness of the closed-loop system are achieved. The matrix $\mathbf{W_s(s)}$ is computed as follows:

$$\mathbf{W_s(s)} = \frac{\mathbf{s/M_p} + \omega_\mathbf{B}}{\mathbf{s} + \omega_\mathbf{B} \mathbf{e_{ss}}} \tag{4.10}$$

where, e_{ss} is the desired minimum steady-state tracking error, ω_B is the desired minimum bandwidth (usually selected where $\frac{1}{|\mathbf{W_s}|}$ crosses 0.707), and M_p is the desired maximum peak magnitude of $\mathbf{W_s}$. Similarly, the weighting matrix $\mathbf{W_T(s)}$ is chosen to constrain the bandwidth such that the gain of $\frac{1}{\mathbf{W_T}}$ forces a roll-off at a desired frequency.

The proposed closed-loop control strategy is depicted in Fig 4.5. Considering the helicopter's equilibrium points discussed in the previous section:

$$\left((\mathbf{x}_*^{[1]}, \bar{\mathbf{u}}_*^{[1]}), (\mathbf{x}_*^{[2]}, \bar{\mathbf{u}}_*^{[2]}), (\mathbf{x}_*^{[3]}, \bar{\mathbf{u}}_*^{[3]}) \right),$$

three distinct H_∞ controllers are designed. Then, the output of these controllers is used with the local model network presented in Fig 4.6 to provide the helicopter with control inputs, $\bar{u}_1$ and $\bar{u}_2$ according to (4.4). It is noteworthy from (2.2) and (2.3) that helicopter's gravitational and centrifugal torques are strongly coupled with the elevation angle ψ. Therefore, this angle is used as an indicator of the operating point as it is illustrated in Fig 4.6.

4.4 Simulation Results

The purpose of this section is to show the tracking error performance of the azimuth angle ψ and the elevation angle φ for the linearized CE-150 helicopter model (2.16). The weight matrices $\mathbf{W}_\ell(s)$, $\ell = 1, 2, 3$, for three different operating points are chosen as:

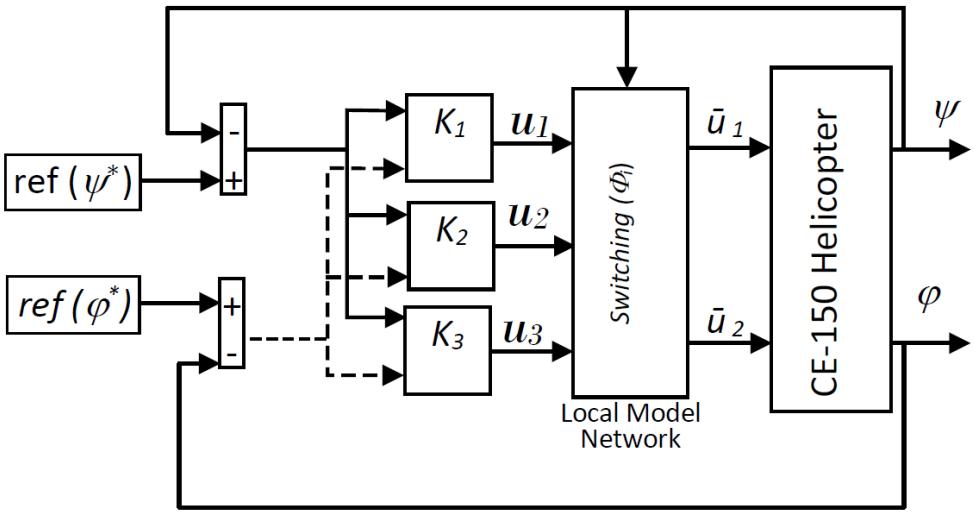

Figure 4.5: control structure for H_∞ local model network.

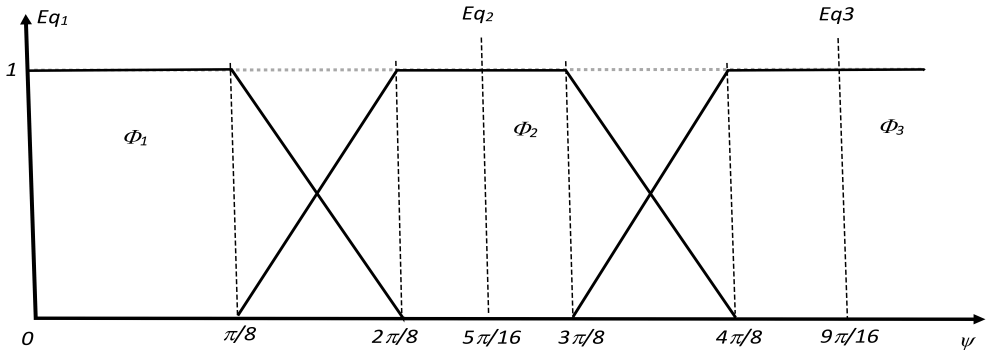

Figure 4.6: Validity function and switching mechanism.

$\mathbf{W}_1(s) = \text{diag}(W_1^1(s),\ W_1^2(s)),\ \ \mathbf{W}_1^t(s) = \text{diag}(0.1, 2.0)$,
for $e_{ss11} = 0.01$, $e_{ss12} = 0.005$, $\omega_{B11} = 0.051$,
$\omega_{B12} = 0.005$, $M_{p11} = 5$, $M_{p12} = 1$,
$\mathbf{W}_2(s) = \text{diag}(W_2^1(s),\ W_2^2(s)),\ \ \mathbf{W}_2^t(s) = \text{diag}(0.2, 1.0)$,
for $e_{ss21} = 0.1$, $e_{ss22} = 0.005$, $\omega_{B21} = 0.05$,
$\omega_{B22} = 0.008$, $M_{p21} = 3$, $M_{p22} = 1$, and
$\mathbf{W}_3(s) = \text{diag}(W_3^1(s),\ W_3^2(s)),\ \ \mathbf{W}_3^t(s) = \text{diag}(0.2, 1.0)$,
for $e_{ss31} = 0.1$, $e_{ss32} = 0.005$, $\omega_{B31} = 0.05$,
$\omega_{B32} = 0.008$, $M_{p31} = 3$, $M_{p32} = 1$.

In order to keep a minimum steady-state tracking error, for azimuth angle control φ, a gain compensator is used, for each local controller (see Fig. 4.2). The performance of the control law (4.6) are summarized in Figs. 4.7–4.12. The step responses for reference azimuth and elevation angles ($\psi^* = 0.25, \varphi^* = 0$) and ($\psi^* = 0, \varphi^* = 0.25$) are shown in Figs 4.7 and 4.8, respectively.

While the desired and actual tracking performances for these reference inputs are shown in Figs 4.7(a) and 4.8(a), a good coupling is observed through the tracking errors shown in Figs 4.7(b) and 4.8(b). We repeat this setup for the reference inputs ($\psi^* = 0.5, \varphi^* = 0$) and ($\psi^* = 0.5, \varphi^* = 0$) and the tracking performance of the azimuth and elevation angles (desired and actual), and the their corresponding tracking errors are revealed in Figs 4.9 and 4.10, respectively. what could be noticed is that the more the settling time decreases, the more performances in terms of oscillations are deteriorated because of the neglected nonlinear dynamics, as expected. Unlike previous simulations, we choose ($\psi^* = 0.5, \varphi^* = 0.5$) to illustrate the controller's ability to sustain the helicopter's dynamic performance on the same azimuth and elevation angles (see Fig. 4.11). Finally, Fig. 4.12 reports the controller's performance due to a sudden change on the desired azimuth and elevation angles.

The above simulation results reveal that the H_∞ controller coupled with the local model network has the ability to track a predefined trajectories of the azimuth and elevation angles regardless of their complexities.

4.5 Conclusion

In this chapter, a local model network based H_∞ control technique is proposed to solve the stabilization problem of CE-150 helicopters. Since the mixed-sensitivity problem is a

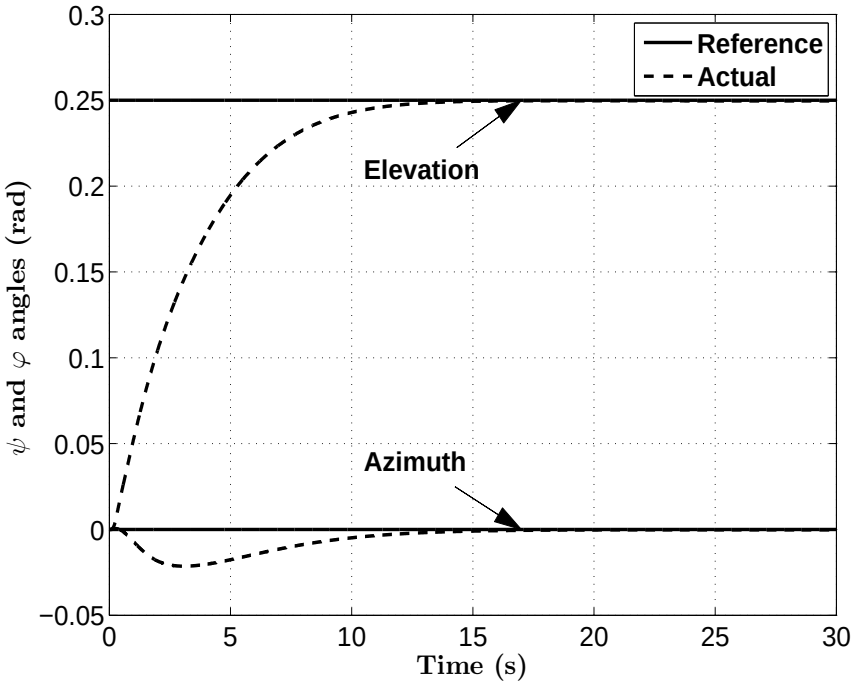

(a)

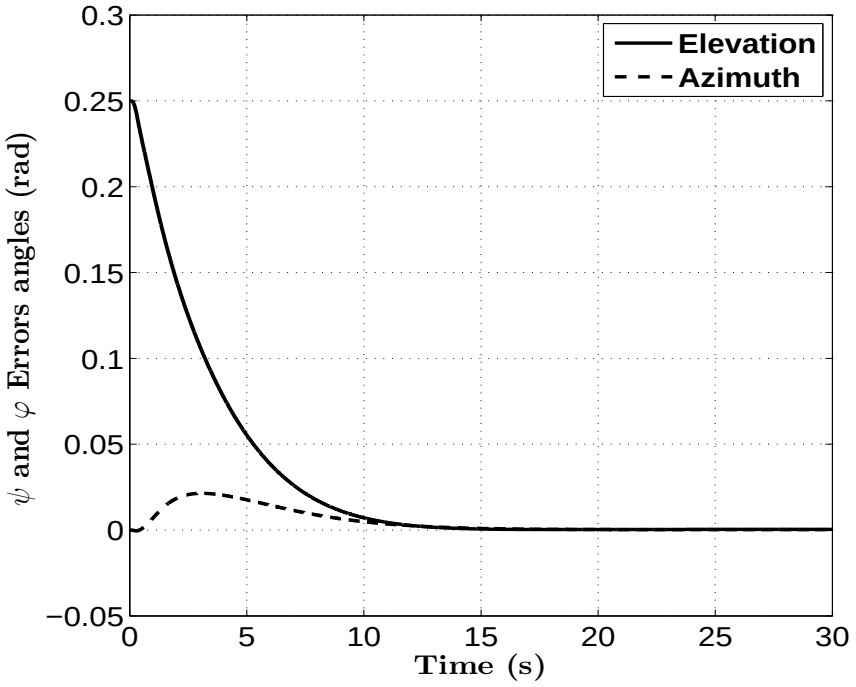

(b)

Figure 4.7: Unit step response for reference $\psi^* = 0,25$ and $\varphi^* = 0$: (a) tracking performance; and (b) tracking error.

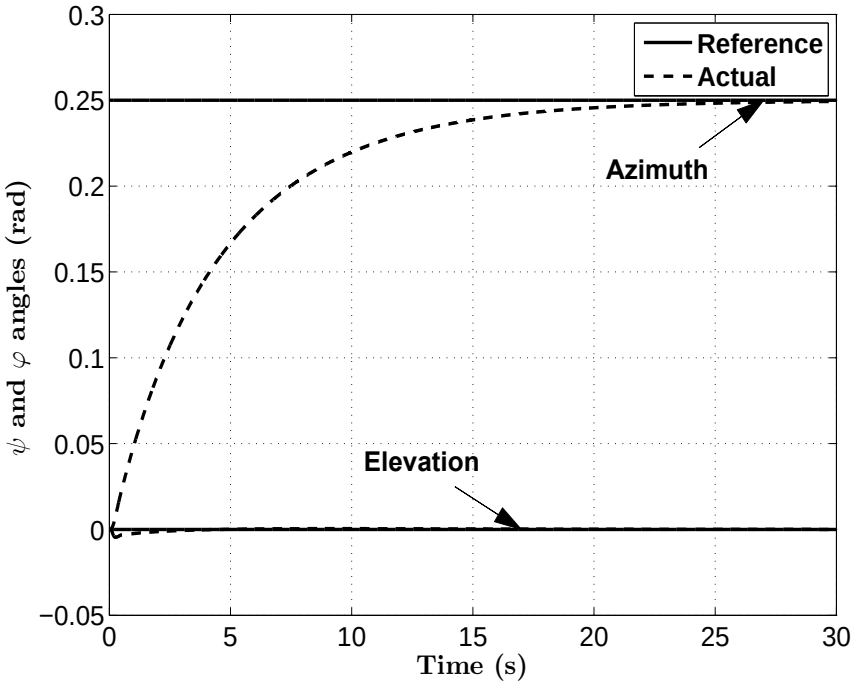

(a)

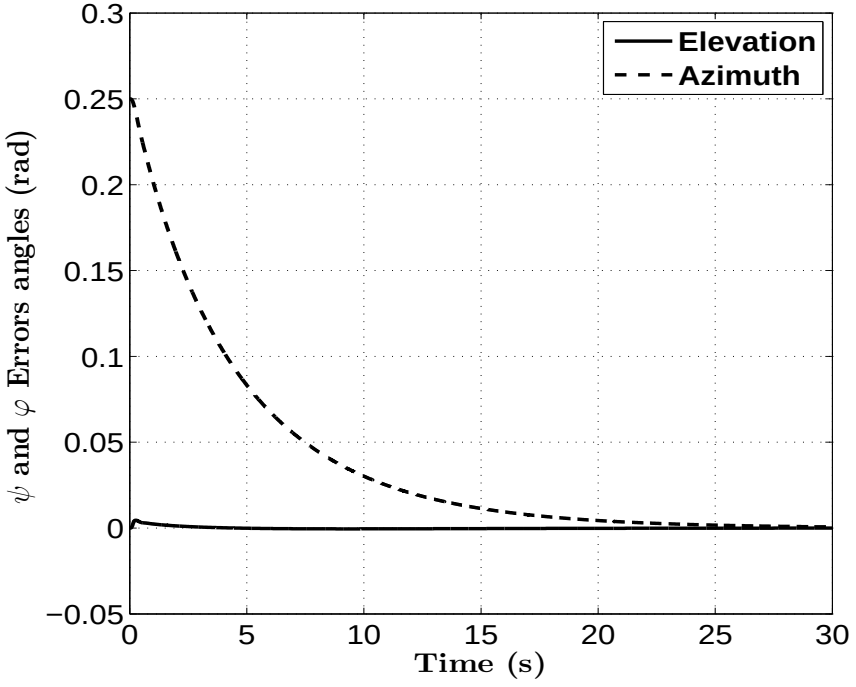

(b)

Figure 4.8: Unit step response for reference $\psi^* = 0$ and $\varphi^* = 0,25$: (a) tracking performance; and (b) tracking error.

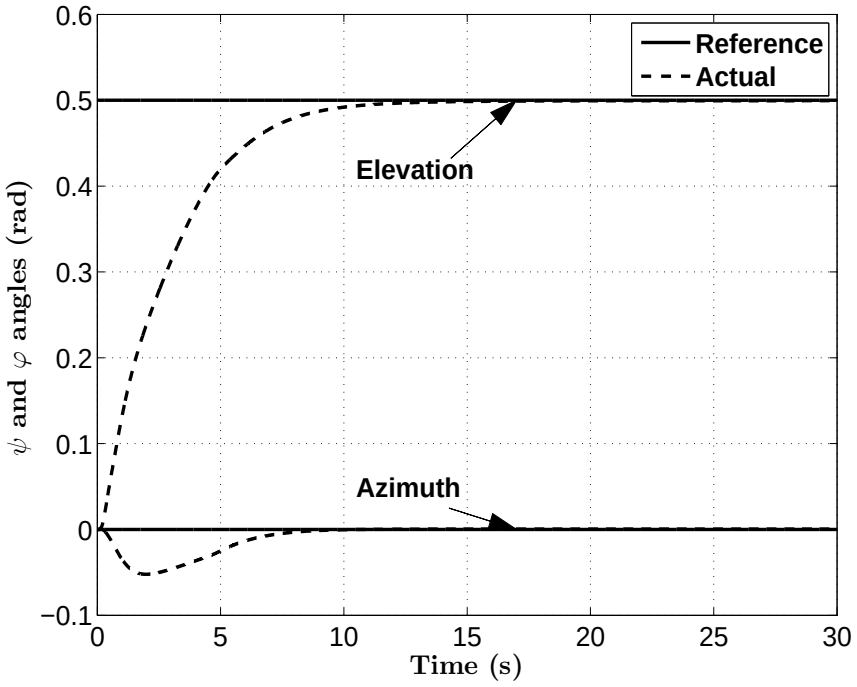

(a)

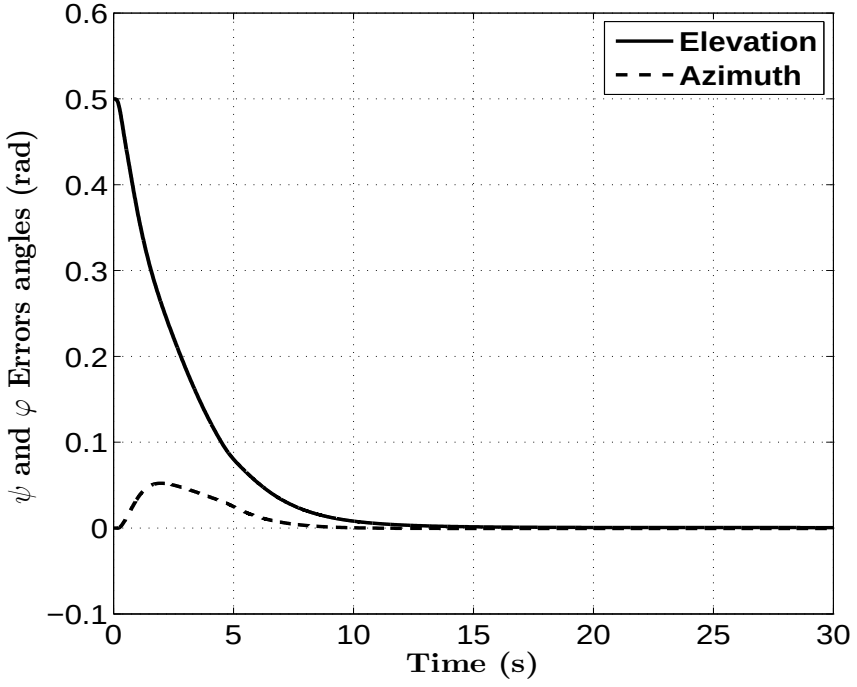

(b)

Figure 4.9: Unit step response for reference $\psi^* = 0,5$ and $\varphi^* = 0$: (a) tracking performance; and (b) tracking error.

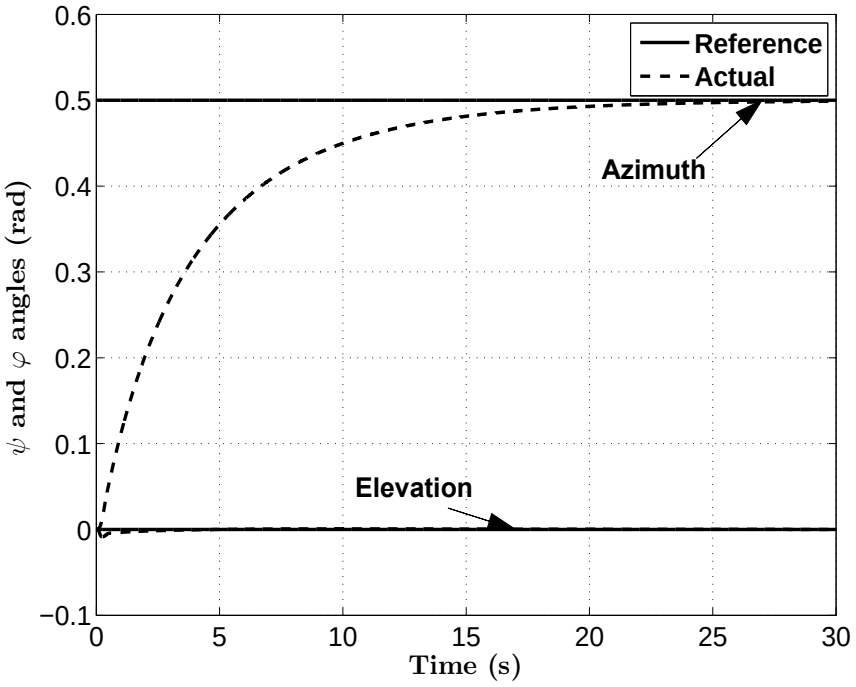

(a)

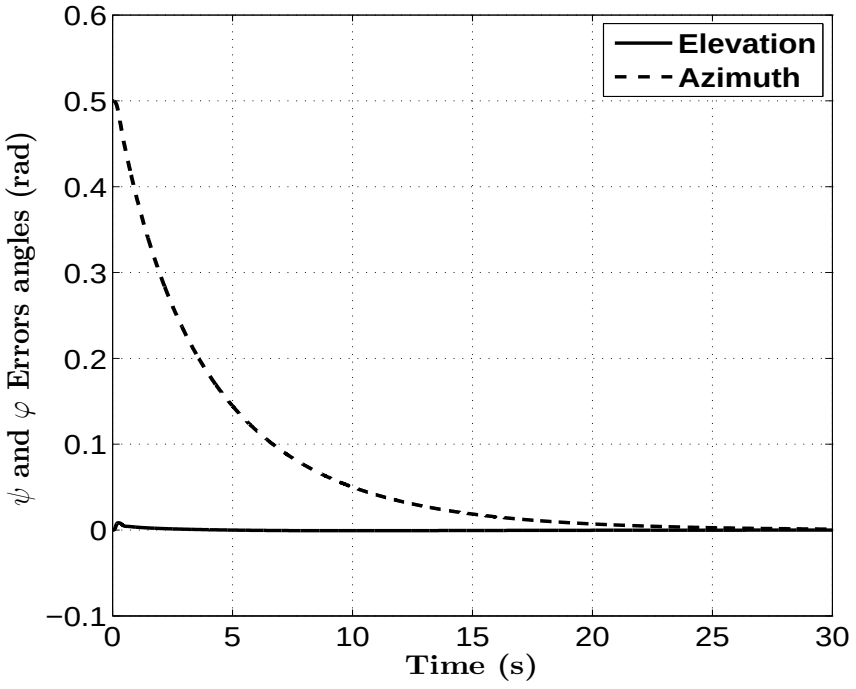

(b)

Figure 4.10: Unit step response for reference $\psi^* = 0$ and $\varphi^* = 0,5$: (a) tracking performance; and (b) tracking error.

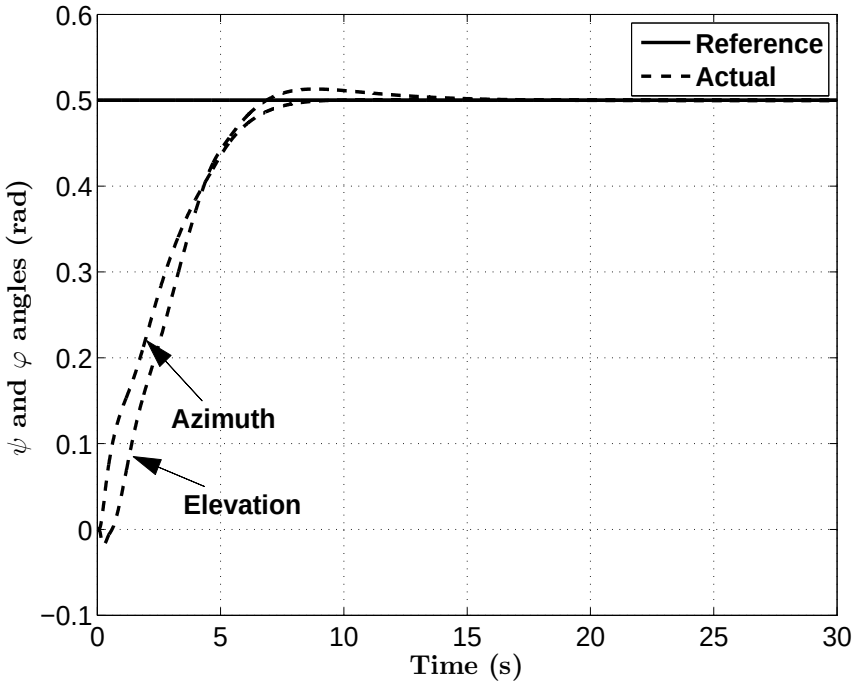

(a)

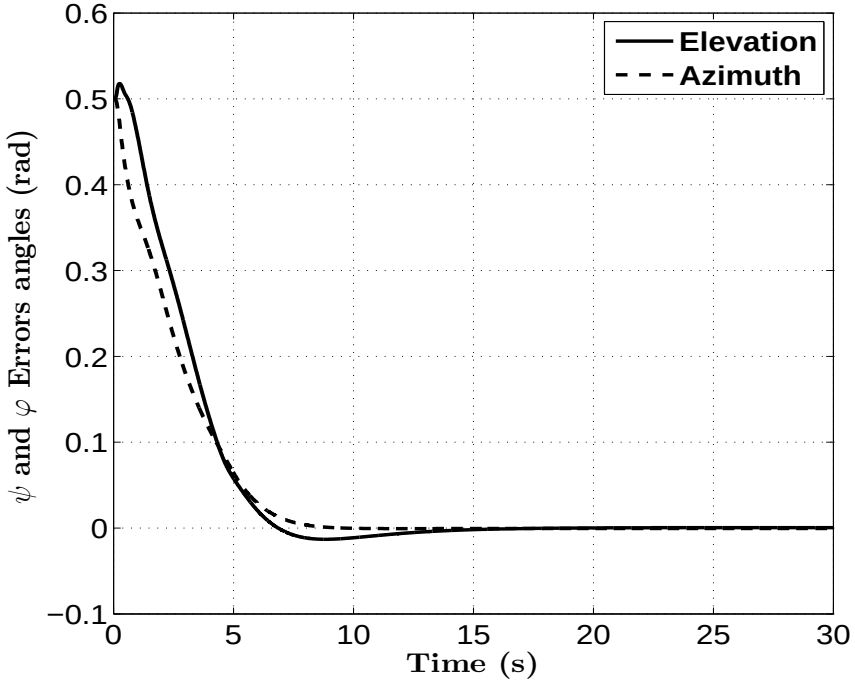

(b)

Figure 4.11: Unit step response for reference $\psi^* = 0,5$ and $\varphi^* = 0,5$: (a) tracking performance; and (b) tracking error.

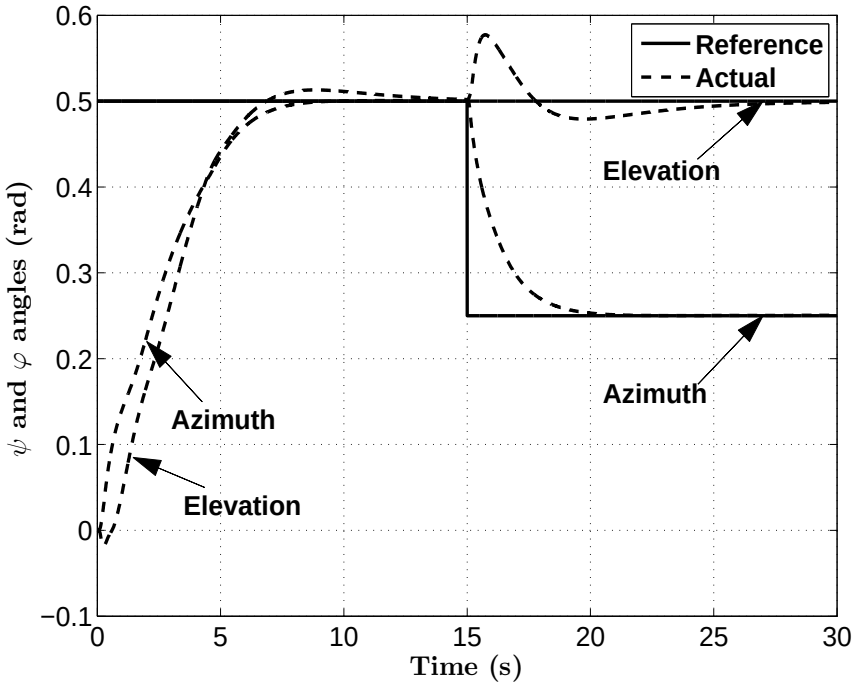

(a)

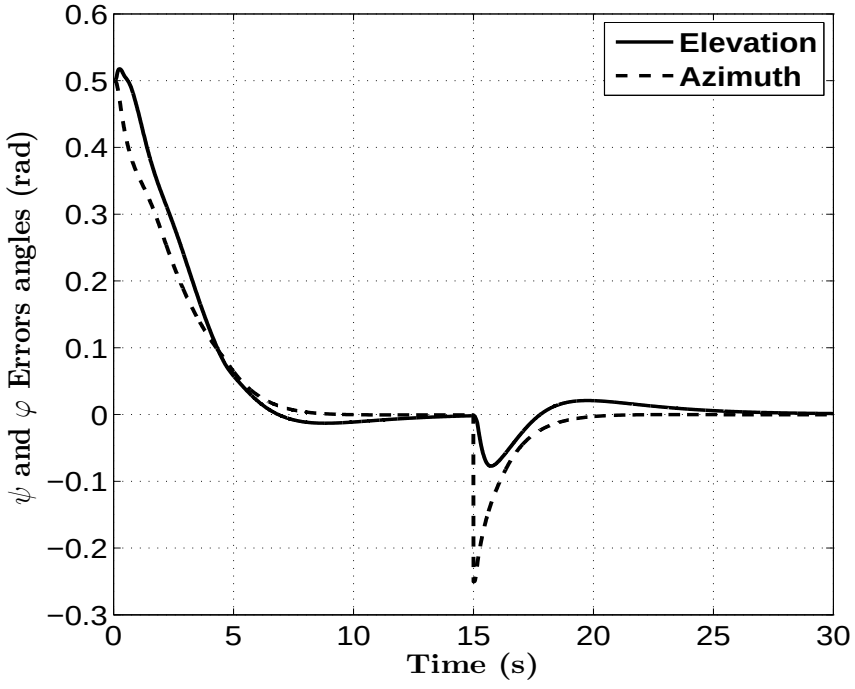

(b)

Figure 4.12: Time change step response for ψ^* and φ^*: (a) tracking performance; and (b) tracking error.

special kind of H_∞ control problem, the system could be linearized around a set of operating points. H_∞ mixed-sensitivity controller for the linearized system has been designed. The problem has been transferred into a standard H_∞ problem and then solved for the stabilizing gain that satisfies the desired criteria. Next the controllers which are based on mixed-sensitivity problems have been embedded within a network. From simulation results, it is noticed that the obtained controller ensures the decoupling of the system dynamics and good performance. The conclusion is that the Local model network based on H_∞ control is suitable for the stabilization of the proposed helicopter simulator model.

Chapter 5

Interval Type-2 Fuzzy Logic Control of a Twin-Rotor Multi-input Multi-output System

5.1 Introduction

The absence of on-board human pilots makes unmanned aerial systems (UASs) increasingly popular and employed in many applications [30, 63]. Recently, twin rotors have received an increasing interest due to their ability to hover and maneuver in tight and dangerous places [8]. But, varying operating conditions along with structured and unstructured uncertainties, such as severe nonlinearities and external disturbances, are among the various challenges that need to be dealt with before their wide-spread use in everyday real-life applications. Unlike quadrotors that exhibit a good degree of decoupling among rotors, which makes them easier to control, twin rotors are open-loop unstable systems due to their inherent characteristics such as nonlinearity, time-varying, uncertainty, and strong coupling between rotors [40, 36, 24]. As such, motion trajectory tracking of a TRMS is a challenging task. This Chapter addresses the control of a TRMS despite its aforementioned inherent characteristics and nonlinearities.

Several existing studies have thoroughly covered the destabilizing effect of high nonlinearities in numerous motion control systems. While controlling such systems and in the absence of meticulous compensation for modeling uncertainties, the latter can have negative consequences, such as severe tracking errors, limit cycles, chattering, and excessive noise [17, 30, 45]. In [74], fuzzy logic is combined with an optimization algorithm in an effort to accurately model the twin rotor system. The control of TRMS has also been rigorously studied, including classical, robust and adaptive control laws [27, 81, 19]. However,

their performance is limited since they generally consider only structured uncertainties. Linear control system design methods [78] are used for their simplicity. But, linearization around a single operating point does not guarantee the stability in all operating conditions. A decoupling deadbeat control technique is proposed for a twin rotor system [94]. Although it shows better convergence than classical PID control, it suffers from sensitivity to parameters that are often changing dynamically and with uncertain dynamics. To overcome this weakness, genetic algorithms are used to tune a PID controller in [49] for a TRMS. Additionally, an adaptive second-order sliding mode controller is proposed in [71] for a TRMS. Yet, robustness to uncertain disturbances and parameter variations is only obtained when sliding mode truly take place. Moreover, most of these controllers do not take into account both structured and unstructured uncertainties. The presence of high, particularly unstructured, uncertainties such as nonlinearities significantly changes the system's dynamics [14]. This raises the urgency to consider alternative approaches for the control of this type of systems to keep up with their increasingly demanding design requirements.

On the other hand, design of robust controllers for mathematically ill-defined systems that may be subjected to structured and unstructured uncertainties is possible with computational intelligence tools, such as artificial neural networks and fuzzy logic controllers [29]. Their approximation capabilities have been the main driving force behind the increasing popularity of such techniques as they are theoretically capable of uniformly approximating any continuous real function to any degree of accuracy. Recent advances in the area of intelligent control has led to satisfactory performance in controlling complex systems [10, 14, 19, 22]. Despite the success of neural control systems, they fail short in incorporating any human-like expertise already acquired about the system's dynamics, which is one of the main shortcomings of such soft-computing methodologies. Conversely, fuzzy logic control is able to provide human reasoning in dealing with uncertainties [52, 88]. Recently, researchers endeavor to combine between the advantages of these two methods which yielded hybrid controllers with more powerful abilities, such as adaptive learning, parallelism, and generalization. Throughout the yesteryears, better control performance had been achieved by using neural networks to adjust and optimize parameters of fuzzy controllers through offline or online learning. However, stability and robustness analysis of such heuristic methods cannot be easily derived.

This work capitalizes on the merits and the latest developments of type-2 fuzzy logic theory to design an interval type-2 fuzzy control scheme for a TRMS. Conventional type-1 fuzzy FLSs can be used to identify the behavior of this highly nonlinear system with various types of uncertainties. However, type-1 fuzzy sets cannot fully capture the uncertainties in

the system due to membership functions and knowledge base imprecision. Hence, higher types of fuzzy sets have to be considered. However, the computational complexity of operations on fuzzy sets increases with the increasing type of the fuzzy set. Therefore, interval type-2 fuzzy sets are used in this work for their simplicity and efficiency. A comparative study between the proposed type-2 FLC and its type-1 counterpart is also presented to better assess their respective performances in various operating conditions.

The rest of the chapter is organized as follows: In section 5.2, interval type-2 FLSs and the functionality of their inference engine are described. The proposed adaptive control technique is detailed in section 5.3. In section 5.4, results are reported and discussed.

5.2 Interval Type-2 FLSs

Since type-2 fuzzy operations are generally more computational demanding than their type-1 counterparts. interval type-2 fuzzy sets are introduced to alleviate their high computational burden [67, 60]. As such, a simplified and efficient alternative is provided to easily process the input and antecedent operations for FLSs offering a balanced tradeoff between complexity and performance. A FLS with an interval singleton type-2 fuzzifiers and product or minimum t-norm satisfies the following properties [67]:

1. The firing strength of the lth fuzzy rule is an interval type-1 fuzzy set defined as:

$$F^l(x') \equiv \sqcap_{i=1}^{p} \mu_{\tilde{F}_i^l}(x'_i) = [\underline{f}^l(x'), \overline{f}^l(x')] \equiv [\underline{f}^l, \overline{f}^l],$$

   where

$$\underline{f}^l(x') = \underline{\mu}_{\tilde{F}_1^l}(x'_1) \star \cdots \star \underline{\mu}_{\tilde{F}_p^l}(x'_p) \tag{5.1}$$

$$\overline{f}^l(x') = \overline{\mu}_{\tilde{F}_1^l}(x'_1) \star \cdots \star \overline{\mu}_{\tilde{F}_p^l}(x'_p) \tag{5.2}$$

   with the t-norm operator denoted by '$\star$'.

2. The fired output consequent set of the l rule is a type-1 fuzzy set characterized by a membership function

$$\mu_{\tilde{B}^l}(y) = \int_{b^l \in [\underline{f}^l \star \underline{\mu}_{\tilde{G}^l}(y), \overline{f}^l \star \overline{\mu}_{\tilde{G}^l}(y)]} 1/b^l \qquad \forall y \in Y \tag{5.3}$$

   with $\underline{\mu}_{\tilde{G}^l}(y)$ and $\overline{\mu}_{\tilde{G}^l}(y)$ being the lower and upper membership grades of $\mu_{\tilde{G}^l}(y)$.

3. If N out of a total of L fuzzy rules in the FLS fire, where $N \leq L$, then the overall aggregated output fuzzy set is defined by a type-1 membership function $\mu_{\tilde{B}}(y)$ obtained by combining the fired output consequent sets into one. In other words, $\mu_{\tilde{B}}(y) = \sqcup_{l=1}^{N} \mu_{\tilde{B}^l}(y)$, where $\mu_{\tilde{B}^l}(y)$ is defined in (5.3).

The following is a brief description of the different stages of the type-2 fuzzy logic inference engine.

5.2.1 Type-2 Fuzzification

During the first stage of the fuzzy inferencing process, i.e., fuzzification, the crisp input vector with n elements $x = (x_1, \ldots, x_n)^T$ in the universe of discourse $X_1 \times X_2 \times \ldots \times X_n$ is mapped into type-2 fuzzy sets [60, 67]. The upper and lower membership functions are computed for each point of the universe of discourse. For rule l, the result of this operation is an interval type-1 set $[\underline{f}^l, \overline{f}^l]$. In this chapter, singleton type-2 fuzzy are adopted to fuzzify the external input signals, as shall be detailed later.

5.2.2 Type-2 Rule Base

The composition of the rules of a type-2 FLC is similar to that of type-1. A type-2 FLS with n inputs, $x_1 \in X_1, \ldots, x_n \in X_n$, and m outputs, $y_1 \in Y_1, \ldots, y_m \in Y_m$, the l^{th} rule is of the form:

$$R^l : \text{IF } x_1 \text{ is } \tilde{F}_1^l \text{ and } x_2 \text{ is } \tilde{F}_2^l \text{ and } \ldots \text{ and } x_n \text{ is } \tilde{F}_n^l$$
$$\text{THEN } y_1 \text{ is } \tilde{G}_1^l \text{ and } y_2 \text{ is } \tilde{G}_2^l \text{ and } \ldots \text{ and } y_m \text{ is } \tilde{G}_m^l$$

where $\tilde{F}_i^l$ and $\tilde{G}_j^l$, $i = 1, \ldots, n, j = 1, \ldots, m$, are input and output fuzzy labels, respectively.

5.2.3 Type-2 Fuzzy Inference Engine

The if-then rules in the knowledge data base are aggregated by the inference engine with the fuzzy set generated after fuzzification. The intersection of multiple rule antecedents is calculated using a t-norm operator while the union of multiple rules is computed through a t-conorm operation. Each rule l in the knowledge base is interpreted as a type-2 fuzzy implication, which, when aggregated with the fuzzified inputs, infers a type-2 fuzzy set $\tilde{B}^l$ such that:

$$\mu_{\tilde{B}^l}(y) = \sqcup_{x \in X} [\mu_{\tilde{A}_x}(x) \sqcap \mu_{R^l}(x, y)].$$

The "minimum" and "maximum" are used for the type-2 FLC as t-norm and t-conorm operators, respectively.

5.2.4 Type Reduction

Since type-2 fuzzy inference engine yields an aggregated output type-2 fuzzy set, type reduction is needed to generate a type-1 fuzzy set called "type-reduced set" of the aggregate type-2 fuzzy set. In this chapter, the center-of-sets type reduction is considered for its computational efficiency [60].

Calculation of the Rule Consequents Centroids Using the centroid method, the center-of-sets type reduction reduces the resulting type-2 fuzzy sets to an interval type-1 fuzzy set $[y_{lk}^p, y_{rk}^p]$ for each rule p. The inferenced interval type-1 fuzzy set is then defined by $[y_{lk}, y_{rk}]$, such as:

$$y_{lk} = \frac{\sum_{p=1}^{R} f_l^p y_{lk}^p}{\sum_{p=1}^{R} f_l^p} \tag{5.4}$$

$$y_{rk} = \frac{\sum_{p=1}^{R} f_r^p y_{rk}^p}{\sum_{p=1}^{R} f_r^p} \tag{5.5}$$

where f_l^p, f_r^p are the firing strengths corresponding to y_{lk}^p and y_{rk}^p of rule p, to minimize y_{lk}^p and maximize y_{rk}^p. The iterative procedures to compute y_{lk} and y_{rk} are revealed in [67].

5.2.5 Defuzzification

The type-reduced set $Y_{cos}(X)_k$ calculated from its left most and right most points, y_{lk} and y_{rk} is defuzzified using the interval set average formula to get a crisp output value. As such, the defuzzified crisp output for each output k is formulated as [60]:

$$Y_k(x) = \frac{y_{lk} + y_{rk}}{2}.$$

5.3 Interval Type-2 Fuzzy Logic Control Strategy

The objective is to design a control law $\mathbf{u}$ to force the TRMS's state vector $\mathbf{q}$ to track their pre-defined time-dependent desired vector $\mathbf{q}^*$. This is to be achieved under unknown

system's dynamics. Let $\mathbf{e} = \mathbf{q} - \mathbf{q}^*$ and $\dot{\mathbf{e}} = \frac{\mathbf{d}}{\mathbf{dt}}\mathbf{q} - \frac{\mathbf{d}}{\mathbf{dt}}\mathbf{q}^*$ denote the state error vector and its derivative. The control approach consists of the design of a fuzzy logic controller that leads to a precise tracking. The fuzzy control strategy is based on a human operator experience to interpret a situation and initiate its control action. A block diagram for the fuzzy logic controller is depicted in Fig. 5.1.

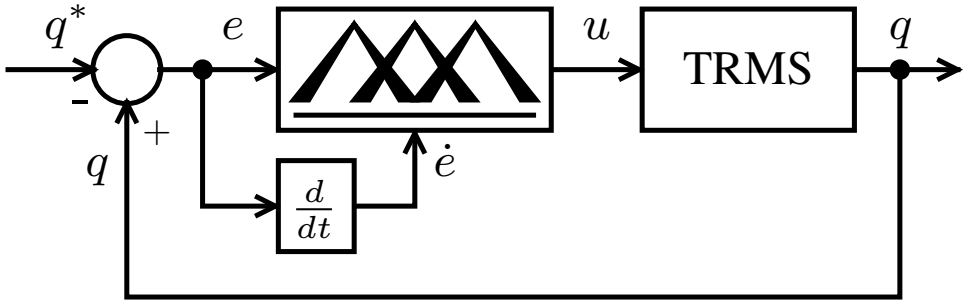

Figure 5.1: Fuzzy logic control scheme.

Given the state vectors $\mathbf{q}^*$ and $\mathbf{q}$, a state error vector $\mathbf{e}$ and its derivative $\dot{\mathbf{e}}$ are computed. The FLC takes these two inputs and provides a control action vector $\mathbf{u}$ that is proportional to the input values. To assess the performance of both types of controllers, the proposed fuzzy controller is implemented in two different ways: the first is based on a type-1 fuzzy control scheme while the second is based on a type-2. The fuzzy rules of the two control techniques are the same; they were chosen heuristically (Table 5.1) and can be refined by an expert. These rules are based on three hypotheses: (i) when the input signals are far from their respective nominal zero-valued surfaces, then the FLC's output assumes a high value; (ii) when the inputs are approaching the nominal zero-valued surfaces, the output is adjusted to a smaller value for a smoother approach; (iii) once the inputs are on the nominal zero-valued surfaces, then the output is set to zero. This way, the FLC forces the error e and the its derivative $\dot{e}$ to approach zero. The input membership functions adopted by both types of control systems are depicted in Fig. 5.2. As it is shown, signals are quantized into 5 levels represented by a set of linguistic variables: Negative Large (NL), Negative Small (NS), Zero (Z), Positive Small (PS), and Positive Large (PL). In this study, triangular membership functions are used, mainly due to their high computational and performance efficiencies. The center of area method is used for defuzzification. It is noteworthy that an empirical study is usually conducted by an expert to tune the input membership functions and the rules until satisfactory performance is achieved. However, this process can be time

consuming especially for nonlinear systems with various types of uncertainties. Moreover, the resultant control system performance is not guaranteed in the presence of unexpected disturbance of high magnitudes. In this work, the input membership functions and the rules of both controller are set for an acceptable performance without any empirical analysis. Then, type-2 fuzzy sets footprint of uncertainty (FOU) is introduced to fully capture the membership functions uncertainties and knowledge base imprecision. Both controllers are compared to evaluate the ability of the FOU in compensating for various and higher types of uncertainties.

Table 5.1: Fuzzy rules for type-1 and type-2 FLCs.

	e				
$\dot{e}$	NL	NS	Z	PS	PL
PL	Z	PL	PL	PL	PL
PS	NS	Z	PS	PS	PL
Z	NL	NS	Z	PS	PL
NS	NL	NS	NS	Z	PS
NL	NL	NL	NL	NL	Z

5.4 Results and Discussion

To show the effectiveness of the proposed intelligent control strategy, a set of computer simulation runs is carried out on a TRMS model. The system's parameters are chosen as in [44] and are summarized in section 2.3.1. The performance of the proposed controller is studied considering the TRMS's angles ψ and φ along with their respective reference angles, and the TRMS control input $\mathbf{u}(t) = [u_1(t), u_2(t)]^T$ to its actuators. To better illustrate the superiority of the proposed controller, a comparison is carried out against the well-known type-1 fuzzy logic control technique.

The aforementioned nominal parameter values are used to assess the ability of type-2 FLC to cope with rules and membership function uncertainties. The elevation and azimuth angle reference signals are set to $\psi^* = 0.5$ rad and $\varphi^* = 0$ rad, respectively. The advantage behind the use of the type-2 fuzzy logic controller is clearly shown in Fig. 5.3 by a better tracking performance. The tracking error under type-1 FLC is fairly fluctuating as opposed to a smoother and steady convergence behavior with the type-2 FLC. On the

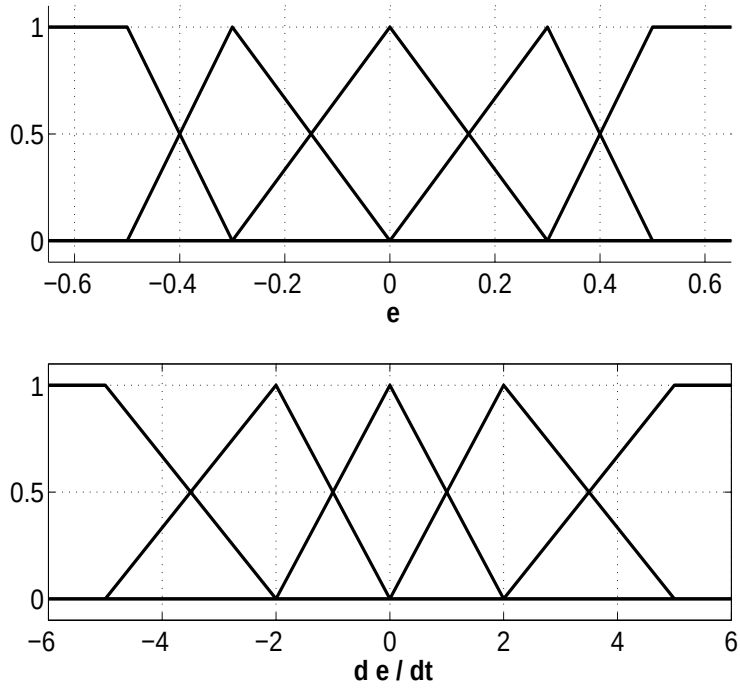

(a)

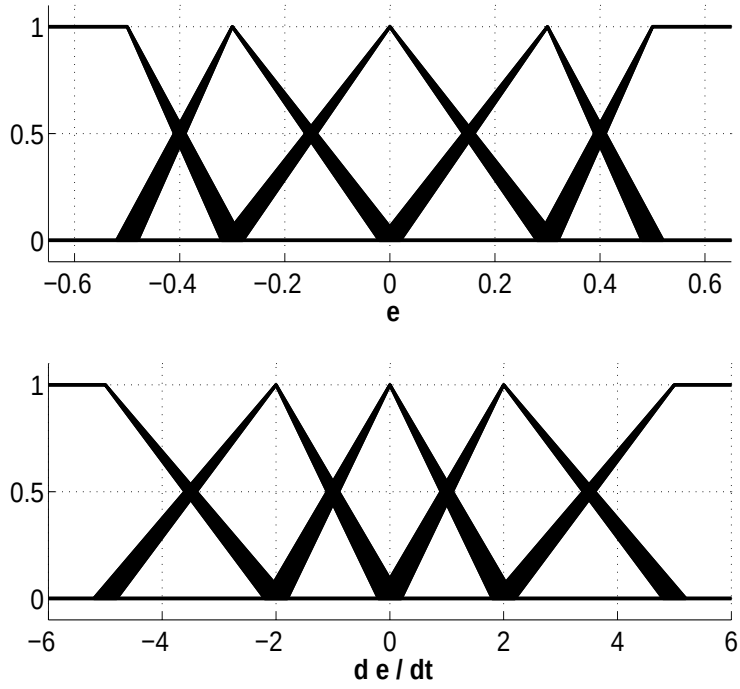

(b)

Figure 5.2: Fuzzy membership functions: (a) type-1; and (b) type-2.

other hand, the type-2 controller is also able to generate high quality control, which yields less oscillations.

Next, the elevation reference angle is set to $\psi^* = 0$ rad and its azimuth counterpart is set to $\varphi^* = 0.5$ rad. As shown in Fig. 5.4, the strong coupling between both angles causes a deviation of the elevation angle from its initial value. This effect is only shown on the type-1 fuzzy logic controller response. Unlike type-1 FLC, the proposed type-2 control method achieves faster and more accurate tracking.

Then, the reference signals of both angles are set to $\psi^* = \varphi^* = 0.5$ rad. Results are depicted in Fig. 5.5. In this case, type-1 FLC shows much slower and oscillatory tracking while type-2 FLC demonstrates a higher ability in providing a better transient response. The high nonlinearities of the TRMS coupled with its complex dynamics make accurate control performance difficult to keep in all operating conditions.

It is important to note that the performance of the type-1 FLC can be further improved by conducting an empirical tuning procedure of the rules and the input membership function parameters. Type-1 fuzzy logic systems (FLSs) are known for their ability to compensate for structured and unstructured uncertainties, to a certain degree. However, type-2 fuzzy engines have been credited to be more powerful in compensating for even higher degrees of uncertainties. As such, they also provide more flexibility to alleviate the problems associated to the uncertainties pertaining to the choice of the system's fuzzy rules and fuzzy membership functions. Conventional type-1 FLSs can be used to identify the behavior of highly nonlinear systems with various types of uncertainties. However, type-1 fuzzy sets cannot fully capture the uncertainties in the system due to membership functions and knowledge base imprecision. Hence, higher types of fuzzy sets have to be considered. Unlike a type-1 fuzzy set where the membership grade is a crisp value, the membership functions of type-2 fuzzy sets are three dimensional functions, with what is known as the set's footprint of uncertainty (FOU) representing the third dimension. In fact, it is this FOU that provides type-2 FLSs with additional degrees of freedom and make it possible for them to directly model and handle more types of uncertainties with higher magnitudes than their type-1 counterparts.

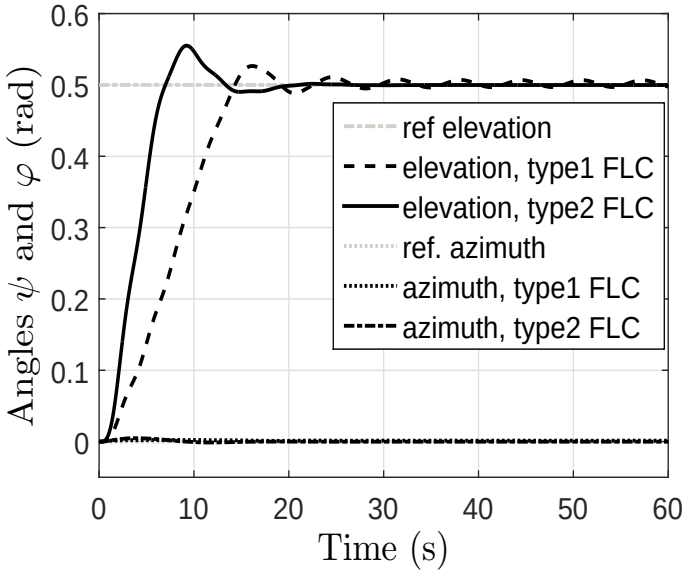

(a)

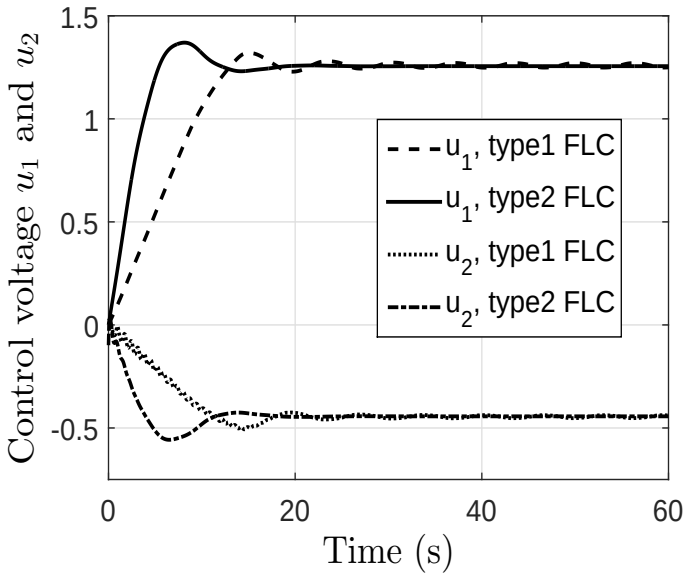

(b)

Figure 5.3: Step response for reference $\psi^* = 0.5$ rad and $\varphi^* = 0$ rad: (a) stabilizing performance, and (b) control inputs (main and tail motors' input voltages).

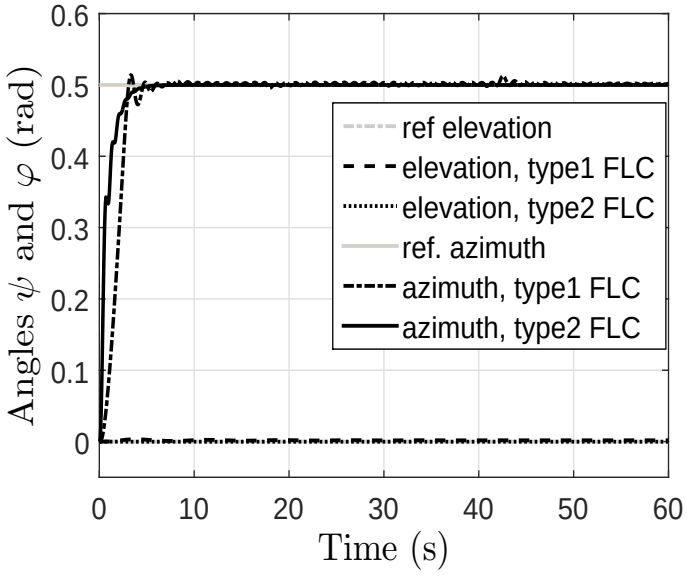

(a)

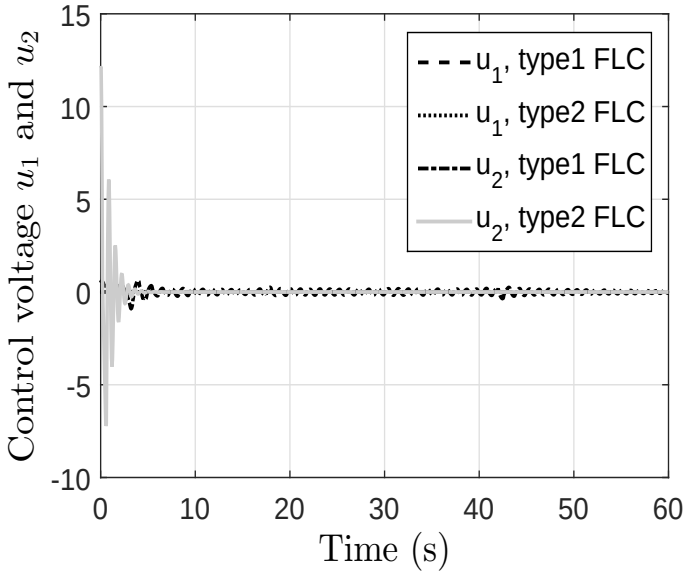

(b)

Figure 5.4: Step response for reference $\psi^* = 0$ rad and $\varphi^* = 0.5$ rad: (a) stabilizing performance, and (b) control inputs (main and tail motors' input voltages).

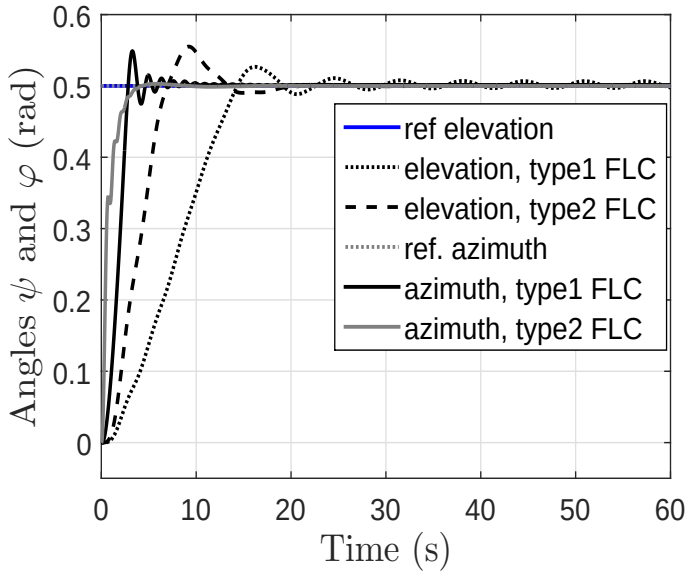

(a)

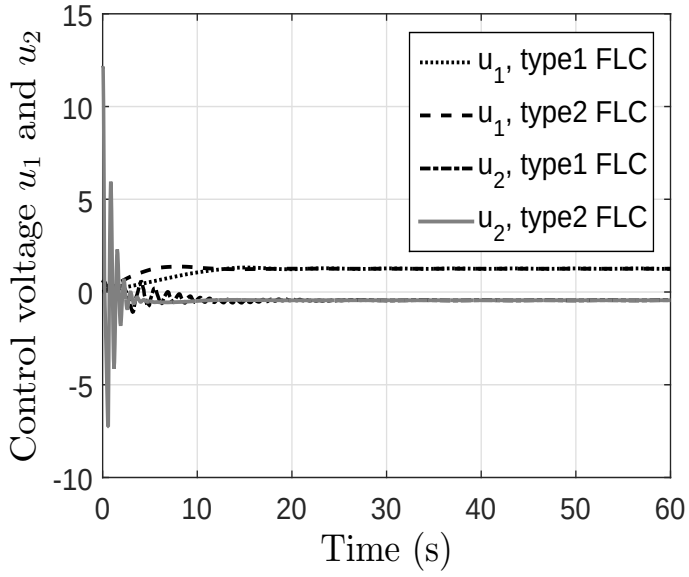

(b)

Figure 5.5: Step response for reference $\psi^* = 0.5$ rad and $\varphi^* = 0.5$ rad: (a) stabilizing performance, and (b) control inputs (main and tail motors' input voltages).

5.5 Conclusion

In this chapter, an interval type-2 fuzzy controller is developed for a TRMS. As such, the naturally inherited high computational complexity of conventional type-2 fuzzy systems is alleviated. A series of tests are carried-out to demonstrate the performance of the proposed control approach. The controller is also compared to its type-1 counterpart in similar operating conditions. Results show the superiority of type-2 FLC in compensating for high-magnitude uncertainties.

Chapter 6

Design and Realization of a Real-Time Control Platform for Quadrotor Unmanned Aerial Vehicles

6.1 Introduction

Quadrotors have become very popular due to their ability to maneuver in both difficult and dangerous conditions and thanks to recent developments in embedded systems, automatic control and artificial intelligence. They have become widely used for many applications such as surveillance, exploration, rescue missions and payload transportation [7]. Reliable positioning and autonomous navigation are fundamental for their use in abundance in everyday real-life applications [39, 37]. Unlike helicopters that use a single main rotor, quadrotors use four rotors making them to have better fault tolerance [23]. However, stabilizing the quadrotor is not an easy task to undertake. They exhibit complex nonlinear and unstable open-loop dynamics. The severe nonlinearities, coupling, varying operating conditions, structured and unstructured uncertainties, and external disturbances are among the typical challenges to be faced.

Similar to aircrafts, quadrotor motion also consists of controlling the pitch, yaw and roll. However, the unique body structure of quadrotors makes the pitch, yaw and roll dynamics strongly coupled [38]. Therefore, controlling them is not trivial. Various control approaches have been proposed for quadrotors [26, 80, 18], including classical, robust and adaptive control laws. Among popular methods, input-output linearization and back-stepping are used for their simplicity. However, linearization does not guarantee the stability in all operating conditions. Moreover, they suffer from sensitivity to parameter variations. So, modeling the system's dynamics based on presumably accurate mathematical models cannot be ap-

plied efficiently in this case. This raises the urgency to consider alternative approaches for the control of this type of systems to keep up with their increasingly demanding design requirements.

Studies have shown that the design of robust controllers for mathematically ill-defined systems that may be subjected to structured and unstructured uncertainties is made possible with computational intelligence tools, such as artificial neural networks and fuzzy logic controllers [20]. The approximation capabilities have been the main driving force behind the increasing popularity of such methods as they are theoretically capable of uniformly approximating any continuous real function to any degree of accuracy [15]. This has led to the recent advances in the area of intelligent control [10, 13]. Satisfactory performance is achieved with various neural network models for complex systems control [18, 21], providing an alternative to conventional control techniques.

This chapter introduces a real-time control platform for quadrotor UAVs. The control framework is meant to be universal but yet flexible to allow implementation of various control and navigation algorithms. The proposed design approach is modular, which favors versatility. System identification is carried out to determine the system's parameters. In addition, a wireless communication unit is designed for remote control and monitoring from a ground station graphical user interface, which simplifies diagnostic. The proposed quadrotor control platform is cost effective, and it is a powerful maquette for a variety of controllers. The performance of the developed control platform is shown by simulation and experiment through PID control implementation. The remaining part of the chapter is organized as follows: Section 6.2 outlines the dynamic model of quadrotor UAVs. The real-time control platform is detailed in Section 6.3 and system identification is presented in Section 6.4. The control strategy is presented in Section 6.5. In Section 6.6, simulation and experimental results are reported and discussed. We conclude with a few remarks.

6.2 Dynamics

The quadrotor depicted in Fig. 6.1 consists of a six degree-of-freedom (DOF) body actuated by four propellers [12]. The four rotors provide upwards propulsion as well direction control. The system consists of two opposite rotor pairs, one rotating clockwise while the other rotates counter clockwise for balance. The difference between the two pairs speed generates either positive or negative yaw acceleration. On the other hand, pitch and roll accelerations are achieved by increasing and decreasing opposite rotors. The dynamic mathematical model based on Euler-Lagrange formulation can be described by the

following equations [26]:

$$\ddot{x} = \frac{1}{m}(\cos\phi\sin\theta\cos\psi + \sin\phi\sin\psi)u_1 \tag{6.1a}$$

$$\ddot{y} = \frac{1}{m}(\cos\phi\sin\theta\sin\psi - \sin\phi\cos\psi)u_1 \tag{6.1b}$$

$$\ddot{z} = -g + \frac{1}{m}(\cos\phi\cos\theta)u_1 \tag{6.1c}$$

$$\ddot{\phi} = \frac{I_y - I_z}{I_x}\dot{\theta}\dot{\psi} - \frac{J_r}{I_x}\dot{\theta}\Omega_r + \frac{l}{I_x}u_2 \tag{6.1d}$$

$$\ddot{\theta} = \frac{I_z - I_x}{I_y}\dot{\phi}\dot{\psi} + \frac{J_r}{I_y}\dot{\phi}\Omega_r + \frac{l}{I_y}u_3 \tag{6.1e}$$

$$\ddot{\psi} = \frac{I_x - I_y}{I_z}\dot{\theta}\dot{\phi} + \frac{1}{I_z}u_4 \tag{6.1f}$$

where,

$m \in \mathbb{R}$:	mass of the quadrotor
$l \in \mathbb{R}$:	length from the rotors to the center of mass
$g \in \mathbb{R}$:	gravitational constant
$\phi \in \mathbb{R}$:	roll angle of the quadrotor
$\theta \in \mathbb{R}$:	pitch angle of the quadrotor
$\psi \in \mathbb{R}$:	yaw angle of the quadrotor
$u_i \in \mathbb{R}$:	control inputs
$J_r \in \mathbb{R}$:	moments of inertia of the propeller blades
$\Omega_r \in \mathbb{R}$:	angular velocity of the propeller blades
$I_x, I_y, I_z \in \mathbb{R}$:	moments of inertia of the quadrotor

The system has four inputs (u_1, u_2, u_3, u_4) and six outputs (x, y, z, ϕ, θ, ψ). The control input u_1 provides thrust on the body in the z-axis, u_2 and u_3 are the roll and pitch inputs and u_4 is used for yaw control. These inputs $u_i \in \mathbb{R}$ can be written in terms of rotor

speeds $\Omega_i \in \mathbb{R}$, $i = 1, \ldots, 4$ [83]:

$$u_1 = b(\Omega_1^2 + \Omega_2^2 + \Omega_3^2 + \Omega_4^2) \tag{6.2a}$$
$$u_2 = b(\Omega_2^2 - \Omega_4^2) \tag{6.2b}$$
$$u_3 = b(\Omega_3^2 - \Omega_1^2) \tag{6.2c}$$
$$u_4 = b(\Omega_1^2 - \Omega_2^2 + \Omega_3^2 - \Omega_4^2) \tag{6.2d}$$
$$\Omega_r = \Omega_2 + \Omega_4 - \Omega_1 - \Omega_3 \tag{6.2e}$$

where b and d are the thrust and drag coefficients, respectively.

Assumption 1 *The body of the quadrotor is assumed to be rigid and symmetric along x, y and z axes.*

Remark 1 *It is noteworthy that the aerodynamic forces and moments are ignored at low speed. These effects are very hard to model, in particular vortex ring state, blade flapping and slip stream of rotors. However, it is reasonable to neglect the aerodynamic effects at low speed for simplicity [97].*

Figure 6.1: GAUI 330 X-S quad flyer.

6.3 Real-Time Control Platform Design

This work aims to develop a quadrotor system capable of autonomous hovering and communication with a control station. For this purpose, various sensors are required to provide the control unit (i.e., microprocessor) with feedback signals through a data acquisition card.

As such, developed feedback control law, localization and navigation algorithms can be implemented in the embedded board and their performance can be evaluated with real-world data. Since the system is also required to have communication capabilities with a ground station, a communication card needs to be installed as well onboard. Moreover, a power interface is necessary between actuators and the embedded board. In this section, a modular architecture, depicted in Fig. 6.2, is proposed to meet the aforementioned requirements, which is divided into three categories:

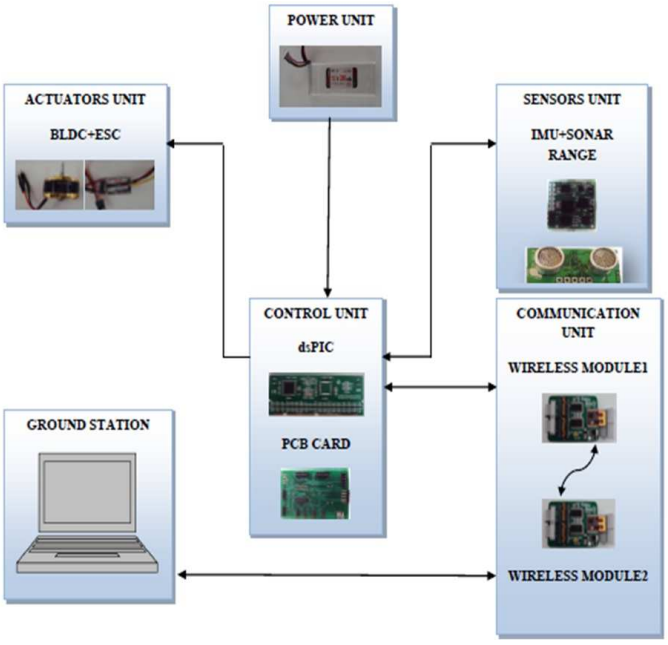

Figure 6.2: Platform architecture.

6.3.1 Hardware

While some engineers and researchers design and build their own quadrotor mechanical structure [95, 42, 50], others prefer to use the so many commercially available platforms such as, Dragan flyer, X-UFO and MD4-200. Since mechanical design is out of the scope of this work, GAUI 330 X-S quad flyer (Fig. 6.1) is purchased for this project at a reasonable price to shorten shortens development time.

The performance of feedback control laws depends significantly on accurate knowledge of quadrotor states. However, accurate sensors for quadrotor altitude, acceleration, global position and other relevant data for the control are costly. The designed sensors' unit makes use of micro-electromechanical systems (MEMS) technology with low-cost sensors.

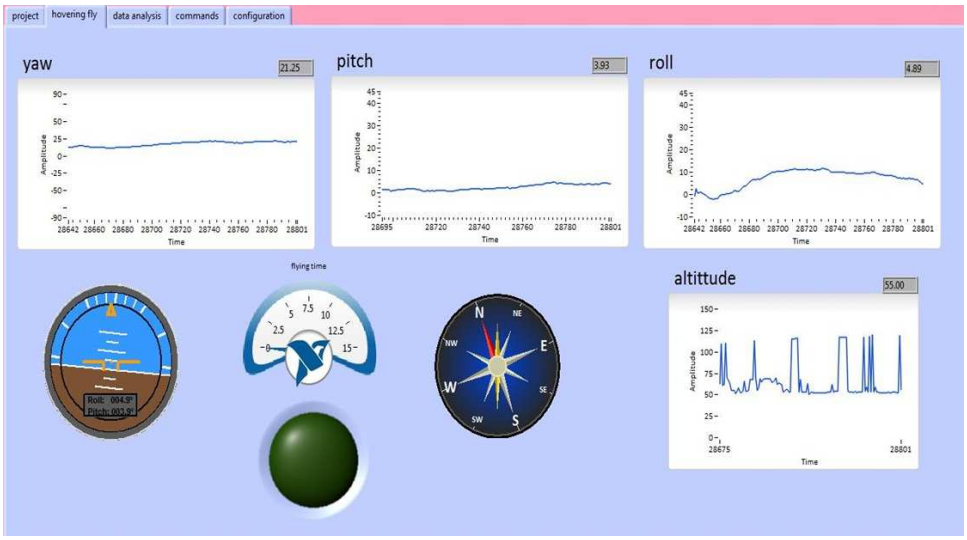

Figure 6.3: Illustration of the ground station interface.

Micro-electromechanical systems (MEMS), however, results in low precision data which yields a weak drift rejection. This imperfection makes control more challenging. This makes of the platform an adequate benchmark to compare the performance of different kinds of controllers.

Various inertial measurement devices are available on the market such as, MT9-B from Xsens and the 3DM-GX1 from Microstrain. Although expensive, both of them offer a good performance and are widely used in many applications. To keep up with our low-cost requirement, CHR-6dm inertial measurement device from CHRobotics is selected for the sensors' unit. Similarly, Devantech sonar range finder (SRF-10) is designated for the project. It is the most popular choice due to its high flexibility of configuration and simple interface on an inter-integrated circuit (I2C) bus, providing measurement at 15 Hz rate.

Actuators unit, on the other hand, receives control signals from the control unit to drive actuators and adjust quadrotor position and orientation. This unit is composed of motors and its associate electronics. In this project, four 40 g brushless dc motors and their electronic speed controllers (ESCs) are provided with the GAUI 330x kit. These motors are rated for 11655 RPM nominal speed and their ESCs weight is 9 g and of small size that can support current up to 10A from various battery types. The PWM switching frequency can be set up to 400 Hz, the fact which yields reduced motor vibration and good control performance.

As for the power unit, it provides necessary power for all units. It is recommended to choose a light weight rechargeable battery to minimize the power consumption and increase the flight time. Nickel Cadmium (NiCd), Nickel Metal Hydride (NiMh) and Lithium

Polymer (Li-Po) are among the most popular batteries in drone applications, especially for quadrotors and helicopters. In this work, Lithium-ion Polymer GAUI 3s (LiPo3s) battery is used for its performance. Moreover, its dimension and weight (150 g) are a perfect fit with our prototype. It is 11 V battery with 2000mAh capacity at discharging rate of 20C.

6.3.2 Communication

The quadrotor is able to communicate with a ground station through a communication unit. Therefore, two modules (i.e., sender and receiver) are needed to perform telemetry and control operations. Several wireless protocols exist but Zigbee is the most suitable for our application due to its low power consumption and acceptable transmission speed. Zigbee protocol is a wireless network protocol designed specifically for low data rate sensors and control networks [1]. Among available products, Xbee module communicates at a rate up to 250 $Kbps$. However, communication with the host controller is done through serial interface. Therefore, faster wireless module is needed to minimize the execution time of the control loop. In this work, Easybee3 module from Mikroelektronika is used for also its compatibility with MRF24J40MA transceiver from microchip. This module has a SPI bus, which allows communication faster than UART bus implemented on the Xbee.

6.3.3 Software

Stabilization, which is achieved by the control unit, is fundamental for a quadrotor system. In this work, dsPIC 128gp710 from microchip is used to implement control laws and acquire sensors data. Moreover, a PCB board is designed to interface the MCU, sensors and built-in ESCs. This card is equipped with 3.3V voltage regulator to power the MCU. Therefore, control and navigation algorithms can be developed and implemented for their experimental validation. Using Labview, a ground station, which is depicted in Fig. 6.3, is developed. It allows bidirectional communication with the quadrotor. As such, quadrotor data is sent to the ground station and displayed in a graphical user interface and remote control signals are sent back for teleoperation. This is useful for control, analysis, monitoring, and system identification. In addition, a PIC18F4520 is connected to a personal computer (PC) through a serial port to read received data from the Zigbee module to be displayed in the GUI. The quadrotor simulator OS4 presented in [6] is used to examine its dynamic behavior. This simulator is modified to include ESCs and motors dynamics. The resultant Simulink model is used for simulation.

6.4 System Identification

Several parameters in the model need to be identified. In this section, quadrotor parameters are identified either by measurements or experiments (Table 6.1) and are then used for control design and simulation. The parameter identification methods are briefly discussed because it is not the focus of the present work. For inertia moments calculation, it is required to identify the dynamic behavior of the quadrotor in rotation around a given axis. Since the body of the quadrotor is symmetric (assumption 1), inertia moments can be represented by a diagonal matrix. On the other hand, the quadrotor is equipped with four nylon propellers driven by four brushless dc motors. In order to control rotational speed of propellers to stabilize the quadrotor, we need to find first the relationship between the rotational speed of each propeller and its generated lift force. Since all motors are considered identical, identification is performed on a single motor for simplicity. Thus, the characteristic of the motors is identified by mounting a permanent magnet on the motor's rotor and by placing close to it a Hall Effect sensor. Then, an additional weight is added to prevent the structure from being lifted by the vertical force of the propeller. By placing the system on an electronic balance as it is shown in Fig. 6.4, the propeller lift force is measured through differential readings. It is noteworthy that mass and length can be directly measured.

Figure 6.4: Trust factor experiment testbed.

6.5 Control Strategy

To demonstrate the performance of the developed quadrotor platform, a controller is designed for altitude and attitude stabilization. The model (6.1) is used to write the system

in a state-space form $\dot{q} = f(q, u)$, where $u = [u_1, u_2, u_3, u_4]^T$ is the inputs vector and $q = [\dot{z}, \dot{\phi}, \dot{\theta}, \dot{\psi}]^T$ is the state vector. Therefore, the quadrotor dynamics is written as:

$$\ddot{z} = -g + \frac{1}{m}(\cos\phi\cos\theta)u_1 \tag{6.3a}$$

$$\ddot{\phi} = \frac{I_y - I_z}{I_x}\dot{\theta}\dot{\psi} - \frac{J_r}{I_x}\dot{\theta}\Omega_r + \frac{l}{I_x}u_2 \tag{6.3b}$$

$$\ddot{\theta} = \frac{I_z - I_x}{I_y}\dot{\phi}\dot{\psi} + \frac{J_r}{I_y}\dot{\phi}\Omega_r + \frac{l}{I_y}u_3 \tag{6.3c}$$

$$\ddot{\psi} = \frac{I_x - I_y}{I_z}\dot{\theta}\dot{\phi} + \frac{1}{I_z}u_4 \tag{6.3d}$$

The control objective is to design a control law $u \in \mathbb{R}^4$ to force the quadrotor state $q \in \mathbb{R}^4$ to track its pre-defined time-dependent desired value $q_d \in \mathbb{R}^4$ as $t \to \infty$ for any initial condition x_0. In this work, the controller uses (z, ϕ, θ, ψ) $\in \mathbb{R}^4$ as system's measurable states. For that, let's define $e_z = z_d - z$, $e_\phi = \phi_d - \phi$, $e_\theta = \theta_d - \theta$, $e_\psi = \psi_d - \psi$ as state errors. Therefore, PID control is used to track these errors to zero with the following control law:

$$u_1 = k_{pz}e_z + k_{iz}\int e_z + k_{dz}\frac{d}{dt}e_z \tag{6.4a}$$

$$u_2 = k_{p\phi}e_\phi + k_{i\phi}\int e_\phi + k_{d\phi}\frac{d}{dt}e_\phi \tag{6.4b}$$

$$u_3 = k_{p\theta}e_\theta + k_{i\theta}\int e_\theta + k_{d\theta}\frac{d}{dt}e_\theta \tag{6.4c}$$

$$u_4 = k_{p\psi}e_\psi + k_{i\psi}\int e_\psi + k_{d\psi}\frac{d}{dt}e_\psi \tag{6.4d}$$

where $k_{p\bullet}$, $k_{i\bullet}$ and $k_{d\bullet}$ are the proportional, integral and derivative control gains, respectively.

The destabilizing effect of nonlinearities can have negative consequences, such as severe tracking errors, limit cycles, chattering, excessive noise and can even lead to instability. For instance, actuator saturation occurs with a large change in setpoint or when starting the system with significant initial conditions [9]. Consequently, the integral term accumulates a significant error during the rise, which is known as windup. Therefore, the anti-windup algorithm is used to cope with actuators saturation [6]. In this algorithm, e is the error of the controlled variable, x_i is the integral action, u is the control input, $\epsilon_\bullet$ is a threshold and T_s is the sampling time.

Algorithm 1: anti-windup

```
begin
    if |e| > ε1 then
        Set x_i = x_i − 1
    else
        if u < ε2 and x_i < ε3 then
            Set x_i = x_i − 1 + (e T_s)
        else
            if (u x_i) > 0 then
                Set x_i = 0
```

6.6 Simulation and Experimental Results

6.6.1 Setup

A simulation and an experiment are carried out on a quadrotor. Table 6.1 summarizes the quadrotor's physical parameters along with their respective values. PID control coefficients are set to $k_{pz} = 5$, $k_{iz} = 0.3$, $k_{dz} = 0.5$, $k_{p\phi} = k_{p\theta} = k_{p\psi} = 3$, $k_{i\phi} = k_{i\theta} = k_{i\psi} = 0.5$, $k_{d\phi} = k_{d\theta} = k_{d\psi} = 1.5$ and the gravitational constant is set to $g = 9.8$ m/s^2. The controller is set to operate at a bandwidth of 200 Hz. For each simulation and experiment, the system's response is studied taking into account the quadrotor's angles (roll, pitch, yaw) and altitude.

Table 6.1: Quadrotor's physical parameters.

Parameter	Value	Unit
Mass	0.68	(kg)
Arm length	0.18	(m)
Thrust coefficient	$6.9 \cdot 10^{-6}$	(N·s^2)
Drag coefficient	$9.3 \cdot 10^{-8}$	(N·m·s^2)
Motor inertia	$4 \cdot 10^{-6}$	(kg·m^2)
Propeller inertia	$1 \cdot 10^{-5}$	(kg·m^2)
Rotor inertia	$1.4 \cdot 10^{-5}$	(kg·m^2)
Inertia on x axis	$3.5 \cdot 10^{-3}$	(kg·m^2)
Inertia on y axis	$4.2 \cdot 10^{-3}$	(kg·m^2)
Inertia on z axis	$7.5 \cdot 10^{-3}$	(kg·m^2)
Twist pitch	0.07	(rad)
Pitch of incidence	0.35	(rad)
Propeller chord	$1.8 \cdot 10^{-2}$	(kg)

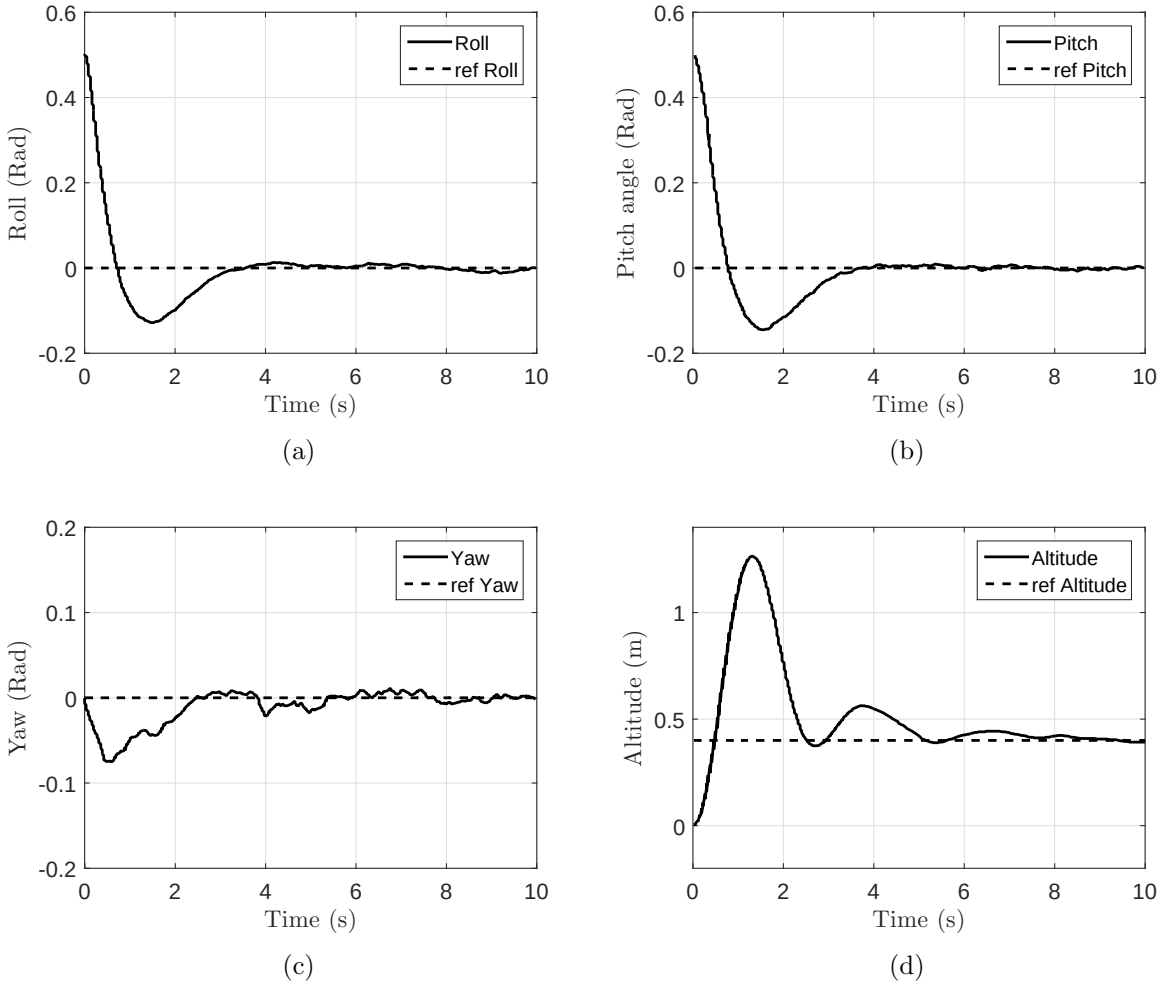

Figure 6.5: Quadrotor platform's simulation: (a) roll; (b) pitch; (c) yaw; and (d) quadrotor's altitude.

6.6.2 Simulation Results

A simulation is carried out to study the developed quadrotor platform's performance. In the first simulation, the aforementioned quadrotor parameter values are used to simulate the system's dynamics. The desired angles are all set to zero, which corresponds to quadrotor horizontal orientation. However, the altitude is set to 40 cm. The altitude controller is composed of two parts: the first which is a constant gain equal to the quadrotor weight to compensate the gravity effect. The second part is the PID controller. It is noteworthy that the controller output is scaled with the factor of $\cos\phi\cos\theta$, which reduces the coupling effect between roll and pitch angles. As it is shown in Fig. 6.5, the quadrotor's angles and altitude errors decay gradually before stabilizing within acceptable amplitude. It is important to note the relatively slow convergence on the altitude (i.e., 8 sec) and its oscillations. This is due to the severe nonlinearities associated with quadrotors that cannot be easily compensated by a linear controller.

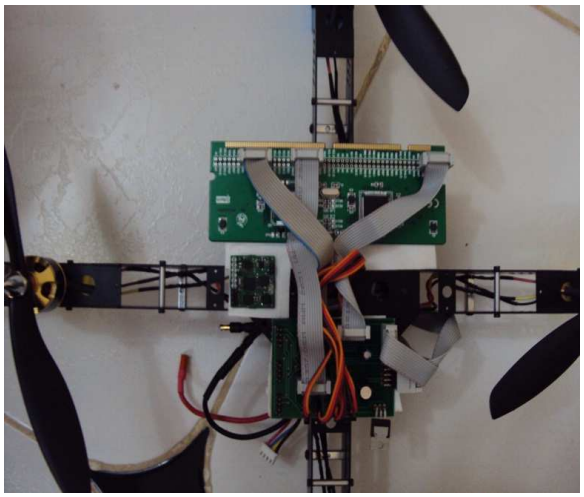

Figure 6.6: Assembled structure.

6.6.3 Experimental results

An experiment is conducted on the developed quadrotor platform (Fig. 6.6). The desired angles are all set to zero for quadrotor horizontal orientation and the altitude is set to 50 cm. Experimental results are depicted in Fig. 6.7. As it is observed, the quadrotor's angles and altitude errors are maintained in the vicinity of zero to obtain a better accuracy for roll and pitch angles. Then, a set of disturbances are introduced manually at $t = 27, 34, 40, 44$ sec for roll angle and at $t = 33, 52, 56$ sec for pitch angle. Although the use of classical

PID control, all perturbations are rejected. Also, altitude control is maintained during disturbance.

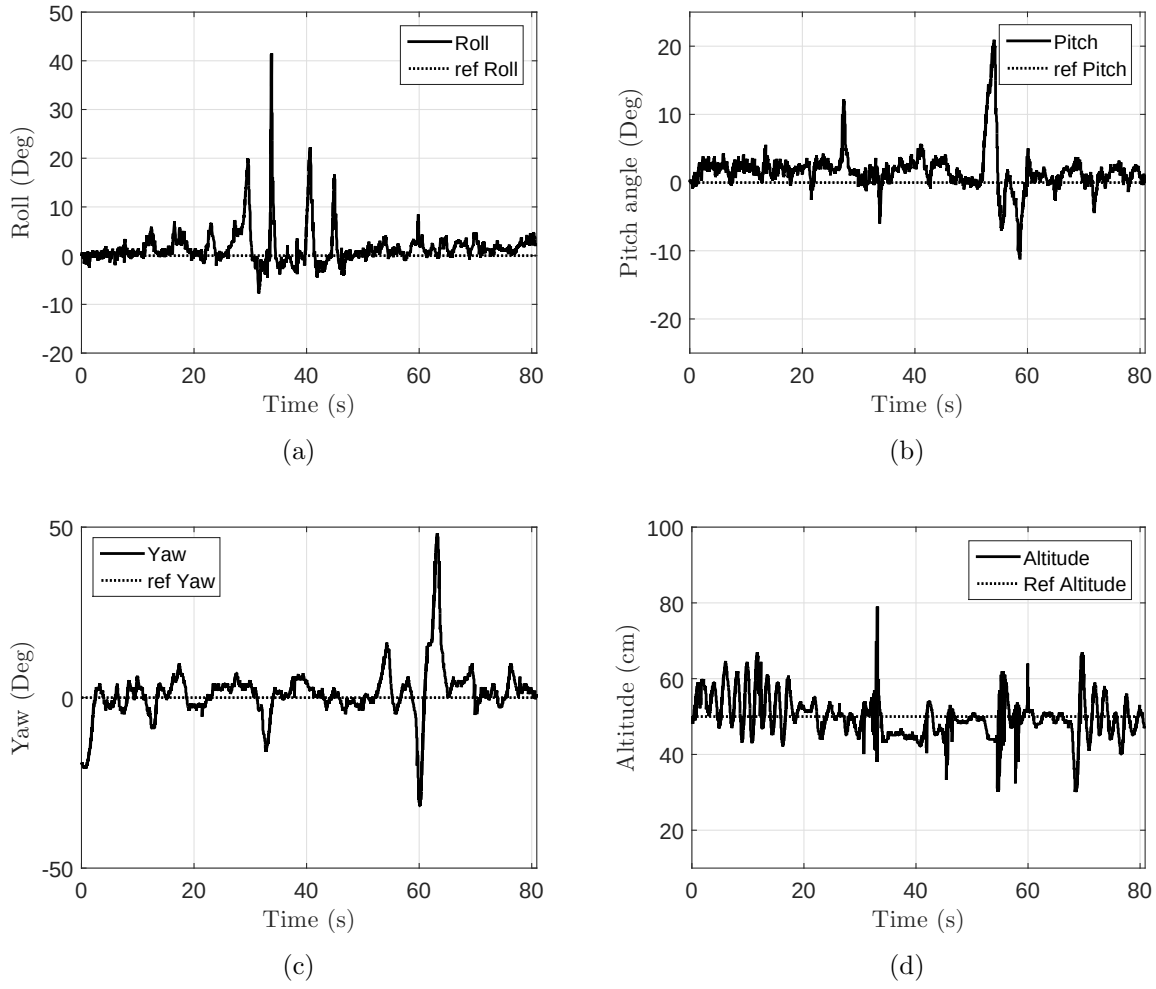

Figure 6.7: Quadrotor platform's experiment: (a) roll; (b) pitch; (c) yaw; and (d) quadrotor's altitude.

6.7 Conclusion

In this chapter, a universal, yet flexible, real-time control platform is designed for quadrotors. This approach allows implementation of various control and navigation algorithms while wireless remote control and monitoring simplify diagnostic. Moreover, the proposed design approach is modular, which makes it versatile. Selection of variety of sensors, communication devices and control boards is cost effective, and their imperfection provides

researchers with additional control challenges. Therefore, it can be used to show the efficiency of different kinds of controllers as it can be considered as a challenging prototype for many nonlinear control problems. In this work, a complete quadrotor system is realized and tested. PID control is chosen for implementation to evaluate the proposed platform's performance due its simplicity. Simulation and experimental results show acceptable control performance of the quadrotor's states (roll, pitch, yaw, altitude). Despite of nonlinearities, the system is successfully stabilized horizontally. A system's identification technique is presented and carried out to derive the system's parameters and coefficients which are then used for simulation. Regardless of modeling uncertainties, experimental results highlight the developed simulation model's accuracy.

Chapter 7

Conclusion and future works

7.1 Conclusion

This thesis is about the synthesis of robust control law for nonlinear multivariable uncertain systems. In fact, classical linear powerful approaches (H_2/H_∞) known for their robustness are applied. Yet the drawbacks are their unsuitability for nonlinear system, in that the performance of these approaches is guaranteed only around separate operating point. Basing on LMN and in order to maintain the obtained performance to a full system operating range, a controllers' network is introduced to ensure transitions between controllers within the network. The LMNs are used for their adaptive feature and their providing powerful combination of conventional linear control techniques. Nevertheless, LMNs are very challenging model knowledge based control techniques. Alternatively, an intelligent control (model free control) is suggested, where no a priori knowledge of system's parameters or dynamics is required.

An interval type-2 fuzzy control scheme is proposed. This strategy uses the effect of uncertainty which is modeled at the level of membership functions to achieve accurate tracking and robustness to both structured and unstructured uncertainties, i.e., this control scheme allows for the incorporation of uncertainty in the input membership levels. The proposed interval type-2 fuzzy controller is compared to type-1 fuzzy control, and it has shown that the former are better able to handle uncertainties than the latter.

Quadrotor as a complete universal flexible real-time control platform, which allows implementation of various control and navigation algorithms, is designed and then realized. Control platform is to eventually used to enhance varied types of controllers, as it could be considered as a scale model for many serious nonlinear control problems. Due to its simplicity, PID control is implemented to evaluate the proposed platform's performance.

Yet, PID is not widely dealt with in the present research because it is not the subject of the foci in this thesis; it is to be let for further future research.

Two types of nonlinear aerodynamic twin rotor multi input multi output (MIMO), the CE-150 and TRMS 33-949 helicopters which are a good example of a highly coupled nonlinear system perturbed by mismatched uncertainty, has been introduced. The models of the systems have been detailed, and Simulation models have been provided. The analysis of these provided models confirm that the systems are multivariable two degree-of-freedom (DOF) and strong cross-coupling. The twin rotor is, therefore, a good example for complex nonlinear multivariable control systems which could not be easily handled by classical control for full range of operating area. This is the reason why new robust controls approaches for full range operation systems are required.

In all the above mentioned robust control techniques, the application of these techniques for the proposed systems (TRMS and CE-150) has given excellent responses when handling uncertainties. In fact, the carried out tests demonstrate that the performance of the proposed control approach LMN and Type 2 FLC provide the desired trajectories of both azimuth and elevation angles which are achieved with satisfactory asymptotic errors. They also ensure the decoupling of the system dynamics and good performance. While the fuzzy approach shows the superiority of type-2 FLC in compensating for high-magnitude uncertainties than Type 1 FLC.

7.2 future works

The thesis writing process has provided me with a certain maturity, and thus raised in my mind some new ideas which might be considered as a platform whereby a new research based on the outcomes could be started.

In fact, myself, I realized after finishing the thesis that it is not enough and even important not to limit the scope of research to the Local Model Network because I have noticed that the Switching mechanism in LMN could be realized by Fuzzy Logic Rules. This is why it is necessary to conduct new research with new directions such as: Fuzzy local model network. Furthermore, intelligent methods are important for they are non model based.

In addition to fuzzy type-2 which was dealt with in present work, an adaptive feature will be useful and advantageous to more handle uncertainties and performance. So, adaptive fuzzy logic interval type-2 control will make a suitable subject for a potential future research avenue.

Implementation of controls methods in real time systems, which were theoretically validated in this thesis through simulation, would be tested experimentally.

Since the developed quadrotor's platform was validated successfully, a need for the implementation of a robust control design becomes prerequisite, and thus a new research avenue is suggested.

References

[1] J. Afruz and M. S. Alam. Non-linear modeling of a twin rotor system using particle swarm optimization. In *Computer Symposium (ICS), 2010 International*, pages 1026–1032, Dec 2010.

[2] Nasir Uddin Ahmed. *Dynamic systems and control with applications*. World Scientific, 2006.

[3] A. Badnjevi, E. uni, T. Uzunovi, and N. Osmi. Design and implementation of three-dimensional simulator for control of laboratory model helicopter. In *MIPRO, 2010 Proceedings of the 33rd International Convention*, pages 1362–1367, May 2010.

[4] T.D. Batzel and K.Y. Lee. An approach to sensorless operation of the permanent-magnet synchronous motor using diagonally recurrent neural networks. *IEEE Transactions on Energy Conversion*, 18(1):100–106, mar 2003.

[5] Alexander Bogdanov and Eric A Wan. State-dependent riccati equation control for small autonomous helicopters. *Journal of guidance, control, and dynamics*, 30(1):47–60, 2007.

[6] S. Bouabdallah. *Design and Control of Quadrotors with Application to Autonomous Flying*. PhD thesis, EPFL, 2006.

[7] D. Cabecinhas, R. Naldi, L. Marconi, C. Silvestre, and R. Cunha. Robust take-off for a quadrotor vehicle. *IEEE Transactions on Robotics*, 28(3):734–742, June 2012.

[8] D. Cabecinhas, R. Naldi, L. Marconi, C. Silvestre, and R. Cunha. Robust Take-Off for a Quadrotor Vehicle. *IEEE Transactions on Robotics*, 28(3):734–742, June 2012.

[9] A. Chamseddine, Y. Zhang, C.A. Rabbath, C. Join, and D. Theilliol. Flatness-Based Trajectory Planning/Replanning for a Quadrotor Unmanned Aerial Vehicle. *IEEE Transactions on Aerospace and Electronic Systems*, 48(4):2832–2848, Oct. 2012.

[10] H. Chaoui and W. Gueaieb. Type-2 Fuzzy Logic Control of a Flexible-Joint Manipulator. *Journal of Intelligent and Robotic Systems*, 51(2):159–186, Feb. 2008.

[11] H. Chaoui, W. Gueaieb, M. Biglarbegian, and M.C.E. Yagoub. Computationally Efficient Adaptive Type-2 Fuzzy Control of Flexible-Joint Manipulators. *Robotics*, 2(2):66–91, May 2013.

[12] H. Chaoui and P. Sicard. Adaptive Fuzzy Logic Motion and Posture Control of Inverted Pendulums with Unstructured Uncertainties. In *IEEE Automation Science and Engineering International Conference*, 2010.

[13] H. Chaoui and P. Sicard. Adaptive fuzzy logic control of permanent magnet synchronous machines with nonlinear friction. *IEEE Transactions on Industrial Electronics*, 59(2):1123–1133, Feb 2012.

[14] H. Chaoui and P. Sicard. Adaptive Fuzzy Logic Control of Permanent Magnet Synchronous Machines with Nonlinear Friction. *IEEE Transactions on Industrial Electronics*, 59(2):1123–1133, Feb. 2012.

[15] H. Chaoui and P. Sicard. Neural Network Modeling of Cold-Gas Thrusters for a Spacecraft Formation Flying Test-bed. In *IEEE Conference on Industrial Electronics Society*, 2012.

[16] H. Chaoui, P. Sicard, and W. Gueaieb. Ann-based adaptive control of robotic manipulators with friction and joint elasticity. *IEEE Transactions on Industrial Electronics*, 56(8):3174–3187, Aug 2009.

[17] H. Chaoui, P. Sicard, and W. Gueaieb. ANN-Based Adaptive Control of Robotic Manipulators with Friction and Joint Elasticity. *IEEE Transactions on Industrial Electronics*, 56(8):3174–3187, Aug. 2009.

[18] C. Coza and C. J. B. Macnab. A new robust adaptive-fuzzy control method applied to quadrotor helicopter stabilization. In *NAFIPS 2006 - 2006 Annual Meeting of the North American Fuzzy Information Processing Society*, pages 454–458, June 2006.

[19] C. Coza and C.J.B. Macnab. A New Robust Adaptive-Fuzzy Control Method Applied to Quadrotor Helicopter Stabilization. In *Annual meeting of the North American Fuzzy Information Processing Society (NAFIPS)*, pages 454–458, 2006.

[20] C. W. de Silva. *Intelligent Control Fuzzy Logic Applications*. CRC Press, 1995.

[21] T. Dierks and S. Jagannathan. Output feedback control of a quadrotor uav using neural networks. *IEEE Transactions on Neural Networks*, 21(1):50–66, Jan 2010.

[22] T. Dierks and S. Jagannathan. Output Feedback Control of a Quadrotor UAV Using Neural Networks. *IEEE Transactions on Neural Networks*, 21(1):50–66, Jan. 2010.

[23] X. Ding and Y. Yu. Motion planning and stabilization control of a multipropeller multifunction aerial robot. *IEEE/ASME Transactions on Mechatronics*, 18(2):645–656, April 2013.

[24] X. Ding and Y. Yu. Motion Planning and Stabilization Control of a Multipropeller Multifunction Aerial Robot. *IEEE/ASME Transactions on Mechatronics*, 18(2):645–656, Oct. 2013.

[25] J.C. Doyle, Keith Glover, P.P. Khargonekar, and B.A. Francis. State-space solutions to standard h_2 and h_∞ control problems. *IEEE Transactions on Automatic Control*, 34(8):831–847, Aug 1989.

[26] Z. T. Dydek, A. M. Annaswamy, and E. Lavretsky. Adaptive control of quadrotor uavs: A design trade study with flight evaluations. *IEEE Transactions on Control Systems Technology*, 21(4):1400–1406, July 2013.

[27] Z.T. Dydek, A.M. Annaswamy, and E. Lavretsky. Adaptive Control of Quadrotor UAVs: A Design Trade Study With Flight Evaluations. *IEEE Transactions on Control Systems Technology*, 21(4):1400–1406, July 2013.

[28] Johnson E.N., Christmann C., Christophersen H., and WU A. Guidance, navigation, control, and operator interfaces for small rapid response unmanned helicopters. In *AHS 64th Annual Forum and Technology Display*, apr 2008.

[29] SI J. Enns R. Helicopter trimming and tracking control using direct neural dynamic programming. *IEEE Transactions on Neural Network*, 14(4):929–939, 2003.

[30] A.L. Fradkov, B. Andrievsky, and Dimitri Peaucelle. Estimation and control under information constraints for laas helicopter benchmark. *Control Systems Technology, IEEE Transactions on*, 18(5):1180–1187, Sept 2010.

[31] Bruce A. Francis. A course in H_∞ control theory. Lecture Notes in Control and Information Sciences, 1987.

[32] Tee K.P. Ge S.S., Ren B. Adaptive neural network control of helicopters with unknown dynamics. In *Proc. 45th IEEE Conf. on Decision and Control*, pages 3022–3027, dec 2006.

[33] M. Golob and B. Tovornik. Identification of non-linear dynamic systems with decomposed fuzzy models. In *Systems, Man, and Cybernetics, 2000 IEEE International Conference on*, volume 5, pages 3520–3525 vol.5, 2000.

[34] M.J Grimble. Optimal h_∞ robustness and the relationship to lqg design problems. *International Journal of Control*, 43(2):351–372, 1986.

[35] M.J Grimble. Polynomial matrix solution of the standard state-feedback h_∞ control problem and relationship to the riccati equation state space solution. Research Report No. ICU/302, 1990.

[36] S. Grzonka, G. Grisetti, and W. Burgard. A Fully Autonomous Indoor Quadrotor. *IEEE Transactions on Robotics*, 28(1):90–100, Feb. 2012.

[37] S. Grzonka, G. Grisetti, and W. Burgard. A fully autonomous indoor quadrotor. *IEEE Transactions on Robotics*, 28(1):90–100, Feb 2012.

[38] N. Guenard, T. Hamel, and R. Mahony. A practical visual servo control for an unmanned aerial vehicle. *IEEE Transactions on Robotics*, 24(2):331–340, April 2008.

[39] B. J. N. Guerreiro, P. Batista, C. Silvestre, and P. Oliveira. Globally asymptotically stable sensor-based simultaneous localization and mapping. *IEEE Transactions on Robotics*, 29(6):1380–1395, Dec 2013.

[40] B.J.N. Guerreiro, P. Batista, C. Silvestre, and P. Oliveira. Globally Asymptotically Stable Sensor-Based Simultaneous Localization and Mapping. *IEEE Transactions on Robotics*, 29(6):1380–1395, Dec. 2013.

[41] H.A. Hagras. A hierarchical type-2 fuzzy logic control architecture for autonomous mobile robots. *IEEE Transactions on Fuzzy Systems*, 12(4):524–539, aug 2004.

[42] B. Herisse?, T. Hamel, R. Mahony, and F.-X. Russotto. Landing a VTOL Unmanned Aerial Vehicle on a Moving Platform Using Optical Flow. *IEEE Transactions on Robotics*, 28(1):77–89, Feb. 2012.

[43] Peter Horaek. Ce 150 helicopter model. Educational manual, 2004.

[44] Feedback Instruments. Twin rotor mimo system control experiments. 33-949s. *Feedback Instruments Ltd., Park Road, Crowborough, East Sussex, TN6 2QR, UK*, 1:89–101, 2006.

[45] Serrni A. Isidor A., Marconi L. Robust nonlinear motion control of a helicopter. *IEEE Transactions on Automatic Control*, 48(3):413–426, 2003.

[46] Kannan S.K. Johnson E.N. Adaptive flight control for an autonomous unmanned helicopter. In *AIAA Guidance, Navigation, and Control Conf. Exhibit*, aug 2002.

[47] Kannan S.K. Johnson E.N. Adaptive trajectory control for autonomous helicopters. *Journal of Guidance Control Dynamics*, 28(3):524–538, 2005.

[48] J. G. Juang, M. T. Huang, and W. K. Liu. Pid control using presearched genetic algorithms for a mimo system. *IEEE Transactions on Systems, Man, and Cybernetics, Part C (Applications and Reviews)*, 38(5):716–727, Sept 2008.

[49] Jih-Gau Juang, Ming-Te Huang, and Wen-Kai Liu. Pid control using presearched genetic algorithms for a mimo system. *IEEE Transactions on Systems, Man, and Cybernetics, Part C: Applications and Reviews*, 38(5):716,727, Sep. 2008.

[50] J. Jun, Q. Juntong, S. Dalei, and H. Jianda. Control Platform Design and Experiment of a Quadrotor. In *Chinese Control Conference (CCC)*, pages 2974–2979, 2013.

[51] Driankov D. Kadmiry B. A fuzzy flight controller combining linguistic and model-based fuzzy control. *Fuzzy Sets Systems*, 146(3):313–347, 2004.

[52] Driankov D. Kadmiry B. A fuzzy gain-scheduler for the attitude control of an unmanned helicopter. *IEEE Transactions on Fuzzy System*, 12(4):502–515, 2004.

[53] Johnson E.N. Kannan S.K. Adaptive trajectory based control for autonomous helicopters. In *21st Digital Avionics Systems Conf.*, oct 2002.

[54] Branko Katalinic, Petr Chalupa, Jan Pikryl, and Jakub Novk. 25th daaam international symposium on intelligent manufacturing and automation, 2014 modelling of twin rotor mimo system. *Procedia Engineering*, 100:249 – 258, 2015.

[55] Naïma Koull and Abdelmadjid Chehma. Soil characteristics and plant distribution in saline wetlands of oued righ, northeastern algeria. *Journal of Arid Land*, 8(6):948–959, 2016.

[56] H Kwakennaak. The polynomial approach to h_∞ optimal regulation. Lecture Notes CIME Course on Recent Developments in H_∞ Control Theory, 1990.

[57] H Kwakennaak. Minimax frequency domain optimization of multivariable linear feedback systems. In *IFAC World Congress, Budapest, Hungary*, 1996.

[58] D. Lee, A. Franchi, H. I. Son, C. Ha, H. H. Blthoff, and P. R. Giordano. Semiautonomous haptic teleoperation control architecture of multiple unmanned aerial vehicles. *IEEE/ASME Transactions on Mechatronics*, 18(4):1334–1345, Aug 2013.

[59] Zhijun Li and Jun Luo. Adaptive robust dynamic balance and motion controls of mobile wheeled inverted pendulums. *IEEE Transactions on Control Systems Technology*, 17(1):233–241, jan 2009.

[60] Qilian Liang and Jerry M. Mendel. Interval type-2 fuzzy logic systems: Theory and design. *IEEE Transactions on Fuzzy Systems*, 8(5):535–550, October 2000.

[61] F.-J. Lin and C.-H. Lin. A permanent-magnet synchronous motor servo drive using self-constructing fuzzy neural network controller. *IEEE Transactions on Energy Conversion*, 19(1):66–72, mar 2004.

[62] Faa-Jeng Lin and Po-Huan Chou. Adaptive control of two-axis motion control system using interval type-2 fuzzy neural network. *IEEE Transactions on Industrial Electronics*, 56(1):178–193, jan 2009.

[63] Hao Liu, Geng Lu, and Yisheng Zhong. Robust lqr attitude control of a 3-dof laboratory helicopter for aggressive maneuvers. *Industrial Electronics, IEEE Transactions on*, 60(10):4627–4636, Oct 2013.

[64] R. Lozano, P. Castillo, P. Garcia, and A. Dzul. Robust prediction-based control for unstable delay systems: Application to the yaw control of a mini-helicopter. *Automatica*, 40(4):603 – 612, 2004.

[65] Benallegue A. Madani T. Backstepping control for a quadrotor helicopter. In *Proc. International Conference on Intelligent Robots and Systems*, pages 3255–3260, oct 2006.

[66] Matsuda H. Mclean D. Helicopter station-keeping: comparing lqr, fuzzy-logic and neural-net controllers. *Engineering Applied Artificial Intelligence*, 11(3):411–418, 1998.

[67] Jerry M. Mendel. *Uncertain Rule-Based Fuzzy Logic Systems: Introduction and New Directions*. Prentice-Hall, 2001.

[68] M Suruz Miah and Wail Gueaieb. Rfid-based mobile robot trajectory tracking and point stabilization through on-line neighboring optimal control. *Journal of Intelligent & Robotic Systems*, 78(3-4):377–399, 2015.

[69] Prasad J.V.R. Mittal M. Three-dimensional modeling and control of a twin-lift helicopter system. *Journal of Guidance Control Dynamics*, 16(1):86–95, 1993.

[70] S. Mondal and C. Mahanta. Adaptive second-order sliding mode controller for a twin rotor multi-input-multi-output system. *IET Control Theory Applications*, 6(14):2157–2167, September 2012.

[71] S. Mondal and C. Mahanta. Adaptive second-order sliding mode controller for a twin rotor multi-input-multi-output system. *IET Control Theory & Applications*, 6(14):2157,2167, 2012.

[72] K.S. Narendra, J. Balakrishnan, and M.K. Ciliz. Adaptation and learning using multiple models, switching, and tuning. *IEEE Control Systems*, 15(3):37–51, Jun 1995.

[73] A. N. K. Nasir and M. O. Tokhi. An improved spiral dynamic optimization algorithm with engineering application. *IEEE Transactions on Systems, Man, and Cybernetics: Systems*, 45(6):943–954, June 2015.

[74] A.N.K. Nasir and M.O. Tokhi. An improved spiral dynamic optimization algorithm with engineering application. *IEEE Transactions on Systems, Man, and Cybernetics Systems*, 45(6):943,954, June 2015.

[75] Katsuhiko Ogata. *Modern control engineering*. Prentice-Hall, Boston, MA, 2010.

[76] P. Poggiolini. Analytical modeling of non-linear propagation in coherent systems. In *Optical Fiber Communication Conference and Exposition and the National Fiber Optic Engineers Conference (OFC/NFOEC), 2013*, pages 1–132, March 2013.

[77] J. K. Pradhan and A. Ghosh. Design and implementation of decoupled compensation for a twin rotor multiple-input and multiple-output system. *IET Control Theory Applications*, 7(2):282–289, Jan 2013.

[78] J.K. Pradhan and A. Ghosh. Design and implementation of decoupled compensation for a twin rotor multiple-input and multiple-output system. *IET Control Theory & Applications*, 7(2):282,289, 2013.

[79] A. P. S. Ramalakshmi and P. S. Manoharan. Non-linear modeling and pid control of twin rotor mimo system. In *Advanced Communication Control and Computing Technologies (ICACCCT), 2012 IEEE International Conference on*, pages 366–369, Aug 2012.

[80] T. Ryan and H. Jin Kim. Lmi-based gain synthesis for simple robust quadrotor control. *IEEE Transactions on Automation Science and Engineering*, 10(4):1173–1178, Oct 2013.

[81] T. Ryan and H.J. Kim. LMI-Based Gain Synthesis for Simple Robust Quadrotor Control. *IEEE Transactions on Automation Science and Engineering*, 10(4):1173–1178, Oct. 2013.

[82] T. s. Kim, J. h. Yang, Y. s. Lee, and O. k. Kwon. Twin rotors system modeling and bumpless transfer implementation algorithm for lq control. In *2006 SICE-ICASE International Joint Conference*, pages 114–119, Oct 2006.

[83] K.D. Sebesta and N. Boizot. A Real-Time Adaptive High-Gain EKF, Applied to a Quadcopter Inertial Navigation System. *IEEE Transactions on Industrial Electronics*, 61(1):495–503, Jan. 2014.

[84] J. Shan, H.-T. Liu, and S. Nowotny. Synchronised trajectory-tracking control of multiple 3-dof experimental helicopters. *Control Theory and Applications, IEE Proceedings -*, 152(6):683–692, Nov 2005.

[85] H. Sira-Ramirez, M. Zribi, and S. Ahmad. Dynamical sliding mode control approach for vertical flight regulation in helicopters. *Control Theory and Applications, IEE Proceedings*, 141(1):19–24, Jan 1994.

[86] Robert F. Stengel. *Optimal Control and Estimation*. Dover Publications, INC., 2012 edition, 2012.

[87] C. W. Tao, J. S. Taur, Y. H. Chang, and C. W. Chang. A novel fuzzy-sliding and fuzzy-integral-sliding controller for the twin-rotor multi-input-multi-output system. *IEEE Transactions on Fuzzy Systems*, 18(5):893–905, Oct 2010.

[88] C. W. Tao, J. S. Taur, Y. H. Chang, and C. W. Chang. A novel fuzzy-sliding and fuzzy-integral-sliding controller for the twin-rotor multi-input multi-output system. *IEEE Transactions on Fuzzy Systems*, 18(5):893–905, Oct 2010.

[89] Chin-Wang Tao, Jin-Shiuh Taur, and YC Chen. Design of a parallel distributed fuzzy lqr controller for the twin rotor multi-input multi-output system. *Fuzzy Sets and Systems*, 161(15):2081–2103, 2010.

[90] C.W. Tao, J.S. Taur, Tzuen Wuu Hsieh, and C.L. Tsai. Design of a fuzzy controller with fuzzy swing-up and parallel distributed pole assignment schemes for an inverted pendulum and cart system. *IEEE Transactions on Control Systems Technology*, 16(6):1277–1288, nov 2008.

[91] J.C. Avila Vilchis, B. Brogliato, A. Dzul, and R. Lozano. Nonlinear modelling and control of helicopters. *Automatica*, 39(9):1583 – 1596, 2003.

[92] Li-Xin Wang. *Adaptive Fuzzy Systems and Control: Design and Stability Analysis*. Prentice-Hall, Inc., Upper Saddle River, NJ, USA, 1994.

[93] P. Wen and T. W. Lu. Decoupling control of a twin rotor mimo system using robust deadbeat control technique. *IET Control Theory Applications*, 2(11):999–1007, November 2008.

[94] P. Wen and T.-W. Lu. Decoupling control of a twin rotor mimo system using robust deadbeat control technique. *IET Control Theory & Applications*, 2(11):999,1007, 2008.

[95] Y. Xu and C. Tong. Design and Attitude Control of a Flying Anchor Node. In *International Conference on Electronics, Communications and Control (ICECC)*, pages 1975–1978, 2011.

[96] G. Zames. Feedback and optimal sensitivity: Model reference transformations, multiplicative seminorms, and approximate inverses. *IEEE Transactions on Automatic Control*, 26(2):301–320, Apr 1981.

[97] Z. Zuo. Trajectory Tracking Control Design with Command-Filtered Compensation for a Quadrotor. *IET Control Theory & Applications*, 4(11):2343–2355, 2010.